Hepatoma-derived growth factor is neuroprotective in models of Huntington's disease

Dissertation an der Fakultät für Biologie
der Ludwig-Maximilians-Universität München
zur Erlangung des akademischen Grades
eines Doktor der Naturwissenschaften (Dr. rer. nat.)

Kerstin Völkl

München, 24. März 2022

Diese Dissertation wurde angefertigt

unter der Leitung von Prof. Dr. Rüdiger Klein und Dr. Irina Dudanova

in der Abteilung Moleküle – Signale – Entwicklung und

der Forschungsgruppe Molekulare Neurodegeneration

am Max-Planck-Institut für Neurobiologie in Martinsried, Deutschland.

Erstgutachter*in:	Prof. Dr. Rüdiger Klein
Zweitgutachter*in:	Prof. Dr. Laura Busse
Tag der Abgabe:	24. März 2022
Tag der mündlichen Prüfung:	21. Juli 2022

Eidesstattliche Erklärung

Ich versichere hiermit an Eides statt, dass die vorgelegte Dissertation von mir selbständig und ohne unerlaubte Hilfe angefertigt ist.

München, den ……24. März 2022…… ……Kerstin Völkl……..

(Unterschrift)

Erklärung

Hiermit erkläre ich,

☒ dass die Dissertation nicht ganz oder in wesentlichen Teilen einer anderen Prüfungskommission vorgelegt worden ist.

☒ dass ich mich anderweitig einer Doktorprüfung ohne Erfolg **nicht** unterzogen habe.

München, den ……24. März 2022…… ……Kerstin Völkl……..

(Unterschrift)

GRAPHICAL SYNOPSIS

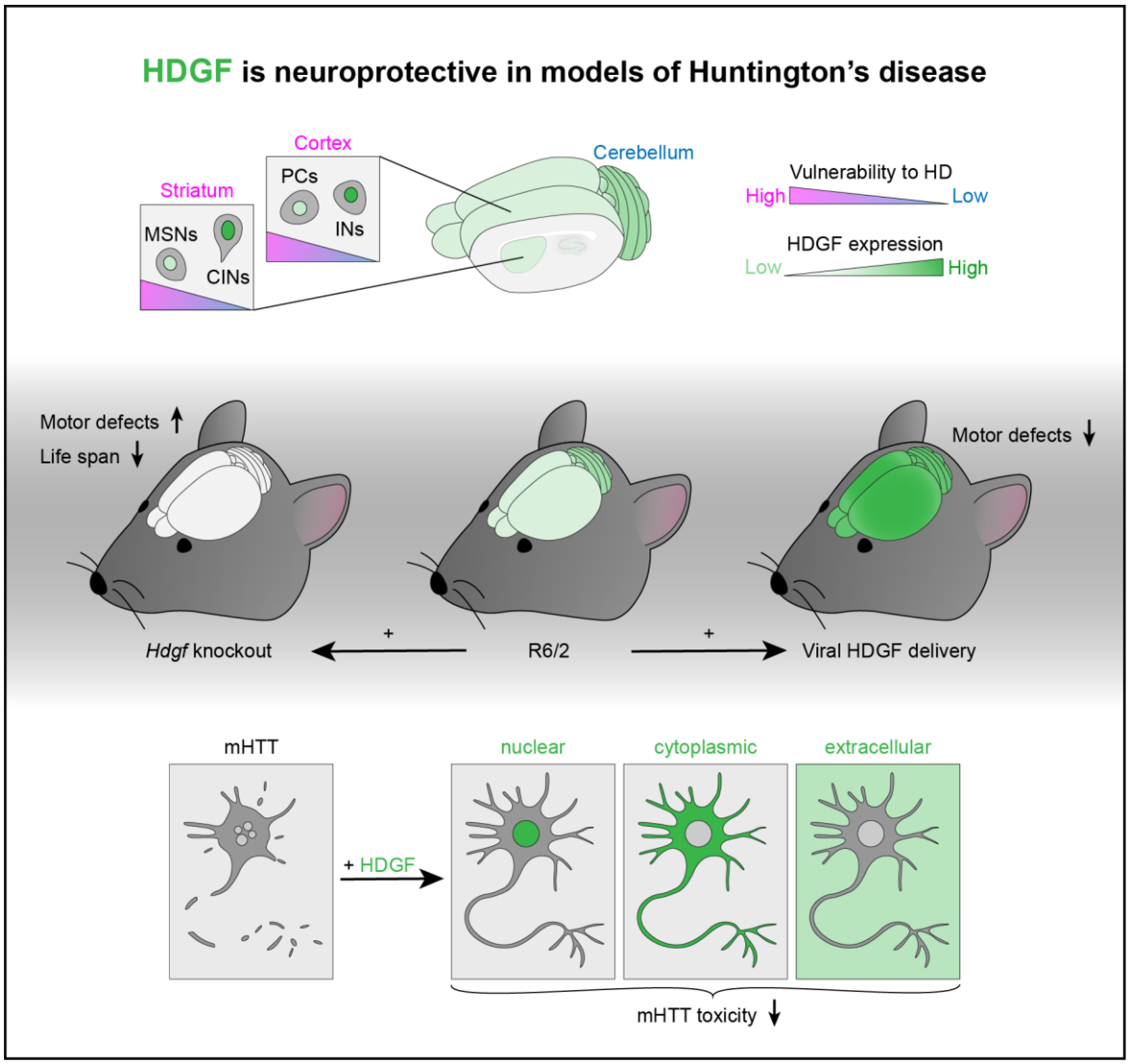

ABSTRACT

Huntington's disease (HD) is a fatal hereditary disorder with severe neurodegeneration in the striatum and cortex. Despite the monogenic nature of HD, disease pathogenesis is insufficiently understood and effective disease-modifying treatments are lacking to date. Here, we uncover hepatoma-derived growth factor (HDGF) as a neuroprotective protein in the context of HD. HDGF counteracts mutant huntingtin aggregation and cell death in murine primary cortical neurons. Expression levels of HDGF in mouse brain are inversely correlated with vulnerability of brain regions and individual neuronal populations to HD. In R6/2 HD model mice, HDGF deficiency exacerbates motor defects and reduces life span, while viral HDGF delivery into the nervous system significantly improves locomotor activity. Mechanistic studies in cell culture models of HD demonstrate that the neuroprotective activity of HDGF is independent of its subcellular localization: Nuclear and cytoplasmic HDGF are equally effective in rescuing mutant huntingtin toxicity. Moreover, extracellular application of recombinant HDGF is sufficient to improve viability of mutant huntingtin-expressing primary neurons via a mechanism distinct from canonical growth factor signaling. Taken together, this study provides new insights into HDGF function in the diseased brain and unravels the therapeutic potential of HDGF in HD.

TABLE OF CONTENTS

LIST OF TABLES

List of Figures

LIST OF ABBREVIATIONS

AAV	adeno-associated virus
AD	Alzheimer's disease
AEBSF	4-(2-aminoethyl)benzenesulfonyl fluoride
ALS	amyotrophic lateral sclerosis
ANOVA	analysis of variance
APC	adenomatous polyposis coli
ASO	antisense oligonucleotide
BCL2	B cell lymphoma 2
BDNF	brain-derived neurotrophic factor
BSA	bovine serum albumin
BW	body weight
ChAT	choline acetyltransferase
CIN	cholinergic interneuron
CNS	central nervous system
cytHDGF	cytoplasmic hepatoma-derived growth factor variant
DAPI	4',6-diamidino-2-phenylindole
DARPP32	dopamine and cyclic adenosine monophosphate-regulated phospho-protein, relative molecular mass 32,000
DIV	day *in vitro*
DMEM	Dulbecco's Modified Eagle Medium
DNA	deoxyribonucleic acid
dNTP	deoxynucleotide triphosphate
DPBS	Dulbecco's Phosphate Buffered Saline
$DPBS_{Ca2+Mg2+}$	Dulbecco's Phosphate Buffered Saline with calcium and magnesium
DTT	dithiothreitol
E	embryonic day
EDTA	ethylenediaminetetraacetic acid

EGFP	enhanced green fluorescent protein
ERK	extracellular signal-regulated kinase
EYFP	enhanced yellow fluorescent protein
F1	first filial generation
FBS	fetal bovine serum
FISH	fluorescence *in situ* hybridization
GABA	gamma-aminobutyric acid
GAD2	glutamate decarboxylase 2
GDNF	glial derived neurotrophic factor
GFAP	glial fibrillary acidic protein
HATH	homologous to the amino-terminus of hepatoma-derived growth factor
HBS	4-(2-Hydroxyethyl)piperazine-1-ethanesulfonic acid-Buffered Saline
HBSS	Hank's Balanced Salt Solution
HD	Huntington's disease
HDGF	hepatoma-derived growth factor
HEPES	4-(2-hydroxyethyl)piperazine-1-ethanesulfonic acid
HRP	hepatoma-derived growth factor-related protein
HTT	huntingtin
IBA1	ionized calcium-binding adaptor molecule 1
IGF2	insulin-like growth factor 2
IN	interneuron
LMU	Ludwig-Maximilians-Universität München
MAPK	mitogen-activated protein kinase
mHTT	mutant huntingtin
mRNA	messenger ribonucleic acid
MSN	medium spiny projection neuron
MTT	3-(4,5-dimethylthiazol-2-yl)-2,5-diphenyltetrazolium bromide
NDS	normal donkey serum
NEAA	Non-Essential Amino Acids Solution
NES	nuclear export signal
NGRN	neurogranin

NLS	nuclear localization signal
nucHDGF	nuclear wild-type hepatoma-derived growth factor
P0	postnatal day 0
PBS	phosphate-buffered saline
PC	pyramidal cell
PCR	polymerase chain reaction
PD	Parkinson's disease
PFA	paraformaldehyde
PI3K	phosphoinositide 3-kinase
RNA	ribonucleic acid
SDS	sodium dodecyl sulfate
SDS-PAGE	sodium dodecyl sulfate-polyacrylamide gel electrophoresis
shRNA	short hairpin ribonucleic acid
SMYD1	(Su(var)3-9, E(z), and trithorax) and (myeloid translocation protein 8, nervy, and deformed epidermal autoregulatory factor 1) domain containing 1
TAE	Tris-acetate-ethylenediaminetetraacetic acid
TBS	Tris-buffered saline
TBS-T	Tris-buffered saline with Tween 20
TCEP	tris(2-carboxyethyl)phosphine
WT	wild-type

1 INTRODUCTION

1.1 Neurodegenerative diseases

Neurodegenerative diseases such as Alzheimer's disease (AD), Parkinson's disease (PD), amyotrophic lateral sclerosis (ALS), and Huntington's disease (HD) are debilitating, to date incurable disorders with a life-changing impact on patients and their family members. AD is the most common cause of dementia in the elderly and primarily affecting cognition (Goodman *et al.*, 2017). PD, on the contrary, is defined by the cardinal motor deficits bradykinesia, rest tremor, and rigidity, although non-motor symptoms can be present (Postuma *et al.*, 2015). Rapidly progressing paralysis culminating in respiratory insufficiency is characteristic for ALS (Kiernan *et al.*, 2011). In HD, patients typically suffer from chorea early in disease and hypokinesia at advanced disease stages, accompanied by cognitive decline and psychiatric symptoms (McColgan and Tabrizi, 2018).

Despite the variety of clinical manifestations, shared pathomechanisms across neurodegenerative diseases have been uncovered in the last decades. Protein misfolding and aggregation, inflammation, mitochondrial dysfunction, altered synaptic transmission, and neuronal loss link their pathogenesis (Gan *et al.*, 2018). Thus, identifying new disease modifiers in one disease cannot only deepen our understanding of disease-specific pathogenesis, but may also yield valuable insights into other neurodegenerative diseases and facilitate the development of common therapies.

1.2 Huntington's disease

HD is named after an American physician, George Huntington, who was the first person to comprehensively describe the disease in 1872. Huntington outlined the autosomal dominant inheritance pattern of "hereditary chorea", a rare progressive adult-onset form of chorea with "a tendency to insanity and suicide" (Huntington, 2003). Sixteen years later, a detailed description of a three-generation family with HD, including two juvenile cases, followed (Hoffmann, 1888). While onset can range from childhood to late adulthood, HD symptoms typically manifest in the fourth to fifth decade of life and progressively worsen until death approximately 20 years later (Foroud *et al.*, 1999; Keum *et al.*, 2016; Rodrigues *et al.*, 2017; Ranganathan *et al.*, 2021). Generally defined by onset before 21 years of age, juvenile HD frequently includes seizures and presents with bradykinesia and dystonia as motor symptoms rather than chorea (Cloud *et al.*, 2012; Fusilli *et al.*, 2018; Achenbach *et al.*, 2020). The leading cause of lethality is pneumonia, most likely owing to aspiration from dysphagia (Sørensen and Fenger, 1992; Heemskerk and Roos, 2012; Rodrigues *et al.*, 2017).

Prevalence of HD was estimated to be 2.7 per 100,000 with geographical differences across the globe: An average prevalence of 5.7 per 100,000 has been reported for North America, Europe, and Australia, whereas in Asia prevalence is low with 0.4 per 100,000 people (Pringsheim *et al.*, 2012). An exceptionally large HD population of genetically related individuals was identified in the region of Lake Maracaibo in Venezuela (The U.S.-Venezuela Collaborative Research Project and Wexler, 2004). Lymphoblast cell lines established from blood samples of this Venezuelan kindred enabled mapping the HD locus to chromosome 4 and eventually led to the discovery of the causative HD mutation in 1993 (Gusella *et al.*, 1983; The Huntington's Disease Collaborative Research Group, 1993).

1.2.1 The causative mutation: A trinucleotide repeat expansion

The cause of HD is an expansion of the polyglutamine-encoding CAG trinucleotide repeat in exon 1 of the huntingtin gene (*HTT*) beyond 35 CAG repeats (The Huntington's Disease Collaborative Research Group, 1993; Nance *et al.*, 1998). Carriers harboring a pathogenic allele with 36 to 39 CAG repeats may or may not develop HD during lifetime, whereas alleles with 40 or more CAG repeats are fully penetrant (Nance *et al.*, 1998). Generally, the longer the CAG repeat tract, the earlier the onset of HD (Andrew *et al.*, 1993; Genetic Modifiers of Huntington's Disease (GeM-HD) Consortium, 2019). Individuals with more than 60 CAG repeats are likely to develop juvenile HD (Andrew *et al.*, 1993; Fusilli *et al.*, 2018; Achenbach *et al.*, 2020). Such long repeat tract lengths are often the result of paternal transmission due to CAG repeat instability in spermatogenesis (Nance *et al.*, 1998; Fusilli *et al.*, 2018). Although the precise underlying mechanisms remain unclear, formation of secondary DNA structures during DNA replication, homologous recombination, and repair are likely to play a key role (Pearson *et al.*, 2005; Khristich and Mirkin, 2020). Repeat instability increases with CAG repeat length and culminates in the phenomenon that offspring tend to have larger CAG repeats and earlier onset than the transmitting parent (genetic anticipation) (Pearson *et al.*, 2005; Wheeler *et al.*, 2007). However, CAG repeat tract length can only explain approximately 60% of individual variation in age at onset (Andrew *et al.*, 1993; Djoussé *et al.*, 2003). Thus, identifying disease-modifying factors that can delay HD onset constitutes a promising approach to deepen our understanding of disease pathogenesis and to uncover novel therapeutic strategies.

1.2.2 HD pathogenesis

HTT encodes for the huntingtin protein (HTT): A large, ubiquitously expressed protein with numerous interaction partners, which is thought to act as a scaffold for protein complex assembly (Saudou and Humbert, 2016). HTT is involved in many cellular processes including regulation of transcription, cargo trafficking along axons and dendrites, and synaptic function (Saudou and Humbert, 2016; Barron *et al.*, 2021).

Hence, haploinsufficiency due to loss-of-function caused by the expanded N-terminal polyglutamine tract in mutant HTT (mHTT) seems likely to drive disease. However, a persuasive line of evidence argues against a major contribution of loss-of-function to HD pathogenesis. While *HTT* knockout is lethal during embryonic development in mice (Duyao *et al.*, 1995; Nasir *et al.*, 1995; Zeitlin *et al.*, 1995), depletion of HTT in adult 4-month-old and 8-month-old mice does not cause neuronal pathology or behavioral abnormalities (Wang *et al.*, 2016). Moreover, huntingtin-lowering approaches decreasing HTT levels in the putamen by 45% were well tolerated in rhesus macaques (McBride *et al.*, 2011; Grondin *et al.*, 2012). Most importantly, heterozygous *HTT* disruption in humans does not cause HD and individuals with two HD alleles grow up normally with similar age at onset as heterozygous carriers matched for CAG repeat length (Ambrose *et al.*, 1994; Squitieri *et al.*, 2003).

Rather than loss-of-function, most findings suggest toxic gain-of-function as the primary effect of CAG repeat expansion in HD. The elongated polyglutamine tract causes mHTT to undergo conformational changes, leading to its aggregation and eventually to the formation of inclusions in neuronal nuclei and neuropil (DiFiglia *et al.*, 1997; Scherzinger *et al.*, 1997; Gutekunst *et al.*, 1999; Peskett *et al.*, 2018). Transgenic mice that express different forms of mHTT in addition to endogenous mouse HTT develop neuropathology and HD-like phenotypes (Mangiarini *et al.*, 1996; Reddy *et al.*, 1998; Hodgson *et al.*, 1999; Schilling *et al.*, 1999; Yamamoto *et al.*, 2000; Laforet *et al.*, 2001; Gray *et al.*, 2008). Consistent with the idea that lengthy polyglutamine stretches convey neurotoxicity, eight other neurodegenerative CAG repeat expansion disorders are known, all resulting in the expression and aggregation of polyglutamine proteins: spinal and bulbar muscular atrophy, dentatorubropallidoluysian atrophy, and spinocerebellar ataxia types 1, 2, 3, 6, 7, and 17 (Lieberman *et al.*, 2019). Moreover, in contrast to gene disruption, insertion of a long CAG repeat in the hypoxanthine phosphoribosyltransferase gene, which is not related to any known CAG repeat disorder, was sufficient to cause inclusion formation and late-onset neurological phenotypes with premature death in mice (Ordway *et al.*, 1997). Thus, abnormal polyglutamine stretches may cause toxicity via mechanisms independent of the protein context in addition to pathomechanisms specific to the affected protein.

In the HD brain, not only full-length mHTT, but also N-terminal polyglutamine-containing fragments of the mutant protein are present (DiFiglia *et al.*, 1997; Gutekunst *et al.*, 1999; Sieradzan *et al.*, 1999; Hoffner *et al.*, 2005). Such truncated forms of mHTT, especially a small exon 1 fragment, can be highly pathogenic, as demonstrated in cellular and animal models of HD (Mangiarini *et al.*, 1996; Hackam *et al.*, 1998; Schilling *et al.*, 1999; Palfi *et al.*, 2007; Yang *et al.*, 2008). While proteolytic cleavage by caspases and calpains can produce fragments of both wild-type and mutant HTT, exon 1 mHTT originates from a short mRNA generated by mis-splicing (Landles *et al.*, 2010; Sathasivam *et al.*, 2013). This process is specific to mutant alleles and seems to be CAG repeat length-dependent: Highest levels of *HTT* exon 1 transcript were detected in postmortem brain samples of juvenile HD cases (Sathasivam *et al.*, 2013; Neueder *et al.*, 2017). To which extent aberrant splicing contributes to disease pathogenesis still needs to be determined. Moreover, the role of other pathogenic mechanisms linked to expanded trinucleotide repeats, including RNA toxic gain-of-function and repeat-associated non-ATG translation (Bañez-Coronel *et al.*, 2015; Malik *et al.*, 2021), remains unclear in HD and requires further studies.

1.2.3 Differential neuronal vulnerability to HD

Although HTT is ubiquitously expressed, the neuropathological changes in HD are most prominent in the striatum and cerebral cortex (Figure 1.1). Up to 95% of striatal GABAergic medium spiny projection neurons (MSNs) are lost in disease, and therefore considered the primarily vulnerable neuronal population in HD (Vonsattel and DiFiglia, 1998). The second most affected population is the cortical glutamatergic pyramidal cells (PCs), including those projecting to the striatum (Hedreen *et al.*, 1991; Macdonald and Halliday, 2002). Already years before motor onset, striatal and cortical atrophy can be detected and becomes more widespread as disease progresses (Rosas *et al.*, 2008; Tabrizi *et al.*, 2009; Nopoulos *et al.*, 2010).

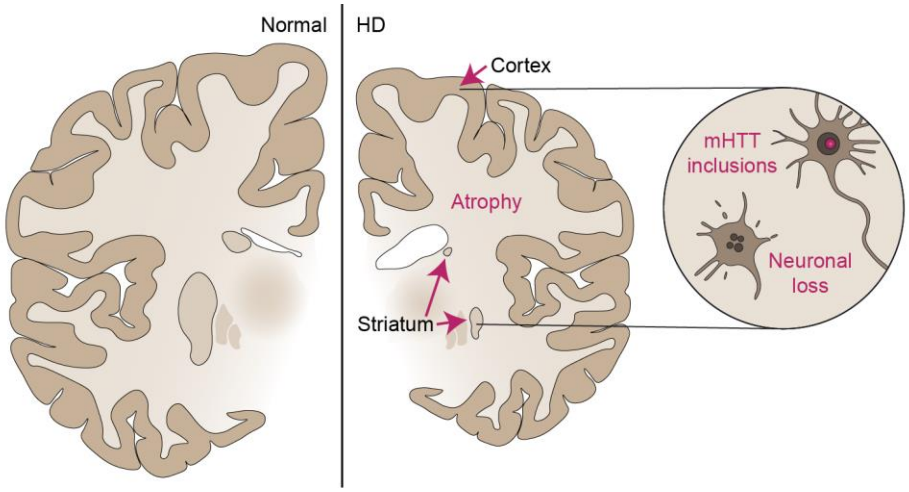

Figure 1.1 HD brain pathology

Schematic drawing of coronal sections through healthy and diseased human brain at the level of the primary motor cortex. Neuropathological changes in HD, which are most prominent in the striatum and cortex, are depicted.

Regional atrophy and neuronal loss are closely linked to the diverse pattern of symptomatology. The early predominance of chorea has been attributed to loss of MSNs projecting to the external segment of the globus pallidus (indirect pathway) prior to degeneration of MSNs that project to the internal segment of the globus pallidus and substantia nigra pars reticulata (direct pathway) (Reiner *et al.*, 1988). While the direct pathway facilitates movement via excitation of the thalamus and cortex, the indirect pathway has the opposing effect suppressing undesired motor programs (Alexander and Crutcher, 1990). In contrast to motor dysfunction, pronounced mood symptoms were associated with profound degeneration in the striosomal compartment of the striatum, which is strongly connected with brain regions related to the limbic system (Tippett *et al.*, 2007). Moreover, cortical changes are likely to contribute to the heterogeneity of symptoms. HD patients with prominent bradykinesia rather than chorea show more widespread cortical thinning including pre-motor and supplementary motor areas (Rosas *et al.*, 2008). Furthermore, stereological cell counting in postmortem HD cortex revealed differences in cell loss depending on motor or mood symptomology: Whereas HD cases with predominant motor dysfunction show pronounced loss of PCs in the primary motor cortex, but not in the

cingulate cortex, cases with a major mood phenotype present neuron loss in the cingulate cortex, but not in the motor cortex (Thu *et al.*, 2010). In conclusion, these findings highlight the role of both striatal and cortical degeneration in disease manifestation.

Why susceptibility to disease differs between tissues and cell populations remains largely unclear. Cell-type specific characteristics such as biochemical signature, morphology, and electrophysiological properties could explain selective vulnerability (Fu *et al.*, 2018). In the striatum, high energy demand, limited ability to counteract oxidative stress and maintain proteostasis, as well as susceptibility to excitotoxicity may render MSNs particularly vulnerable to mHTT toxicity (Fu *et al.*, 2018). Somatic CAG repeat expansion might also contribute to differential susceptibility. Repeat instability is especially prominent in the striatum and cortex with repeats of more than 1,000 CAGs detected in postmortem tissue (Telenius *et al.*, 1994; Kennedy *et al.*, 2003; Shelbourne *et al.*, 2007; Larson *et al.*, 2015). Interestingly, many HD-modifying loci identified by genome-wide association studies suggest a role of DNA repair mechanisms in HD pathogenesis with variants likely to influence the rate of somatic expansion (Genetic Modifiers of Huntington's Disease (GeM-HD) Consortium, 2015; Moss *et al.*, 2017; Flower *et al.*, 2019; Genetic Modifiers of Huntington's Disease (GeM-HD) Consortium, 2019; Goold *et al.*, 2019). However, selective neuropathology and motor deficits developed in a HD mouse model harboring a stable CAA-CAG tract (Gray *et al.*, 2008), arguing against a central role of somatic instability in differential vulnerability. A better understanding of disease pathology and physiology of neuronal subtypes will be essential to dissect why specific cells are particularly vulnerable in neurodegenerative diseases.

1.2.4 The R6/2 mouse model of HD

Since possibilities to study HD in humans are limited, animal models constitute an essential tool to advance understanding of pathogenic processes in disease and develop therapeutic approaches to treat patients effectively in future. The R6 lines, including R6/2, were the first mice genetically engineered to carry the HD mutation

(Mangiarini *et al.*, 1996). Although various animal models of HD have been generated thereafter (Chang *et al.*, 2015), the R6/2 mouse line is among the most widely studied and best characterized HD animal models. These transgenic mice express human mHTT-exon 1 under the control of the *HTT* promotor (Mangiarini *et al.*, 1996). Originally harboring 144 CAG repeats on average, many different R6/2 sublines with varying CAG tract length have been established on the basis of intergenerational repeat instability (Mangiarini *et al.*, 1997; Dragatsis *et al.*, 2009; Menalled *et al.*, 2009; Morton *et al.*, 2009; Cowin *et al.*, 2011; Cummings *et al.*, 2012). While the phenotype becomes more severe up to approximately 160 CAG repeats, longer CAG tracts tend to delay onset in R6/2 mice (Dragatsis *et al.*, 2009; Morton *et al.*, 2009; Cummings *et al.*, 2012). The reason for this non-linear U-shaped relationship is not clear, but reduced mHTT expression and limited nuclear access of mHTT with very large CAG repeats (>300 CAGs) may contribute to phenotype attenuation (Dragatsis *et al.*, 2009).

R6/2 mice develop progressive pathological and behavioral HD-like alterations until death at around 12 to 21 weeks of age (for mice with 145 to 225 CAGs) (Figure 1.2) (Mangiarini *et al.*, 1996; Stack *et al.*, 2005; Dragatsis *et al.*, 2009; Morton *et al.*, 2009). Overt neurological signs include impaired balance, motor coordination deficits, stereotypic movements, and tremor (Mangiarini *et al.*, 1996; Carter *et al.*, 1999). Prominent neuronal nuclear inclusions were first detected in R6/2 mice, leading to the discovery of mHTT aggregates in human HD brain (Davies *et al.*, 1997; DiFiglia *et al.*, 1997). However, despite widespread aggregate pathology and brain atrophy, only mild striatal cell death is detectable in R6/2 mice at advanced disease stage, suggesting that behavioral deficits arise from neuronal dysfunction preceding cell loss (Stack *et al.*, 2005; Dodds *et al.*, 2014).

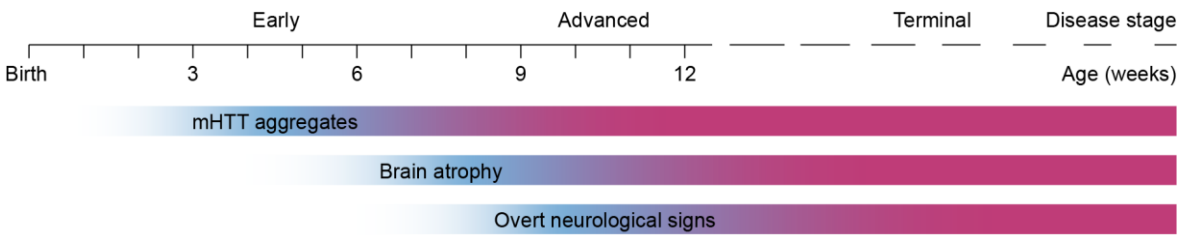

Figure 1.2 Timeline of phenotypes in the R6/2 mouse model

While neuronal dysfunction likely plays a role in human disease as well, to which extent it contributes to human symptomology compared to cell death is not fully understood. Since HD naturally only occurs in humans, none of the animal models can perfectly recapitulate human disease. Nevertheless, HD animal models have provided valuable insights into disease pathogenesis and are key to preclinical drug development (Rubinsztein, 2002; Chang *et al.*, 2015). Fast progression with a clear behavioral phenotype is the major advantage of the R6/2 mouse model. Thus, R6/2 mice represent a suitable model for initial drug testing, although validation in other HD models, such as full-length mHTT models, should be considered as a complementary approach.

1.2.5 HD therapeutics

Almost three decades after the genetic cause of HD was uncovered, available treatment options for HD are still palliative and limited to symptom relief (Kim *et al.*, 2021). Hence, identification of disease-modifying therapies will be absolutely vital to delay or halt progression of this devastating disease in future. Current preclinical and clinical investigations aim at various targets including mitochondrial function, immune response, neurotrophic support, protein aggregation, and somatic CAG repeat expansion, but the main focus is on mHTT-lowering strategies (Tabrizi *et al.*, 2019a; Kumar *et al.*, 2020; CHDI Foundation, 2021; Kim *et al.*, 2021). Great promise was held for tominersen (previously RG6042 or IONIS-HTT_{Rx}), a non-allele-selective antisense oligonucleotide (ASO), which was well tolerated and showed dose-dependent reduction of mHTT in the cerebrospinal fluid in a phase I/IIa clinical trial (Tabrizi *et al.*, 2019b). Being the first HTT-lowering drug entering a pivotal phase III trial (NCT03761849), tominersen's failure to show efficacy with discontinuation of dosing in March 2021 is a major setback for the field (Roche, 2021). In the same month, Wave Life Sciences suspended further clinical development of two allele-specific ASOs (WVE-120101 and WVE-120102) after they failed to reduce mHTT levels in phase I/II studies (NCT03225833, NCT04617847, NCT03225846, NCT04617860) (Wave Life Sciences, 2021). While these outcomes do not argue against mHTT lowering as a promising

therapeutic approach, they highlight the need for further refinement with regard to dosing, drug distribution and timing of treatment. In manifest human disease, targeting mHTT alone might not be sufficient to halt or slow down progression since secondary pathogenic processes could be self-enforcing, driving further neurodegeneration. Pursuing different therapeutic approaches – targeting both primary and secondary pathogenic processes to act complementary or in synergy – is likely the best strategy to maximize patient benefit.

1.3 Hepatoma-derived growth factor

Hepatoma-derived growth factor (HDGF) is a widely expressed 26 kDa protein of the family of HDGF-related proteins (HRPs) (Abouzied *et al.*, 2004). Originally purified from conditioned medium of human hepatoma cells, HDGF was reported as a secreted factor with mitogenic activity (Nakamura *et al.*, 1994). Thereafter, several other studies have described HDGF release from various cell types, including mesenchymal cells, muscle cells, and neurons (Oliver and Al-Awqati, 1998; Zhou *et al.*, 2004; Ooi *et al.*, 2010; Ojima *et al.*, 2014). The N-terminal part of HDGF was shown to mediate extracellular release, but lacks a canonical signal sequence for secretion via the endoplasmic reticulum/Golgi secretory pathway (Nakamura *et al.*, 1994; Thakar *et al.*, 2010; Nüße *et al.*, 2017). Thus, secretion must occur through alternative pathways (Rabouille, 2017). Nüße *et al.* (2017) have previously demonstrated exosomal release as one possibility for HDGF secretion. However, HDGF was also found in exosome-depleted supernatant, suggesting additional release of protein not associated with extracellular vesicles (Nüße *et al.*, 2017). Uptake of such free HDGF is likely mediated by a cell-surface receptor, whose identity is not yet clarified. One proposed candidate is nucleolin, a multifunctional protein which shuttles between the nucleus, cytoplasm and plasma membrane (Chen *et al.*, 2015). Inside cells, HDGF is targeted to the nucleus by two nuclear localization signals (NLSs) within its sequence, but can also reside in the cytoplasm (Nakamura *et al.*, 1994; Oliver and Al-Awqati, 1998; Everett *et al.*, 2000; Kishima *et al.*, 2002; Abouzied *et al.*, 2004; Zhou *et al.*, 2004) (Figure 1.3). Differences in

subcellular distribution might reflect different functions of HDGF within cells. Nuclear localization for instance has been shown to play an important role for growth-stimulating activity of HDGF (Everett *et al.*, 2001; Kishima *et al.*, 2002).

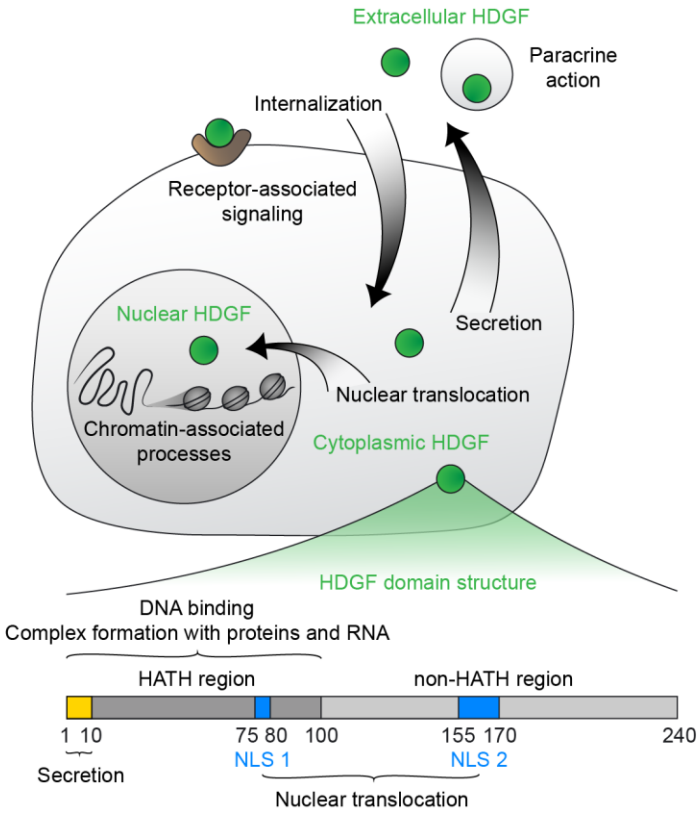

Figure 1.3 The multiple facets of HDGF

Schematic representation of HDGF structure, subcellular localization and potential modes of action. Inside cells, HDGF can reside in the cytoplasm, but mostly localizes to the nucleus where it can bind DNA and regulate chromatin-associated processes. Nuclear translocation of HDGF is mediated by two NLSs in its sequence. The N-terminal HATH domain is key for DNA binding and complex formation with proteins and RNA. In the extracellular space, HDGF can be present as free protein or in association with vesicles. Secretion of HDGF requires the first 10 residues of the protein. Extracellular HDGF can activate receptor-associated signaling and might act in a paracrine manner to mediate cell-to-cell communication.

The identification of various HDGF interactors suggested the protein's involvement in many cellular processes including translation, ribosome biogenesis, RNA processing, chromatin remodeling, DNA damage repair, and transcriptional regulation (Zhao *et al.*, 2011). In accordance with a potential function as transcriptional modulator, HDGF was

shown to downregulate transcription of the striated muscle specific SET and MYND domain containing 1 gene (SMYD1) by binding to the SMYD1 promotor in complex with the C-terminal binding protein, a transcriptional corepressor (Yang and Everett, 2007; Yang and Everett, 2009). DNA binding and complex formation with proteins and RNA is dependent on the N-terminal homologous to the amino-terminus of HDGF (HATH) region, also known as PWWP domain (Lukasik *et al.*, 2006; Yang and Everett, 2007; Zhao *et al.*, 2011) (Figure 1.3). More than twenty human PWWP domain-containing proteins have been identified and most of them are implicated in chromatin-associated processes (Qin and Min, 2014), strengthening the idea of a predominant nuclear role of HDGF.

In neurons, also mostly nuclear localization has been reported (Abouzied *et al.*, 2004; Zhou *et al.*, 2004; El-Tahir *et al.*, 2006). Expression is widespread in the brain (Abouzied *et al.*, 2004; Zhou *et al.*, 2004; El-Tahir *et al.*, 2006; Uhlén *et al.*, 2015) (Human Protein Atlas available from http://www.proteinatlas.org), but studies about HDGF function in the nervous system are scarce. In neuronal cultures, HDGF was found to promote neurite extension and survival following extracellular application, whereas suppression of endogenous HDGF promoted cell death, suggesting that HDGF acts as a neurotrophic factor (Zhou *et al.*, 2004; Marubuchi *et al.*, 2006). In line with these findings, treatment with recombinant HDGF provided neuroprotection after optic and facial nerve transection *in vivo* (Marubuchi *et al.*, 2006; Hollander *et al.*, 2012). However, to which extent receptor-mediated signaling plays a role, or if neuroprotection is solely due to nuclear functions of HDGF remains to be elucidated. Moreover, the disease-modifying potential of HDGF in the context of neurodegenerative diseases such as HD has not yet been explored.

1.4 Ultimate goal and specific aims

Identifying novel disease modifiers in HD cannot only advance our understanding of pathogenesis, but also holds great promise to uncover new therapeutic strategies against neurodegeneration. This study aimed to investigate the neuroprotective ability of HDGF in HD. The four specific aims were (1) to unravel the disease-modifying potential of HDGF in primary neurons, (2) to thoroughly characterize the expression of HDGF in the central nervous system, (3) to decipher the impact of HDGF deficiency and overexpression on HD phenotypes in HD mouse models, and (4) to provide first insights into the mechanism of action by which HDGF provides neuroprotection.

2 Material and Methods

2.1 Plasmid generation and preparation

All plasmids used in this study are specified in Table 2.1.

Table 2.1 Plasmid constructs

ID	Insert	Vector	Origin
1	mCherry-Myc-His	pcDNA3.1	Hipp *et al.* (2012) [1]
2	HTTQ25-mCherry-Myc-His		
3	HTTQ97-mCherry-Myc-His		
4	HTTQ25-His		Cloned, with support from Sophie Keeling
5	HTTQ72-His		
6	EGFP-HA	pCI-neo	Schulz-Trieglaff (2018)
7	HDGF-Myc-Flag	pCMV6-Entry	OriGene, RC204148
8	cytHDGF-Myc-Flag		Cloned
9	-	psPAX2	Addgene plasmid # 12260; gift from Didier Trono [2]
10	VSV-G	pcDNA3.1	Kuhn *et al.* (2010) [2]
11	EYFP	pFhSynW2 [2,3]	Gutiérrez-Ángel (2019)
12	EYFP-P2A-Flag-HDGF		
13	EYFP-P2A-Flag-cytHDGF		Cloned, with support from Maximilian Gantz
14	HDGF-Flag-TEV-His	pET-17b	
15	cytHDGF-Flag-TEV-His		

[1] Kindly provided by Franz-Ulrich Hartl, Max Planck Institute of Biochemistry, Martinsried, Germany

[2] Kindly provided by Dieter Edbauer, German Center for Neurodegenerative Diseases, Munich, Germany

[3] May *et al.* (2014)

Plasmids were cloned as detailed in Table 2.2 using the In-Fusion HD Cloning Plus kit (Takara Bio, 638909) according to the manufacturer's instructions. In brief, the target insert was amplified using the CloneAmp HiFi PCR Premix (included in the In-Fusion HD Cloning Plus kit package) with adequate primers (Eurofins Genomics). As annealing temperature, the melting temperature of the 3' portion of the primers was chosen for the first 10 cycles and changed to the melting temperature calculated on the entire length of the primers for the following 25 cycles to improve specific primer binding. If the calculated melting temperature exceeded the extension temperature of 72°C, annealing temperature was set to 72°C. For linearization of the vector, 10 µg DNA was digested using the appropriate restriction enzymes (New England Biolabs) as directed by the supplier. The target PCR product and the linearized vector were purified by agarose gel extraction using the NucleoSpin Gel and PCR Clean-Up kit (included in the In-Fusion HD Cloning Plus kit package). The DNA fragments were excised from the gel utilizing a Molecular Imager Gel Doc XR+ System (Bio-Rad). DNA concentration was determined with a NanoDrop 1000 spectrophotometer (Peqlab). In-Fusion cloning procedure and transformation in Stellar Competent Cells (included in the In-Fusion HD Cloning Plus kit package) followed as instructed by the manufacturer. Bacterial cultures were grown from single colonies and plasmids isolated using QIAprep Spin Miniprep Kit (Qiagen, 27106) according to the supplier's instructions. Prior to cell lysis, glycerol stocks were prepared from bacterial cultures with 20% glycerol and stored at -80°C. For quality control, 0.5-1 µg plasmid DNA was linearized by restriction digestion with an appropriate restriction enzyme (New England Biolabs) as directed by the manufacturer and analyzed by agarose gel electrophoresis. The DNA sequence of the insert and correct insertion into the vector was confirmed by sequencing (Eurofins Genomics).

Transfection-grade plasmid DNA was prepared using NucleoBond Xtra Maxi kit (Macherey-Nagel, 740414.50) following the manufacturer's instructions. DNA was reconstituted in distilled water and the concentration adjusted to 1 µg/µl using NanoDrop 1000. Aliquots were stored at -20°C. Plasmid identity was confirmed by sequencing.

Table 2.2 Cloning strategy

ID (Table 2.1)	**Insert**	**C-terminal sequence(s)** (introduced via primers)	**PCR template**	**Vector, cloning sites**
4	HTTQ25	-	pPGK-HTTQ25 (Jeong *et al.*, 2012) [1]	ID 2 (Table 2.1), *XhoI* and *AgeI*
5	HTTQ72		pPGK-HTTQ72 (Jeong *et al.*, 2012) [1]	
8	HDGFmN1mN2	Nuclear export signal (NES) [2] → cytHDGF	pCC1-EYFP-P2A-Flag-HDGFmN1mN2 (GenScript) [3]	ID 7 (Table 2.1), *AsiSI* and *MluI*
13	cytHDGF	-	ID 8	ID 12 (Table 2.1), *SmaI* and *NheI*
14	HDGF	Flag-TEV-His	ID 12 (Table 2.1)	pET-17b-Ub [4], *NdeI* and *XhoI*
15	cytHDGF		ID 13	

[1] Kindly provided by Dimitri Krainc, Northwestern University Feinberg School of Medicine, Chicago, USA

[2] NES sequence (SELQNKLEELDLDSYK) adopted from Addgene plasmid # 36206 (Goedhart *et al.*, 2012)

[3] Mutagenesis of HDGF (NM_004494) according to Kishima *et al.* (2002)

[4] Kindly provided by Kathrin Lang, Center for Integrated Protein Science Munich, Technical University of Munich, Garching, Germany

2.2 Agarose gel electrophoresis

DNA was separated in 1-2% agarose gels prepared with Tris-acetate-EDTA (TAE) buffer containing 40 mM Tris, 20 mM acetic acid, and 1 mM EDTA pH 8.0. Gels were pre-stained with SYBR Safe DNA Gel Stain (Invitrogen, S33102). Electrophoresis was performed in TAE buffer at 80-200 V until separation was complete. GeneRuler 1 kb Plus DNA Ladder (Thermo Scientific, SM1333) was used to estimate DNA fragment size. Gels were imaged using the Molecular Imager Gel Doc XR+ System.

2.3 Lentivirus preparation

For lentivirus production, HEK 293T cells (Takara Bio, 632180) were expanded until 80% confluency in a 3-layer 525 cm^2 culture flask (Corning, 353143) at 37°C, 5% CO_2 in 60 ml Dulbecco's Modified Eagle Medium (DMEM; Gibco, 41965-039) supplemented with 10% heat-inactivated fetal bovine serum (FBS; Biochrom, S0115), 1% Geneticin (Gibco, 10131-019), 1% Non-Essential Amino Acids Solution (NEAA; Gibco, 11140-050), and 10 mM HEPES pH 7.4. Cells were washed with 10 ml pre-warmed Dulbecco's Phosphate Buffered Saline (DPBS; Sigma-Aldrich, D8537) and detached using 5 ml pre-warmed Trypsin-EDTA solution (Sigma-Aldrich, T4299) at 37°C, 5% CO_2. 20 ml pre-warmed growth medium, containing 10% FBS, 1% NEAA, and 10 mM HEPES pH 7.4 in DMEM, was added, followed by centrifugation at 140 *g* for 2 min. Cells were resuspended and seeded in 60 ml pre-warmed growth medium at a split ratio of 1:2 in a new 3-layer 525 cm^2 culture flask. The next day, transfection mix was prepared by combining 59.5 µg of the respective pFhSynW2 expression plasmid, 35.2 µg psPAX2, and 20.5 µg pcDNA3.1-VSV-G in 4.9 ml DMEM with 345 µl TransIT-Lenti Transfection Reagent (Mirus Bio, MIR 6600) added to 4.8 ml DMEM, followed by incubation for 20 min. Growth medium was exchanged and transfection mix was added to cells. After overnight incubation, medium was replaced by fresh pre-warmed growth medium, collected 48-52 h later, and centrifuged at 1,200 *g* for 10 min. Lentiviral supernatant was filtered through a 0.45 µm filter and concentrated using Lenti-X Concentrator (Takara Bio, 631232) according to the manufacturer's instructions. Virus was suspended in 600 µl buffer containing 50 mM Tris-HCl pH 7.8, 130 mM NaCl, 10 mM KCl, and 5 mM $MgCl_2$. Single-use aliquots were stored at -80°C. Viral titers were estimated using Lenti-X GoStix Plus (Takara Bio, 631280) following the manufacturer's instructions using a reference value of 6.014 (TU/ml)/GV. Calculated titers were in the range of $1.35*10^6$ to $2.77*10^6$ TU/ml.

2.4 Recombinant protein production

Brain-derived neurotrophic factor (BDNF) was purchased from R&D Systems (248-BD/CF). Recombinant HDGF protein was produced by Leopold Urich at the Protein Production Core Facility, Max Planck Institute of Biochemistry, Martinsried, Germany. In brief, pET17-HDGF-Flag-TEV-His and pET17-cytHDGF-Flag-TEV-His were transformed into Rosetta (DE3) cells and expressed via autoinduction (Studier, 2005) at 20°C overnight. After pelleting, cells were resuspended in His Binding Buffer (50 mM sodium phosphate pH 8, 500 mM NaCl, 10 mM imidazole, 1 mM TCEP, and 10% glycerol) supplemented with protease inhibitor mix (prepared in-house; 1 mM AEBSF HCl, 2 µg/ml aprotinin, 1 µg/ml leupeptin, 1 µg/ml pepstatin), 2.4 U/ml benzonase (produced in-house), and 2 mM $MgCl_2$. Cell disruption was conducted using an Emulsiflex C5 homogenizer (Avestin). Lysates were centrifuged for 30 min at 50,833 *g*, 4°C. Per 50 ml supernatant, 2.5 ml of 5% polyethyleneimine solution was added for nucleic acid removal, followed by stirring for 10 min and centrifugation for 30 min at 50,833 *g*, 4°C. Proteins were precipitated by stirring for 1 h with 21.8 g ammonium sulfate per 50 ml supernatant. After centrifugation for 30 min at 50,833 *g*, 4°C, the pellet was resuspended in 50 ml His Binding Buffer and applied to a 1 ml BabyBio Ni-NTA column (Bio-Works, 45 655 103) equilibrated in His Binding Buffer. The column was washed with 4% His Elution Buffer (50 mM sodium phosphate pH 8, 500 mM NaCl, 250 mM imidazole, 1 mM TCEP, and 10% glycerol), followed by protein elution in a straight gradient from 4% to 100% His Elution Buffer. The purest fractions were identified via SDS-polyacrylamide gel electrophoresis (SDS-PAGE) and pooled accordingly. His-tag cleavage was performed by adding His-tagged TEV protease (produced in-house) and dialysis in phosphate-buffered saline (PBS; 137 mM NaCl, 2.7 mM KCl, 8.1 mM Na_2HPO_4, 1.5 mM KH_2PO_4, pH 7.4) with 1 mM TCEP overnight. The remaining tag and protease were removed by reverse nickel-nitrilotriacetic acid purification in batch mode (Ni-Sepharose High Performance; GE Healthcare, 17-5268-02). Final polishing of the target proteins was done through size exclusion on a HiLoad 26/600 Superdex 75 prep grade column (GE Healthcare) eluting in PBS with 1 mM DTT.

Proteins were concentrated to 1 mg/ml using an Amicon Ultra 15 column (Amicon). Quality of recombinant proteins was checked via SDS-PAGE and dynamic light scattering analysis. Identity was confirmed through liquid chromatography-mass spectrometry (micro-ToF). Protein aliquots were snap frozen in liquid nitrogen and stored at -80°C.

2.5 Transfection of HEK 293T cells

HEK 293T cells were maintained in DMEM (Gibco, 41966-029) with 1% Penicillin/Streptomycin (Sigma-Aldrich, P0781) and 10% FBS at 37°C, 5% CO_2, and passaged at 70-80% confluency. Cover glasses were sterilized at 180°C for 2 h to overnight and coated with sterile filtered 1 mg/ml poly-D-lysine (Sigma-Aldrich, P7886) in borate buffer (50 mM boric acid and 12.5 mM sodium tetraborate, pH 8.5) for 4 h to overnight at 37°C, 5% CO_2, followed by washing three times with DPBS. Cells were washed with pre-warmed DPBS, detached using pre-warmed Trypsin-EDTA solution at 37°C, 5% CO_2, and plated at a density of 25,000 cells/cm^2 in 500 µl pre-warmed DMEM with 1% Penicillin/Streptomycin and 10% FBS on the coated cover glasses in 24-well plates. The next day, transfection was performed using jetPEI transfection reagent (Polyplus-transfection, 101-10N) according to the manufacturer's instructions. Per well, 0.5 µg DNA and 1.5 µl jetPEI in 50 µl 150 mM NaCl were applied.

2.6 Primary neuronal cultures

Cultureware was coated with sterile filtered 1 mg/ml poly-D-lysine in borate buffer for 4 h to overnight at 37°C, 5% CO_2. After washing three times with DPBS with calcium and magnesium ($DPBS_{Ca2+Mg2+}$; Sigma-Aldrich, D8662), 5 µg/ml laminin (Gibco, 23017-015) in $DPBS_{Ca2+Mg2+}$ was applied for 2-4 h at 37°C, 5% CO_2. Meanwhile, a pregnant CD-1 female was anesthetized using isoflurane (CP-Pharma, 400806.00.00) and sacrificed by cervical dislocation at embryonic day (E) 15.5. The uterus was dissected and washed

in ice-cold $DPBS_{Ca2+Mg2+}$. Embryos were harvested and decapitated in ice-cold dissection medium containing 1x Penicillin/Streptomycin, 10 mM HEPES pH 7.4, and 10 mM $MgSO_2$ in Hank's Balanced Salt Solution (HBSS; Gibco, 24020-091). Brains were extracted and meninges removed prior to dissection of neocortices. Digestion of collected neocortices was conducted at 37°C for 15 min in pre-warmed Trypsin-EDTA solution with 7.5 µg/ml DNase I (Roche, 10104159001). Trypsin activity was blocked by washing with pre-warmed Neurobasal medium (Gibco, 21103-049) supplemented with 5% FBS. After washing with pre-warmed culture medium containing 1x B-27 (Gibco, 17504-044), 1x Penicillin/Streptomycin, and 2 mM L-Glutamine (Gibco, 25030-024) in Neurobasal medium, cells were dissociated in pre-warmed culture medium by triturating and pelleted by centrifugation at 130 *g* for 5 min. Meanwhile, coated plates were washed twice with $DPBS_{Ca2+Mg2+}$. The cell pellet was resuspended in 1 ml/embryo pre-warmed culture medium, followed by cell counting at 10-fold dilution using an Improved Neubauer counting chamber (Brand). Cells were plated in pre-warmed culture medium according to Table 2.3 and maintained at 37°C, 5% CO_2.

Table 2.3 Plating conditions for primary neuron cultures

	Cell number	**Culture medium**	
Cultureware	per dish/well		**Experiment**
100 mm culture dish	$3*10^6$	10 ml	Western blot
24-well plate with cover glasses [1]	120,000	500 µl	Immunocytochemistry
96-well plate	20,000	100 µl	MTT assay

[1] Sterilized at 180°C for 2 h to overnight

2.7 Transfection of primary neurons

Neurons were transfected at day *in vitro* (DIV) 7 using CalPhos Mammalian Transfection Kit (Takara Bio, 631312). Transfection solution was prepared by adding

1.5 µg DNA per construct (3 µg in total) in 200 mM $CaCl_2$ dropwise to 2x HEPES-Buffered Saline (HBS) at a ratio of 1:1, followed by incubation for 30 min. Cells on cover glasses were equilibrated in fresh pre-warmed culture medium and incubated with 30 µl transfection solution for 3 h at 37°C, 5% CO_2. Fresh culture medium was acidified for at least 30 min at 37°C, 10% CO_2 prior to transfer of transfected cells and incubation for 30 min at 37°C, 5% CO_2. Cells on cover glasses were transferred back to the original medium and incubated at 37°C, 5% CO_2 for protein expression.

2.8 Transduction of primary neurons

At DIV 7, 50 µl culture medium was removed and lentiviral vectors added with 100 µl fresh pre-warmed culture medium. The amount of virus was adjusted according to the titer ranging from 0.25 to 0.50 µl.

2.9 MTT assay

Medium was exchanged with a 5:1 mixture of pre-warmed culture medium and 5 mg/ml MTT (Sigma-Aldrich, M5655) in PBS for a total volume of 120 µl. Following incubation for 3-4 h at 37°C and 5% CO_2, 100 µl solubilizer containing 10% SDS and 45% dimethylformamide, adjusted to pH 4.5 with acetic acid, was added. Crystals were dissolved at 37°C, 5% CO_2 for 4 h to overnight and absorbance measured at 570 nm using a TriStar^2 S LB 942 Multimode Reader (Berthold Technologies).

2.10 Cell lyses for western blotting

Primary neurons were washed with ice-cold $DPBS_{Ca2+Mg2+}$, followed by cell lysis in 100 µl ice-cold lysis buffer containing 50 mM Tris-HCl pH 7.5, 150 mM NaCl, 1% Triton-X 100,

2 mM EDTA, protease inhibitor cocktail (Roche, 04693159001), and phosphatase inhibitor (Roche, 04906837001). Lysates were collected using a cell scraper and centrifuged for 10 min at 4,000 *g*, 4°C. Supernatant was stored at -80°C until use for western blotting.

2.11 Immunocytochemistry

Cells were fixed with 4% paraformaldehyde (PFA) in PBS (ChemCruz, sc-281692) for 20 min. After washing twice with PBS, 50 mM NH_4Cl in PBS was applied for 10 min. Cells were rinsed with PBS and permeabilized with 0.3% Triton X-100 in PBS for 5 min, followed by washing 5 min with PBS. To prevent unspecific antibody binding, cells were incubated in blocking solution containing 0.2% bovine serum albumin (BSA; Carl Roth, 8076), 5% normal donkey serum (NDS; Jackson ImmunoResearch Laboratories, 017-000-121), 0.2% L-lysine hydrochloride, 0.2% glycine, and 0.02% NaN_3 in PBS for 30 min. Primary antibodies (Table 2.4) were applied for 1 h in primary antibody solution (0.3% Triton X-100, 2% BSA, and 0.02% NaN_3 in PBS). Cells were washed for 5 min in PBS and incubated for 30 min in the dark with Alexa Fluor 488, Cyanine Cy3, and/or Alexa Fluor 647-conjugated secondary antibodies derived from donkey (Jackson ImmunoResearch Laboratories) at 1:250 dilution and 0.5 µg/ml DAPI in secondary antibody solution containing 0.3% Triton X-100, 3% NDS, and 0.02% NaN_3 in PBS. Following three 5 min washes with PBS, coverslips were dipped in Milli-Q water and mounted with ProLong Glass Antifade Mountant (Invitrogen, P36984). After curing overnight, slides were stored at 4°C until image acquisition with a Leica TCS SP8 confocal microscope.

Table 2.4 Primary antibodies for immunocytochemistry

Antibody	Reference	Dilution
Goat anti-mCherry	Origene, AB0040-200	1:500
Mouse anti-His	Dianova, DIA-900-100	1:1,000
Chicken anti-EGFP	Invitrogen, A10262	1:1,000
Mouse anti-Flag	Origene, TA50011	1:1,000
Goat anti-Flag	Abcam, ab1257	1:2,000
Rabbit anti-cleaved Caspase-3	Cell Signaling Technology, 9661	1:500

2.12 Mouse lines

All animal experiments were approved by the Government of Upper Bavaria (permit numbers 55.2-1-54-2532-168-14, 55.2-1-54-2532-19-2015, ROB-55.2-2532.Vet_02-20-05, and ROB-55.2-2532.Vet_02-19-083) and conducted in accordance with the German guidelines for animal welfare. Mice were housed in a specific pathogen-free environment with *ad libitum* access to food and water in the animal facilities of the Max Planck Institutes of Biochemistry and Neurobiology. All mouse lines used are detailed in Table 2.5. For maintenance, Hdgf KO, Gad2-IRES-Cre, and Ai9 mice were kept heterozygous on C57BL/6 background. Transgenic R6/2 mice were maintained by breeding hemizygous R6/2 males with the first filial generation (F1) female progeny of a cross between CBA and C57BL/6 mice. To generate HDGF-deficient R6/2 mice, hemizygous R6/2 males were crossed to homozygous Hdgf KO females, followed by mating the F1 offspring R6/2 transgenic males with heterozygous Hdgf KO females.

Table 2.5 Mouse lines

Line	Official name	Origin
C57BL/6	C57BL/6NRj	Janvier Labs
CBA	CBA/JRj	Janvier Labs
CD-1	Crl:CD1(ICR)	Charles River Laboratories
R6/2	B6CBA-Tg(HDexon1)62Gpb/1J	The Jackson Laboratory (Stock No: 002810); Mangiarini *et al.* (1996)
Hdgf KO	B6.129P2-HDGF^{tm1Sefr}	Kindly provided by Søerge Kelm, University of Bremen, Bremen, Germany; Gallitzendoerfer *et al.* (2008)
Gad2-IRES-Cre	STOCK Gad2$^{tm2(cre)Zjh}$/J	The Jackson Laboratory (Stock No: 010802); Taniguchi *et al.* (2011)
Ai9	B6.Cg-Gt(ROSA)26 Sor$^{tm9(CAG-tdTomato)Hze}$/J	The Jackson Laboratory (Stock No: 007909); Madisen *et al.* (2010)

2.13 Genotyping and CAG repeat sizing

For genotyping, DNA was extracted from hair follicles or if indicated from tail or ear biopsies. Mouse hair was incubated with 20 µl Dilution Buffer and 0.5 µl DNARelease Additive (Thermo Scientific, F170S) for 5 min, followed by 2 min at 98°C. Polymerase chain reaction (PCR) mix was prepared with 1 µl DNA extract, 5 µl Platinum II Hot-Start Green PCR Master Mix (Invitrogen, 14001013), and 0.5 µM of each primer in a total volume of 10 µl. Tail or ear punch biopsies were boiled in 100 µl 50 mM NaOH three times for 15 min at 95°C with vortexing in between. 10 µl 1.5 M Tris-HCl pH 8.8 was added and 2 µl DNA extract was used for PCR. Reaction mix of 25 µl (Hdgf KO and Ai9) or 50 µl (Gad2-IRES-Cre and R6/2) in total contained 0.05 units/µl Taq DNA Polymerase with 1x ThermoPol Buffer (New England Biolabs, M0267), 250 µM dNTPs, and 0.25 µM of each primer. Primers (Eurofins Genomics) and PCR programs used are

detailed in Table 2.6 and 2.7, respectively. PCR products were separated by agarose gel electrophoresis. Genotyping was conducted with support from Magdalena Böhm. CAG repeat length was determined from tail or ear punch biopsies by Laragen, Inc. The SEQ CAG No. is reported.

Table 2.6 Genotyping primers and product size

PCR	Reaction	Primer	Sequence (5'→3')	Product (bp)
R6/2	1	Forward	CCG CTC AGG TTC TGC TTT TA	170
		Reverse	TGG AAG GAC TTG AGG GAC TC	
Hdgf KO	1	Forward	GGC TTG TTG GGC TTT TCT ATC	236
		Wild-type reverse	CTT GGT ATT TGT TGG CTG TTG A	
	2	Forward	GGC TTG TTG GGC TTT TCT ATC	517
		Mutant reverse	GTC GTC CTT GAA GAA GAT GGT G	
Gad2-IRES-Cre	1	Forward	GTG GCA GAT GGC GCG GCA ACA CCA TT	726
		Reverse	GCC TGC ATT ACC GGT CGA TGC AAC GA	
Ai9	1	Wild-type forward	AAG GGA GCT GCA GTG GAG TA	297
		Wild-type reverse	CCG AAA ATC TGT GGG AAG TC	
		Mutant forward	GGC ATT AAA GCA GCG TAT CC	196
		Mutant reverse	CTG TTC CTG TAC GGC ATG G	

Table 2.7 Genotyping PCR programs

Tissue	PCR	Step	Temperature	Time	Note
Hair follicles	R6/2, Hdgf KO, Gad2-IRES-Cre, and Ai9	1	94°C	2 min	
		2	94°C	15 sec	Repeat steps 2-4 for 30 cycles
		3	60°C	15 sec	
		4	68°C	15 sec	
		5	12°C	∝	
Tail and ear punch biopsies	R6/2	1	94°C	2 min	
		2	94°C	20 sec	Repeat steps 2-4 for 10 cycles
		3	65°C with -0.5°C/cycle	15 sec	
		4	68°C	30 sec	
		5	94°C	15 sec	Repeat steps 5-7 for 28 cycles
		6	60°C	15 sec	
		7	72°C	30 sec	
		8	72°C	2 min	
		9	12°C	∝	
	Hdgf KO	1	94°C	2 min	
		2	94°C	20 sec	Repeat steps 2-4 for 10 cycles
		3	60°C with -0.5°C/cycle	15 sec	
		4	68°C	1 min	
		5	94°C	15 sec	Repeat steps 5-7 for 28 cycles
		6	55°C	15 sec	
		7	72°C	1 min	
		8	72°C	2 min	
		9	12°C	∝	

Tissue	PCR	Step	Temperature	Time	Note
Tail and ear punch biopsies	Gad2-IRES-Cre	1	92°C	2 min	
		2	92°C	10 sec	Repeat steps 2-4 for 30 cycles
		3	58°C	15 sec	
		4	68°C	1 min	
		5	68°C	5 min	
		6	12°C	∝	
	Ai9	1	94°C	2 min	
		2	94°C	20 sec	Repeat steps 2-4 for 10 cycles
		3	65°C with -0.5°C/cycle	15 sec	
		4	68°C	30 sec	
		5	94°C	15 sec	Repeat steps 5-7 for 28 cycles
		6	60°C	15 sec	
		7	72°C	30 sec	
		8	72°C	2 min	
		9	12°C	∝	

2.14 Viral injections *in vivo*

Viral vectors (Table 2.8) were produced by the Viral Vector Production Unit at Universitat Autònoma de Barcelona.

Table 2.8 Viral vectors for *in vivo* injections

Viral vector	Backbone plasmid (cloning sites)	Promotor	Insert	Titer (gc/ml)
AAV8	pAAV-CAG-WPRE (*Spe*I and *Eco*RI)	CAG	EYFP	$2.40*10^{12}$
			EYFP-P2A-Flag-HDGF	$5.59*10^{12}$

Intracerebroventricular viral injections at postnatal day 0 (P0) were performed similarly as previously described (Kim *et al.*, 2014). In brief, pregnant females were monitored for birth at least every 12 h starting 17 days after the plug date to ensure surgery of newborn pups within 24 h after birth. Anesthesia was induced with 5% isoflurane and maintained at 2% isoflurane using an O_2 flow rate of 1 l/min. Xylocaine 2% Jelly (Aspen, 6077215.00.00) was applied on the prospective injection sites for local anesthetic blockade. Per hemisphere, 2 µl adeno-associated virus (AAV) was stereotactically injected with 15 nl/sec using a microinjection system (Nanoliter 2010, WPI) at (X, Y, Z) = (±0.8, 1.5, -1.5) mm from lambda. Xylocaine 2% Jelly was again applied on injection sites to seal wounds. During surgery and for recovery, neonates were kept on a warming pad. To ensure success of fostering with CD-1 females, fecal pellets from the foster mother were solved in water and rubbed on the back of the injected pups. Neonates were placed in the foster mother's cage as soon as they have recovered and were moving normally. Striatal injections were performed by Sara Gutiérrez-Ángel as described in Gutiérrez-Ángel (2019). Mice were transferred to inverted light cycle after surgery.

2.15 Behavior and life span analysis

All behavioral assessments were conducted during the dark phase of the diurnal cycle. For the open field test, mice were video recorded while exploring a custom-made squared box (40 x 40 x 40 cm) with black walls and white floor for 10 min with lights on. EthoVision XT 14 software (Noldus Information Technology) was used for automated tracking to quantify distance traveled. Rearing activity was manually analyzed by counting the number of rearing bouts. Rotarod analysis was conducted on a RotaRod NG (Ugo Basile). Mice were trained twice on two consecutive days at 5 rpm for 5 min. On the third day, the latency to fall was measured with accelerating speed from 5 to 40 rpm over a 5 min period, and averaged over three trials. Forepaw grip strength was determined using the BIO-GS3 Grip Strength Test (Bioseb) with the BIO-GRIPBS bar for mice (Bioseb) as grasping tool. Measurements were averaged from

three consecutive trials. For survival analysis, endpoint measures were severe burden according to behavior, appearance, and body weight or loss of righting reflex.

2.16 Transcardial perfusion

Mice were anesthetized by intraperitoneal injection of 240 mg/kg body weight (BW) ketamine (MEDISTAR Arzneimittelvertrieb, 13690.00.00) and 12 mg/kg BW xylazine (Serumwerk Bernburg, 3100265.00.00) diluted in isotonic saline (DELTAMEDICA, 1299.99.99). Surgical anesthesia plane was confirmed by absence of palpebral, tail-pinch, and pedal withdrawal reflexes. Thorax was opened and the perfusion cannula inserted through the apex of the left ventricle. The right atrium was cut open right after the start of perfusion. Mice were perfused with ice-cold PBS for 4 min, followed by 4% PFA in PBS for 6 min at 3-3.5 ml/min using a Perimax 12 peristaltic pump (SPETEC). Brains and if indicated spinal cords were extracted and post-fixed overnight in 4% PFA in PBS at 4°C. Until further processing for immunostaining, brains and spinal cords were stored in 0.05% NaN_3 in PBS at 4°C. For fluorescence *in situ* hybridization (FISH) with immunostaining, brains were processed immediately after overnight fixation.

2.17 Immunostaining of free floating sections

To cut spinal cords and sagittal brain sections, tissue was embedded in 4% agarose in PBS. Meninges were carefully removed from spinal cords beforehand. For coronal brain sections, instead of embedding in agarose, the cerebellum was cut off evenly to form a straight base. Serial 70 µm thick sections were cut in PBS with a Leica VT1000 S vibratome and stored in 0.05% NaN_3 in PBS at 4°C.

Sections selected for immunostaining were briefly washed in PBS, followed by permeabilization in 0.5% Triton X-100 in PBS for 15 min with gentle shaking. If indicated, antigen retrieval was performed in 10 mM trisodium citrate pH 6 with 0.05%

Tween 20 at 80°C for 15 min at 300 rpm in an Eppendorf ThermoMixer. To prevent unspecific antibody binding, sections were incubated in blocking solution for 1 h on a shaker. Primary antibodies (Table 2.9) were applied in primary antibody solution overnight at 4°C on a shaker. After three 10 min washes in PBS, sections were incubated for 1 h in the dark with Alexa Fluor 488, Cyanine Cy3, and/or Alexa Fluor 647-conjugated secondary antibodies derived from donkey at 1:250 dilution in secondary antibody solution with gentle shaking. NeuroTrace 640/660 (Invitrogen, N21483) was added at 1:500 dilution to the secondary antibody solution if indicated. Sections were washed three times for 10 min in PBS with DAPI added in the middle washing step at a concentration of 0.5 µg/ml. ProLong Glass Antifade Mountant was used for mounting. After curing overnight, mounted sections were stored at 4°C until image acquisition with a Leica TCS SP8 confocal microscope.

Table 2.9 Primary antibodies for immunostaining of mouse tissue

Antibody	Reference	Dilution
Rabbit anti-HDGF	Abcam, ab128921	1:500
Mouse anti-HTT (EM48)	Chemicon, MAB5374	1:500
Mouse anti-Flag	Origene, TA50011	1:1,000
Goat anti-ChAT	Chemicon, AB144	1:500
Goat anti-DARPP32	LifeSpan Biosciences, LS-C150127	1:300
Mouse anti-NGRN	R&D Systems, MAB7947	1:60
Chicken anti-GFAP [1]	Origene, AP31806PU-N	1:2,000
Mouse anti-APC [1]	Calbiochem, OP80	1:20
Goat anti-IBA1 [1]	Abcam, ab107159	1:1,000

[1] With antigen retrieval

2.18 Fluorescence *in situ* hybridization with immunostaining

After a brief wash in DPBS, perfused brains were immersed in 15% sucrose in DPBS, followed by 30% sucrose in DPBS, at 4°C with gentle shaking until tissue has sunk. Cryopreserved brains were frozen in Tissue-Tek O.C.T. Compound (Sakura Finetek, 4583) and stored at -80°C. Coronal 10 µm thick brain sections were obtained at -20 °C using a Leica CM3050 S cryostat and stored at -80°C on SuperFrost Plus Slides (Epredia, J1800AMNZ).

For FISH, RNAscope Fluorescent Multiplex Assay (ACD, 320850, 322000, and 322340) was conducted according to the manufacturer's instructions (ACD, 320293-USM and 320535-TN) with RNAscope Probe against *Hdgf* (ACD, 524601). Immunostaining against HDGF protein was performed prior to counterstaining with DAPI similar as immunostaining of free floating sections. Briefly, brain slices were incubated in blocking solution for 2 h, followed by overnight incubation with rabbit anti-HDGF antibody (Table 2.9) in primary antibody solution at 4°C. After washing four times for 5 min with RNAscope 1x Wash Buffer, Alexa Fluor 488-conjugated secondary antibody raised in donkey was applied at 1:250 dilution in secondary antibody solution for 2 h. Sections were washed four times for 5 min with RNAscope 1x Wash Buffer, counterstained with RNAscope DAPI and mounted with ProLong Glass Antifade Mountant. After curing overnight, mounted sections were stored at 4°C until image acquisition with a Leica TCS SP8 confocal microscope.

2.19 Brain dissection and preparation of tissue lysates

Mice were sacrificed by cervical dislocation under isoflurane anesthesia. Brains were extracted, washed in ice-cold PBS, and dissected on ice. Cerebella, hippocampi, cortices, and striata were snap frozen in liquid nitrogen and stored at -80°C.

To obtain tissue lysates, dissected brain regions were thawed on ice and homogenized in ice-cold lysis buffer. After incubation on ice for at least 30 min,

homogenates were centrifuged at 15,000 *g* for 15 min at 4°C. Supernatants were further processed for western blotting or stored at -80°C until use. Protein concentrations were determined with DC Protein Assay Kit (Bio-Rad, 5000112) following the manufacturer's instructions using the TriStar^2 S LB 942 Multimode Reader to measure absorbance.

2.20 Western blotting

Samples were boiled at 95°C for 5 min with Laemmli sample buffer (Bio-Rad, 1610747) containing 2-mercaptoethanol as reducing agent. Per lane, 25 µl cell lysate and 50 µg protein for tissue lysates was loaded on 4-15% (Bio-Rad, 5678084) and 10% TGX Stain-Free Protein Gels (Bio-Rad, 4568034 and 5678034), respectively. Proteins were separated along with 5 µl Precision Plus Protein All Blue Prestained Protein Standards (Bio-Rad, 1610373) at 80-120 V in SDS-PAGE running buffer containing 25 mM Tris, 192 mM glycine, and 0.1% SDS. After electrophoretic separation, stain-free gels were activated using the ChemiDoc MP Imaging System (Bio-Rad, 17001402). Transfer onto low fluorescence polyvinylidene fluoride membranes (Bio-Rad, 1620264) was conducted at 2.5 A, up to 25 V for 10 min with the Trans-Blot Turbo Transfer System (Bio-Rad, 1704150) according to the manufacturer's instructions for using traditional semi-dry consumables. Once protein transfer was complete, the stain-free blot image was acquired using the ChemiDoc MP imager. Membranes were then blocked for 1 h with 3% BSA and 5% powdered milk (Carl Roth, T145) in Tris-buffered saline (TBS; 20 mM Tris-HCl pH 8, 150 mM NaCl) with 0.1% Tween 20 (TBS-T). Blocking and all following incubation procedures were conducted with gentle shaking. After rinsing twice and washing for 5 min in TBS-T, primary antibodies (Table 2.10) were applied overnight at 1:1,000 dilution in 3% BSA and 0.01% NaN_3 in TBS-T at 4°C. The next day, membranes were rinsed twice and washed three times for 10 min in TBS-T. Rhodamine-conjugated anti-tubulin antibody (Bio-Rad, 12004166) and StarBright Blue 520/700 secondary antibodies (Bio-Rad) were applied at 1:2,500 dilution in TBS for 1 h,

followed by rinsing twice and washing three times for 10 min in TBS-T. Blot image was acquired using the ChemiDoc MP imager.

Table 2.10 Primary antibodies for western blotting

Antibody	Reference
Rabbit anti-HDGF	Abcam, ab244498
Mouse anti-AKT	Cell Signaling Technology, 2920
Rabbit anti-p-AKT	Cell Signaling Technology, 4060
Rabbit anti-ERK	Cell Signaling Technology, 9102
Mouse anti-p-ERK	Cell Signaling Technology, 9106

2.21 Immunohistochemistry on human brain sections

Formalin-fixed paraffin-embedded tissue sections of 5 µm thickness from the primary motor cortex of three HD autopsy cases and three age-matched controls were provided by the Neurobiobank Munich, Ludwig-Maximilians-Universität München (LMU), Munich, Germany. Informed consent was available for all cases and usage of the material for this project was approved by the ethics committee of the Max Planck Society. The experiments were performed in accordance with the relevant guidelines and regulations.

Immunohistochemistry was performed on a VENTATA BenchMark ULTRA (Roche) by Michael Schmidt, Center for Neuropathology, LMU, Munich, Germany. In brief, after standard pretreatment in CC1 buffer (Roche), sections were incubated with rabbit anti-HDGF antibody (Abcam, ab244498) at a dilution of 1:100 for 32 min. The UltraView Universal DAB Detection Kit (Roche) was used for detection and counterstaining was performed with hematoxylin for 4 min. Images were acquired with a Leica THUNDER imager.

2.22 Data analysis and statistics

Images were analyzed and/or processed with the open-source image analysis software Fiji (Schindelin *et al.*, 2012). Western blot images were quantified with Image Lab version 6.0.1, build 34 software (Bio-Rad). GraphPad Prism 9.2.0 (GraphPad Software) was used for graphical representation and statistical analysis. Statistics are detailed in the figure legends. Differences were considered statistically significant with $P < 0.05$.

3 RESULTS

3.1 HDGF rescues mHTT toxicity in primary neurons

To investigate whether HDGF is neuroprotective in the context of HD, we first evaluated the impact of HDGF overexpression on cell viability and aggregate formation in mHTT-transfected primary cortical neurons. Cell death was assessed by immunostaining for active caspase-3, an apoptosis marker, and by nuclear staining with DAPI to visualize changes in nuclear morphology. Caspase-3 activation precedes nuclear fragmentation, enabling detection of early apoptotic cells, while nuclear labeling with DAPI ensured inclusion of cell corpses lacking an active caspase-3 signal. Only neurons with intact nuclear morphology and absent active caspase-3 immunoreactivity were categorized as viable (Figure 3.1 A, bottom row). As expected, expression of pathological HTTQ97-mCherry, but not HTTQ25-mCherry or mCherry control, significantly reduced viability. Remarkably, HDGF co-expression resulted in full rescue of neuronal survival (Figure 3.1 B). Moreover, the frequency of mHTT inclusions was markedly reduced for HDGF-transfected neurons compared to EGFP control (Figure 3.1 C). Together, these data show that HDGF counteracts mHTT-induced cell death and mHTT aggregation in primary neurons.

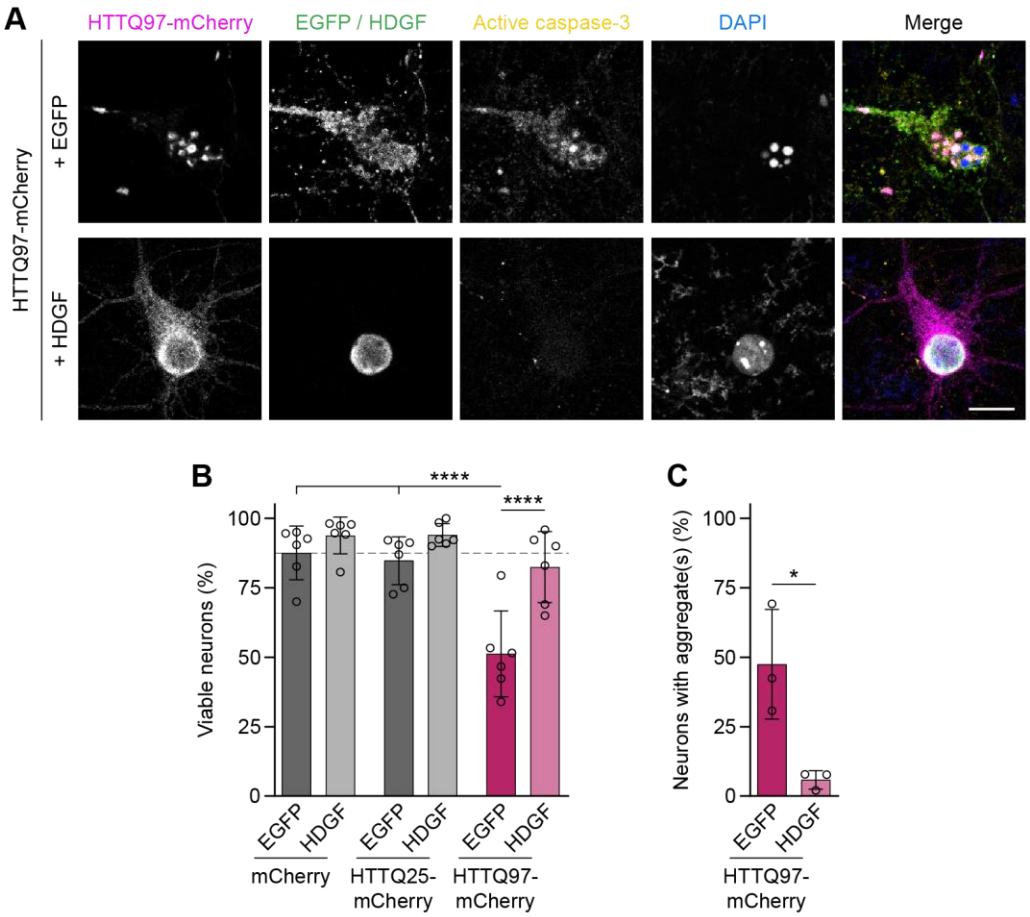

Figure 3.1 HDGF rescues mHTT toxicity in primary neurons

Cortical neurons were co-transfected with the indicated constructs at DIV 7 and fixed 2 days later. HDGF-transfected cells were identified by immunostaining against Flag-tag. Viability was assessed by immunostaining for active caspase-3 and nuclear labeling with DAPI.

A. Example of an apoptotic EGFP-transfected cell with mHTT aggregates (top) and a living neuron transfected with HDGF (bottom). Cells negative for active caspase-3 with intact nuclear morphology were categorized as viable.

B. Quantification of the fraction of viable neurons. N = 6 biological replicates, with N = 3 biological replicates contributed by Sara Gutiérrez-Ángel. Two-way ANOVA with Bonferroni's multiple comparisons test. ANOVA: HTT, **** $P < 0.0001$; HDGF, **** $P < 0.0001$; HTT x HDGF, * $P < 0.0107$. Significant pairwise multiple comparisons are indicated on the graph.

C. Quantification of the fraction of neurons with mHTT aggregates. N = 3 biological replicates. Unpaired two-tailed *t*-test.

Data information: Columns with error bars represent mean ± standard deviation. Significance: * $P < 0.05$, **** $P < 0.0001$. Scale bar in A, 10 µm.

3.2 HDGF expression levels correlate with neuronal resistance to HD

To start addressing the role of HDGF *in vivo*, we analyzed HDGF expression in the central nervous system (CNS) of wild-type (WT) mice. While previous studies have shown that HDGF is expressed in neurons and glial cells in mouse and human brain (Abouzied *et al.*, 2004; Zhou *et al.*, 2004; El-Tahir *et al.*, 2006; Uhlén *et al.*, 2015) (Human Protein Atlas available from http://www.proteinatlas.org), a more detailed quantitative analysis comparing protein expression levels in different cell types and brain regions is still missing.

We first confirmed widespread expression of HDGF in the CNS of adult mice by immunostaining, including expression in striatum and cerebral cortex (Figure 3.2). Except for some neurons in the spinal cord, where HDGF was cytoplasmic (Figure 3.2 B, white arrows), protein localization was confined to the nucleus. Of note, expression levels seemed to differ between cells (Figure 3.2 C, yellow arrows and arrowheads).

Since HDGF can be secreted (Nakamura *et al.*, 1994; Oliver and Al-Awqati, 1998; Zhou *et al.*, 2004; Ooi *et al.*, 2010; Ojima *et al.*, 2014), we asked whether some cells positive for HDGF protein exclusively take it up from the extracellular space instead of expressing the protein endogenously. We therefore combined HDGF staining with FISH. Antibody and probe specificity was confirmed by the absence of signal in *Hdgf* knockout tissue (Figure 3.3 A, bottom row). In line with a scenario, where HDGF is endogenously expressed by cells containing HDGF protein in the brain, we detected *Hdgf* mRNA in nearly all cells positive for HDGF protein in striatum and cortex (Figure 3.3).

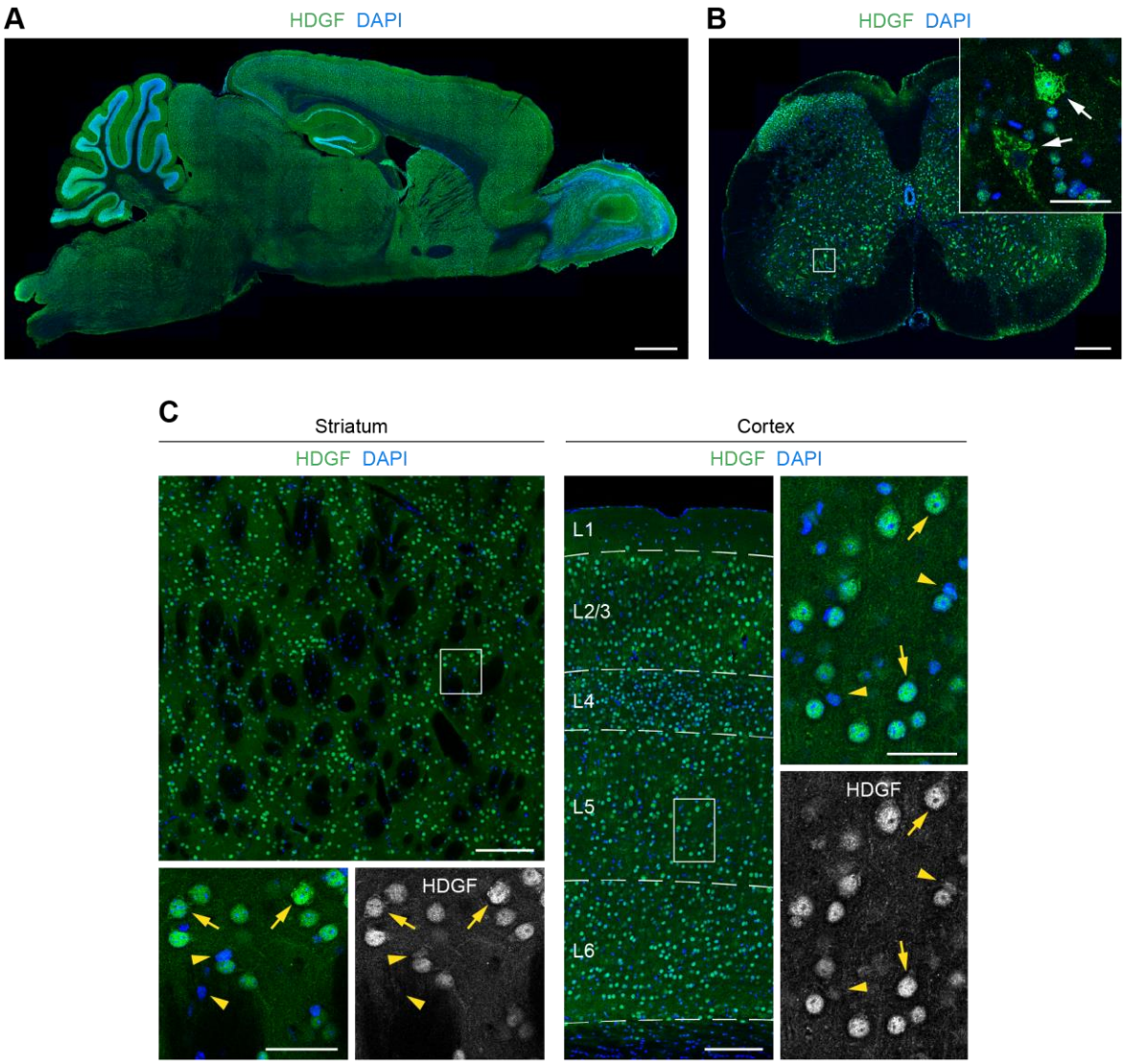

Figure 3.2 HDGF is expressed throughout the CNS

Brain and spinal cord sections from adult WT mice were immunostained against HDGF. Nuclei were counterstained with DAPI.

A, B. Overview images of a sagittal brain (A) and transverse lumbar spinal cord (B) section. In B, inset shows higher magnification of the boxed area. Examples of cells with cytoplasmic HDGF are marked by white arrows. Images representative for N = 4 12-week-old WT female mice.

C. Representative images of the dorsal striatum and cerebral cortex. Cortical layers are indicated and marked with dashed lines. Magnifications of the boxed areas are shown next to the overview images. Yellow arrows point towards cells with high levels of HDGF, whereas yellow arrowheads indicate cells with low levels of HDGF. Similar results were obtained from N = 4 (3 ♀, 1 ♂) 8-week-old WT mice.

Data information: Scale bars in A, 1 mm; B, 200 µm; C, 150 µm; magnifications in B and C, 40 µm.

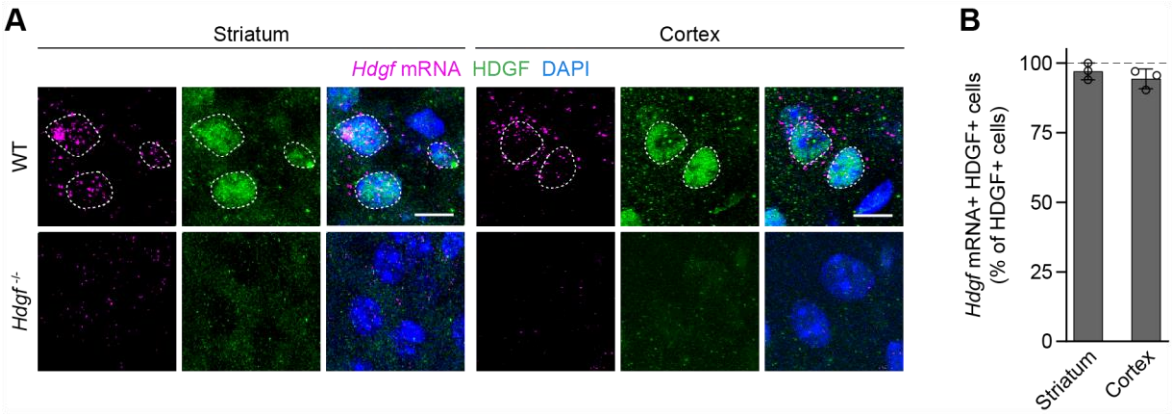

Figure 3.3 HDGF is endogenously expressed in mouse striatum and cortex

In brain sections, FISH was combined with HDGF immunostaining to label *Hdgf* mRNA and HDGF protein, respectively. N = 3 (2 ♀, 1 ♂) WT and 3 (1 ♀, 2 ♂) *Hdgf* $^{-/-}$ mice at 8 weeks of age.

A. Representative images of cells in striatum and cortex of WT and *Hdgf* $^{-/-}$ mice. Nuclei positive for HDGF protein are marked with dashed lines.

B. Quantification of the fraction of HDGF-immunopositive cells containing *Hdgf* mRNA in WT brain. Two-tailed one-sample *t*-test, not significant.

Data information: Columns with error bars represent mean ± standard deviation. Scale bars in A, 10 µm.

With support from Sophie Keeling in brain cutting, FISH with immunostaining, image acquisition, and image quantification.

To investigate differential expression between cell types, we combined HDGF staining with immunolabeling and genetic labeling of various neuronal and glial markers. For reliable quantification of cell type-specific HDGF expression by fluorescence intensity, background-subtracted values were normalized to the fluorescence intensity of the highest expressing cell in the field of view. We observed clearly higher HDGF levels in neurons compared to glial cells (Figure 3.4 A, B). Lowest HDGF expression was detected in microglia followed by oligodendrocytes and astrocytes (Figure 3.4 A, C). Interestingly, in neurons, HDGF expression levels were higher in cell types with a higher resistance to HD. In the striatum, cholinergic interneurons (CINs) had higher levels of HDGF compared to MSNs. Similarly, in the cortex, HDGF expression was higher in interneurons (INs) compared to PCs (Figure 3.4 A, C). While striatal CINs and cortical INs are relatively spared, striatal MSNs and cortical PCs are the cell types most susceptible to HD (Han *et al.*, 2010).

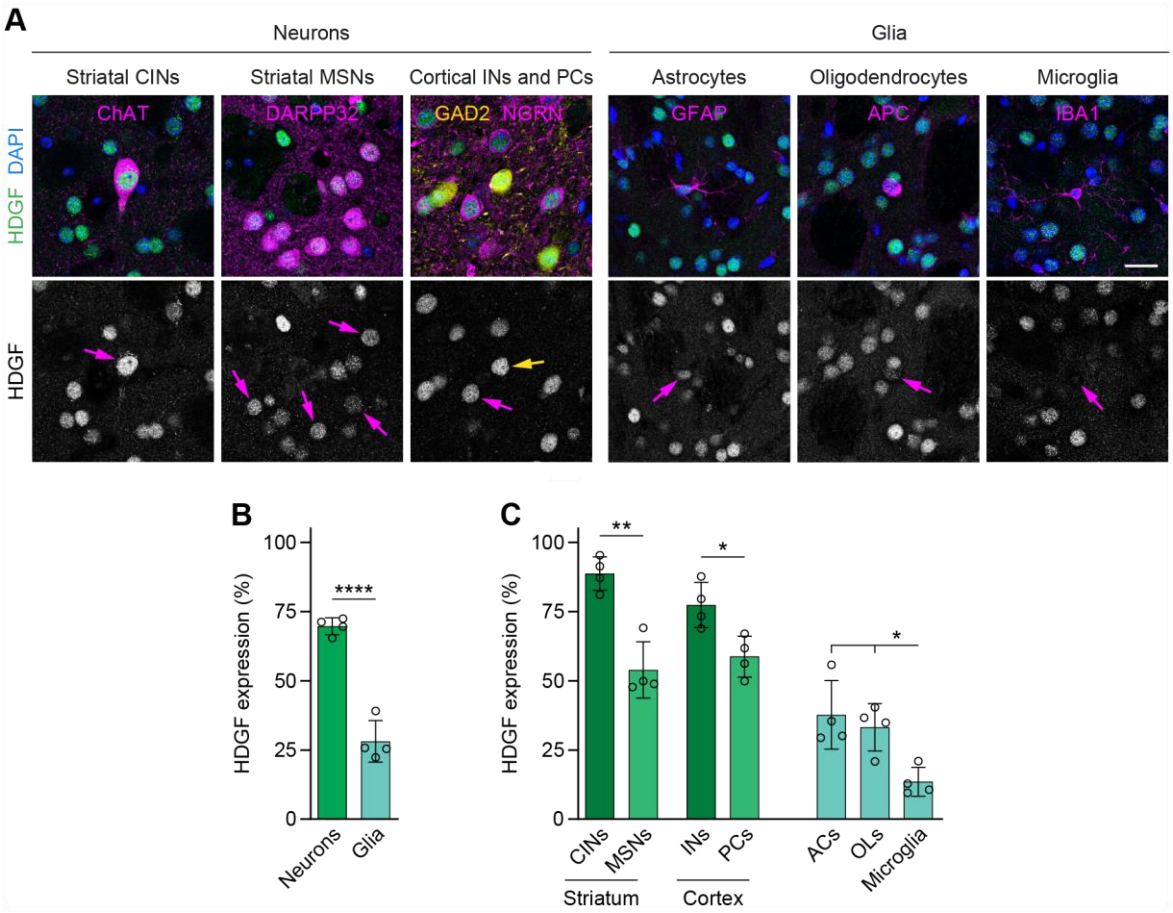

Figure 3.4 HDGF is differentially expressed in neuronal and glial cell types

Brain sections from 8-week-old mice were immunostained against HDGF. Neuronal and glial cell types in striatum and cortex were identified by co-staining (magenta) or genetic labeling (yellow, Cre-dependent tdTomato expression) of indicated cell markers. Cortical INs and PCs were identified by glutamate decarboxylase 2 (GAD2) and neurogranin (NGRN) expression, respectively. Nuclei were counterstained with DAPI. N = 4 (3 ♀, 1 ♂) heterozygous Gad2-IRES-Cre; Ai9 mice.

A. Representative images of HDGF immunostaining in striatal and cortical neurons as well as glial cells. Arrows point to nuclei of the respective cell types.

B. Quantification of HDGF staining fluorescence intensity in all examined neurons and glia. Unpaired two-tailed *t*-test.

C. Quantification of HDGF staining fluorescence intensity separated by neuronal (green) and glial (turquoise) cell types. Neuronal populations with a higher resistance to HD (dark green) and neuronal cell types most susceptible to HD (light green) were included in analysis. Glial HDGF expression was averaged for striatal and cortical cells. Neurons: Unpaired two-tailed *t*-test, per brain region. Glia: One-way ANOVA with Tukey's multiple comparisons test. ANOVA: * P = 0.0107. Significant pairwise multiple comparisons are indicated on the graph. ACs, astrocytes; OLs, oligodendrocytes.

Data information: Columns with error bars represent mean ± standard deviation. Significance: * $P < 0.05$, ** $P < 0.01$, **** $P < 0.0001$. Scale bar in A, 20 µm.

With support from Maximilian Gantz, Florian Leiß-Maier, and Sophie Keeling in brain cutting, immunostaining, image acquisition, and image quantification.

We then quantified HDGF levels in brain regions with differential vulnerability to HD by western blot analysis. Highest HDGF levels were detected in the cerebellum of 8 and 12-week-old WT mice, while significantly less HDGF was found in hippocampus, cortex and striatum (Figure 3.5), brain regions with more pronounced pathology in disease (Vonsattel and DiFiglia, 1998; Rosas *et al.*, 2008; Cepeda-Prado *et al.*, 2012). Collectively, these findings indicate that low HDGF amounts correlate with increased neuronal vulnerability to HD.

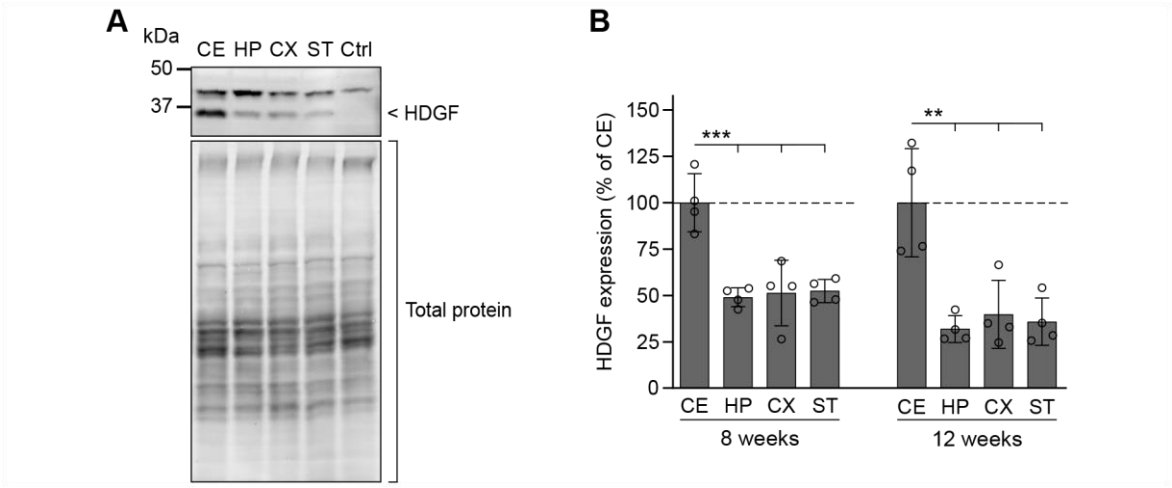

Figure 3.5 HDGF is differentially expressed in different brain regions

HDGF protein levels were measured in cerebellum (CE), hippocampus (HP), cortex (CX), and striatum (ST) of 8 and 12-week-old WT mice by western blot analysis. Total protein, determined using stain-free technology, was used as loading control. N = 4 (3 ♀, 1 ♂) 8-week-old and 4 (2 ♀, 2 ♂) 12-week-old WT mice.

A. Representative western blot of indicated brain lysates collected at 12 weeks of age. The lower molecular weight band at ~37 kDa was specific to HDGF as confirmed by the absence of signal in control brain lysates from *Hdgf* $^{-/-}$ mice (Ctrl).

B. HDGF protein quantity normalized to total protein and to cerebellar lysates mean for the indicated ages. One-way ANOVA with Tukey's multiple comparisons test, per age. ANOVA: 8 weeks, *** $P = 0.0002$; 12 weeks, *** $P = 0.0007$. Significant pairwise multiple comparisons are indicated on the graph.

Data information: Columns with error bars represent mean ± standard deviation. Significance: ** $P < 0.01$, *** $P < 0.001$.

With support from Nicole Martin in tissue homogenization, determination of protein concentration, western blotting, and image quantification.

3.3 HDGF expression is not altered in HD

We next asked whether HDGF expression is dysregulated in HD. Western blot analysis revealed no changes in HDGF levels in R6/2 mice, neither at 8 weeks of age, before the mice display overt symptoms, nor at 12 weeks of age, an advanced disease stage (Figure 3.6). To explore the possibility of alterations in cellular localization or cell type-specific expression of HDGF in neurons susceptible to HD, immunostaining was performed in 12-week-old R6/2 and control brain sections. However, expression pattern and cell type-specific HDGF expression in striatal MSNs and in cortical PCs was unaltered (Figure 3.7).

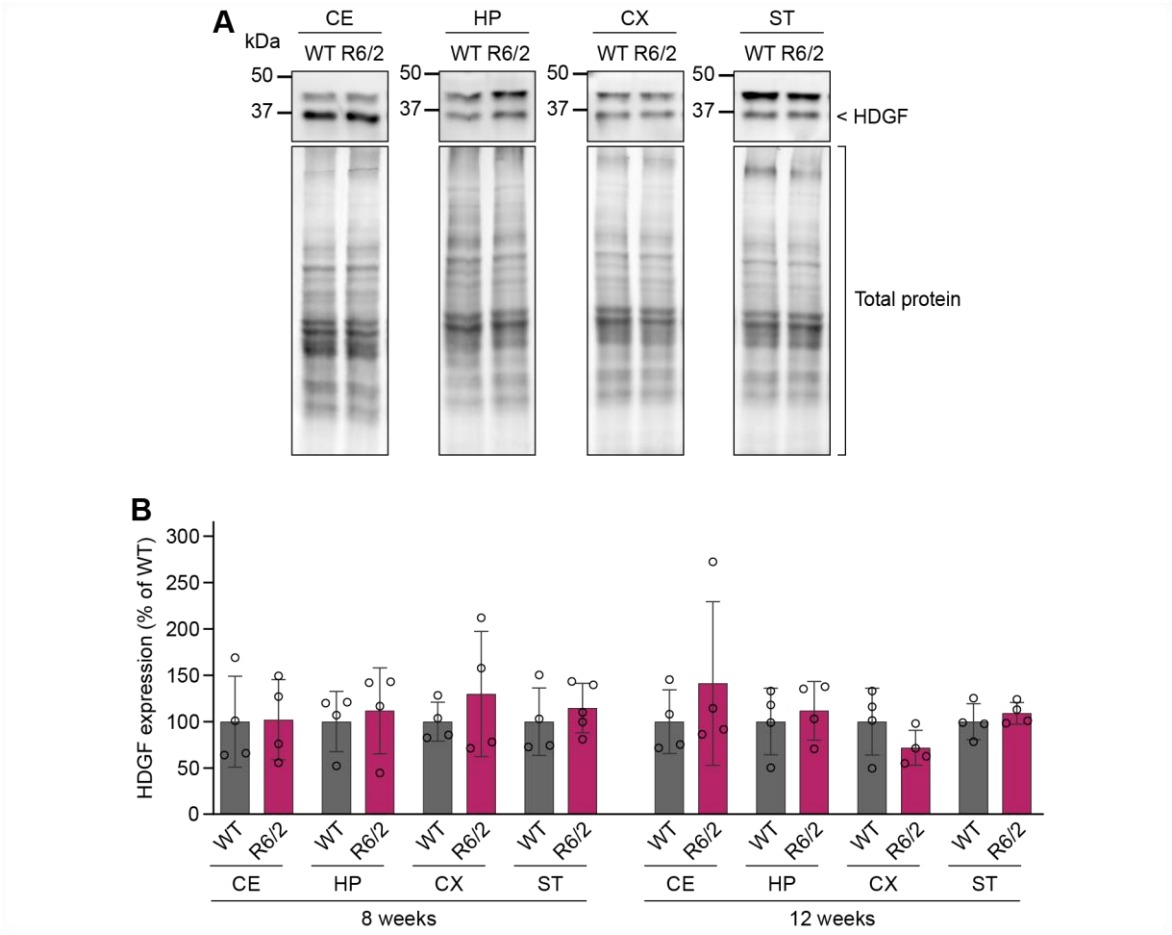

Figure 3.6 HDGF expression levels are maintained in R6/2 mouse brain

HDGF protein levels were measured in cerebellum (CE), hippocampus (HP), cortex (CX), and striatum (ST) of 8 and 12-week-old R6/2 and WT mice by western blot analysis. Total protein, determined using stain-free technology, was used as loading control. N = 4-5 (WT: 3 ♀, 1 ♂; R6/2: 3-4 ♀, 1 ♂) 8-week-old and 4 (WT: 2 ♀, 2 ♂; R6/2: 3 ♀, 1 ♂) 12-week-old mice.

A. Representative western blots of indicated brain lysates collected at 8 weeks of age. HDGF was specifically detected at ~37 kDa (lower molecular weight band).

B. HDGF protein quantity normalized to total protein and to the corresponding WT mean. Unpaired two-tailed *t*-test, per brain region and age, not significant.

Data information: Columns with error bars represent mean ± standard deviation.

With support from Nicole Martin in tissue homogenization, determination of protein concentration, western blotting, and image quantification.

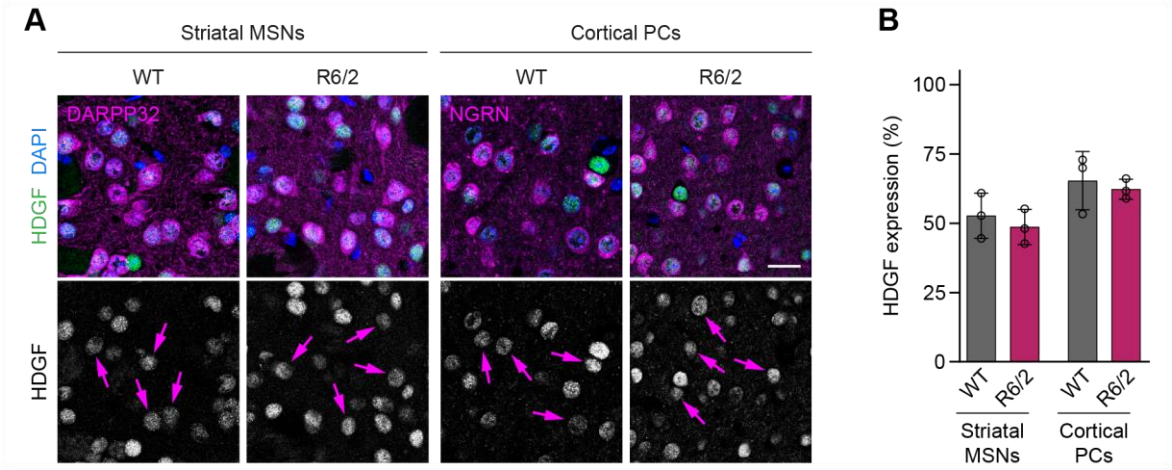

Figure 3.7 Cell type-specific HDGF expression is maintained in R6/2 mouse brain

Brain sections from 12-week-old R6/2 mice and WT controls were immunostained against HDGF. Striatal MSNs and cortical PCs were identified by co-staining of indicated cell markers (magenta). Nuclei were counterstained with DAPI. N = 3 female mice.

A. Representative images of HDGF immunostaining in striatal MSNs and cortical PCs. Arrows point to nuclei of the respective cell types.

B. Quantification of HDGF staining fluorescence intensity. Unpaired two-tailed *t*-test, per cell type, not significant.

Data information: Columns with error bars represent mean ± standard deviation. Scale bar in A, 20 µm.

With support from Florian Leiß-Maier and Maximilian Gantz in brain cutting, immunostaining, image acquisition, and image quantification.

In line with these results, we found HDGF expressed in the motor cortex of human control brains and HD cases with a similar expression pattern (Figure 3.8). Interestingly, in human brain HDGF is cytoplasmic in cortical neurons with a rather weak signal compared to glial cells, where HDGF is localized to the nucleus and its signal intensity is higher (Figure 3.8, arrowheads and arrows for neurons and glia, respectively). Overall, our findings suggest that HDGF expression is not altered in HD. However, whether the mechanism of action and downstream pathways of HDGF are maintained in HD remains to be elucidated.

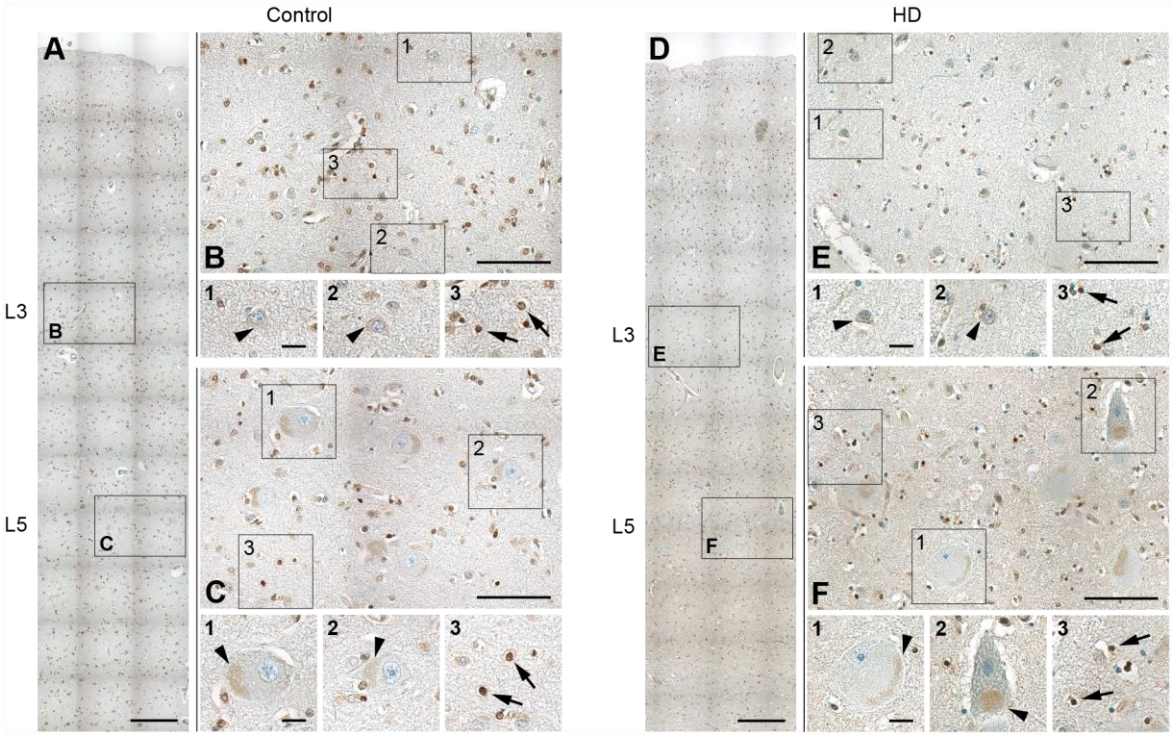

Figure 3.8 HDGF expression is maintained in human HD brain

Brain sections from primary motor cortex of human HD autopsy cases and controls were immunostained against HDGF (brown). Nuclei were counterstained with hematoxylin (blue). Similar results were obtained from N = 3 cases and 3 controls.

A, D. Representative images of control (A) and HD (D) primary motor cortex. Pyramidal cell layers (L3, L5) are indicated on the left.

B, C, E, F. Magnifications of the areas in cortical layer 3 (B, E) and layer 5 (C, F) indicated by boxes in A and D. Higher magnifications of boxed areas with representative neurons (1, 2) and glial cells (3) are shown below. Arrowheads point to cytoplasmic HDGF in neurons, whereas arrows indicate nuclear HDGF in glial cells.

Data information: Scale bars in A, D, 250 µm; B, C, E, F, 100 µm; magnifications 1-3, 20 µm.

With support from Neurobiobank Munich, Thomas Arzberger and Michael Schmidt (Center for Neuropathology, LMU, Munich) in providing tissue and conducting immunostaining.

3.4 Deletion of endogenous HDGF worsens HD phenotypes *in vivo*

To study the neuroprotective potential of endogenous HDGF *in vivo*, we crossed the R6/2 line to *Hdgf* knockout mice (Gallitzendoerfer *et al.*, 2008). Behavioral tests were conducted at 5, 8, and 12 weeks of age with R6/2 mice and non-transgenic littermates with and without HDGF deficiency. Apart from a decrease in rearing activity detected at 6 months of age, *Hdgf* $^{-/-}$ mice have been reported to be phenotypically normal without motor abnormalities or other significant alterations in exploratory behavior (Gallitzendoerfer *et al.*, 2008). Contrary to Gallitzendoerfer *et al.* (2008), we observed a mild hyperactivity of HDGF-deficient mice in the open field test. Both distance traveled and rearing frequency were increased compared to WT controls. Remarkably, H*dgf* $^{-/-}$; R6/2 mice did not show a hyperactive phenotype (Figure 3.9 A, B). On the rotating rod, HDGF deficiency worsened the performance of R6/2 mice. We detected a clearly reduced latency to fall for H*dgf* $^{-/-}$; R6/2 mice compared to R6/2 littermates at 8 weeks of age (Figure 3.9 C), pointing towards an accelerated decline in motor function. Forepaw grip strength, as a measure of muscle strength, was unaffected by HDGF deficiency (Figure 3.9 D).

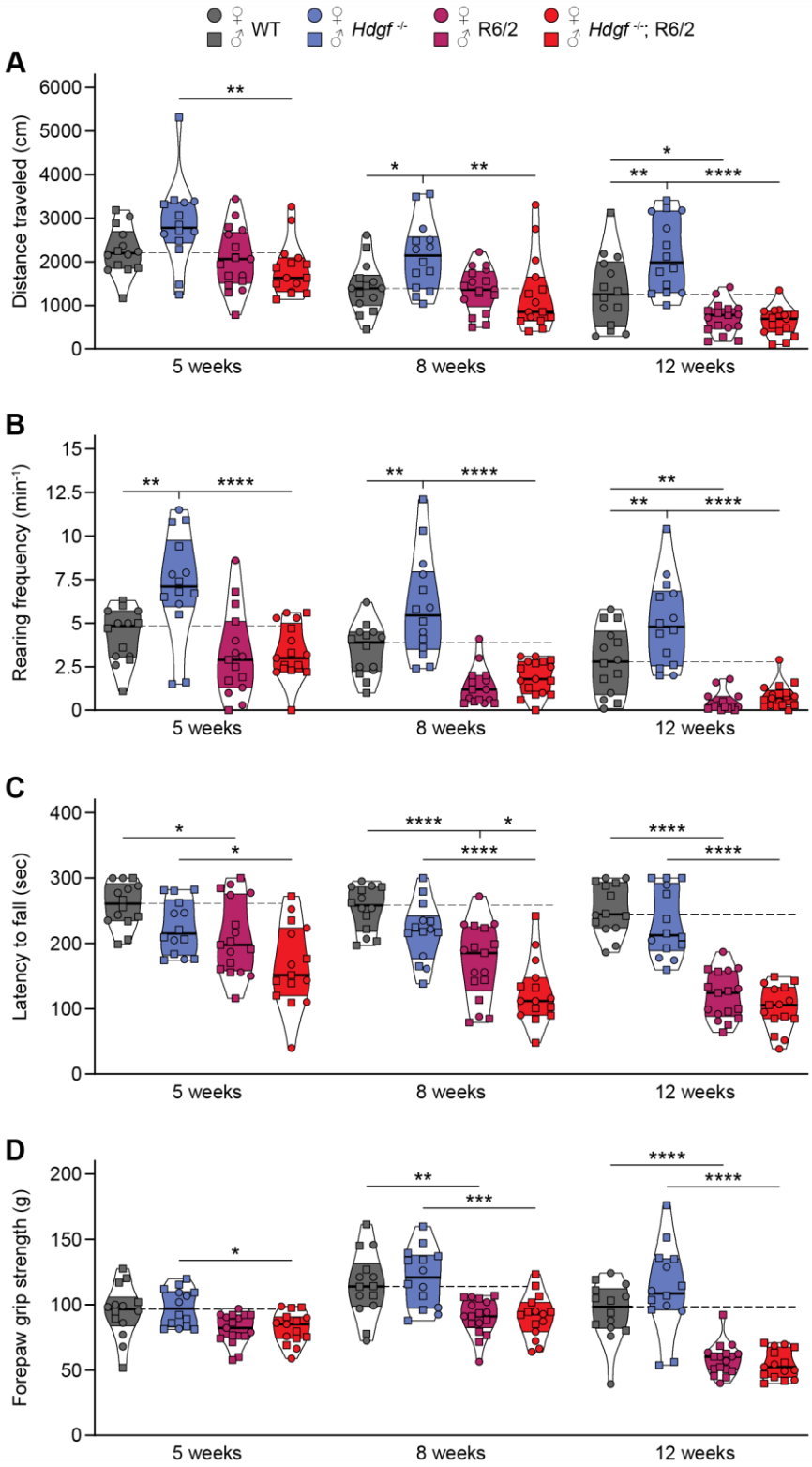

Figure 3.9 **HDGF deficiency causes hyperactivity, and exacerbates motor defects in R6/2 mice**

Behavior of R6/2 and non-transgenic littermates with and without HDGF deficiency was analyzed in the same cohorts of mice at 5, 8, and 12 weeks of age. N = 14 (7 ♀, 7 ♂) WT mice, 14 (4 ♀, 10 ♂) *Hdgf* $^{-/-}$ mice, 17 (7 ♀, 10 ♂) R6/2 mice, and 15 (7 ♀, 8 ♂) *Hdgf* $^{-/-}$; R6/2 mice.

A. Distance traveled in the open field test. Repeated measures three-way ANOVA with Bonferroni's multiple comparisons test per age group. ANOVA: Age, **** $P < 0.0001$; HTT, **** $P < 0.0001$; HDGF, $P = 0.0560$; Age x HTT, *** $P = 0.0008$; Age x HDGF, $P = 0.5773$; HTT x HDGF, ** $P = 0.0054$; Age x HTT x HDGF, $P = 0.9482$. Significant pairwise multiple comparisons are indicated on the graph.

B. Rearing frequency in the open field test. Repeated measures three-way ANOVA with Bonferroni's multiple comparisons test per age group. ANOVA: Age, **** $P < 0.0001$; HTT, **** $P < 0.0001$; HDGF, * $P = 0.0115$; Age x HTT, $P = 0.1218$; Age x HDGF, $P = 0.4487$; HTT x HDGF, ** $P = 0.0013$; Age x HTT x HDGF, $P = 0.8055$. Significant pairwise multiple comparisons are indicated on the graph.

C. Latency to fall off the accelerating rotarod. Repeated measures three-way ANOVA with Bonferroni's multiple comparisons test per age group. ANOVA: Age, **** $P < 0.0001$; HTT, **** $P < 0.0001$; HDGF, ** $P = 0.0017$; Age x HTT, **** $P < 0.0001$; Age x HDGF, $P = 0.1624$; HTT x HDGF, $P = 0.7995$; Age x HTT x HDGF, $P = 0.8124$. Significant pairwise multiple comparisons are indicated on the graph.

D. Forepaw grip strength. Repeated measures three-way ANOVA with Bonferroni's multiple comparisons test per age group. ANOVA: Age, **** $P < 0.0001$; HTT, **** $P < 0.0001$; HDGF, $P = 0.2832$; Age x HTT, **** $P < 0.0001$; Age x HDGF, $P = 0.7028$; HTT x HDGF, $P = 0.2008$; Age x HTT x HDGF, $P = 0.2316$. Significant pairwise multiple comparisons are indicated on the graph.

Data information: Violin plots with thick black line and colored area representing median and interquartile range, respectively. Significance: * $P < 0.05$, ** $P < 0.01$, *** $P < 0.001$, **** $P < 0.0001$.

In addition to behavior, life span of R6/2 mice was analyzed. Strikingly, we found a significant reduction in survival by 6 days on average for the HDGF-deficient cohort (Figure 3.10 A). By CAG repeat sizing, we excluded the possibility that observed phenotypic alterations were due to differences in CAG tract length. A similar number of CAG repeats was confirmed for *Hdgf* $^{-/-}$; R6/2 and R6/2 mice (Figure 3.10 B). Taken together, these experiments demonstrate that deletion of endogenous HDGF exacerbates motor defects and shortens life span in R6/2 mice, consistent with a neuroprotective role of HDGF in disease.

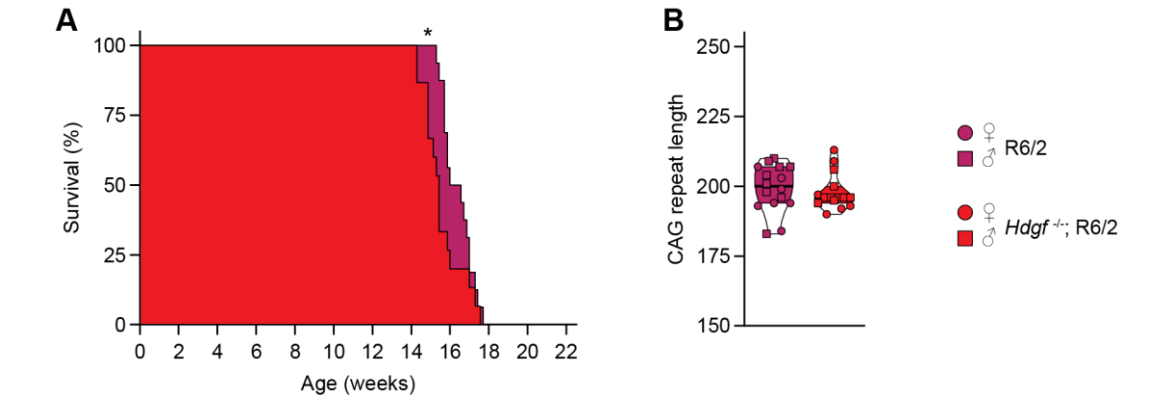

Figure 3.10 HDGF deficiency reduces life span of R6/2 mice

Life span of HDGF-deficient R6/2 mice and R6/2 littermates was determined. N = 16 (7 ♀, 9 ♂) R6/2 mice and 15 (7 ♀, 8 ♂) *Hdgf* $^{-/-}$; R6/2 mice.

A. Kaplan-Meier survival curves. Unpaired two-tailed *t*-test.

B. CAG repeat tract length. Unpaired two-tailed *t*-test, not significant.

Data information: B: Violin plot with thick black line and colored area representing median and interquartile range, respectively. Significance: * $P < 0.05$.

3.5 HDGF overexpression ameliorates HD phenotypes *in vivo*

We next asked whether increasing neuronal HDGF levels *in vivo* has a therapeutic effect leading to an improvement of R6/2 phenotypes. Since R6/2 mice display early-onset and widespread pathology, AAV8-EYFP-P2A-Flag-HDGF or AAV8-EYFP control (from here on referred to as HDGF and EYFP, respectively) was injected into the lateral ventricles of newborn mice for early treatment with brain-wide delivery (Kim *et al.*, 2014). We confirmed Flag-HDGF expression by immunostaining in 3-week-old WT mice (Figure 3.11 A, B), an age when HTT aggregates begin to form in R6/2 mice (Morton *et al.*, 2000; Landles *et al.*, 2020; Kumar *et al.*, 2021). Expression was stable beyond the lifespan of R6/2 mice, with high HDGF levels in hippocampus and cortex (Figure 3.11). Of note, striatal transduction efficiency was generally rather low and

varied between mice ranging from no or very sparse expression to a denser, but locally restricted expression (Figure 3.11 A, B, D).

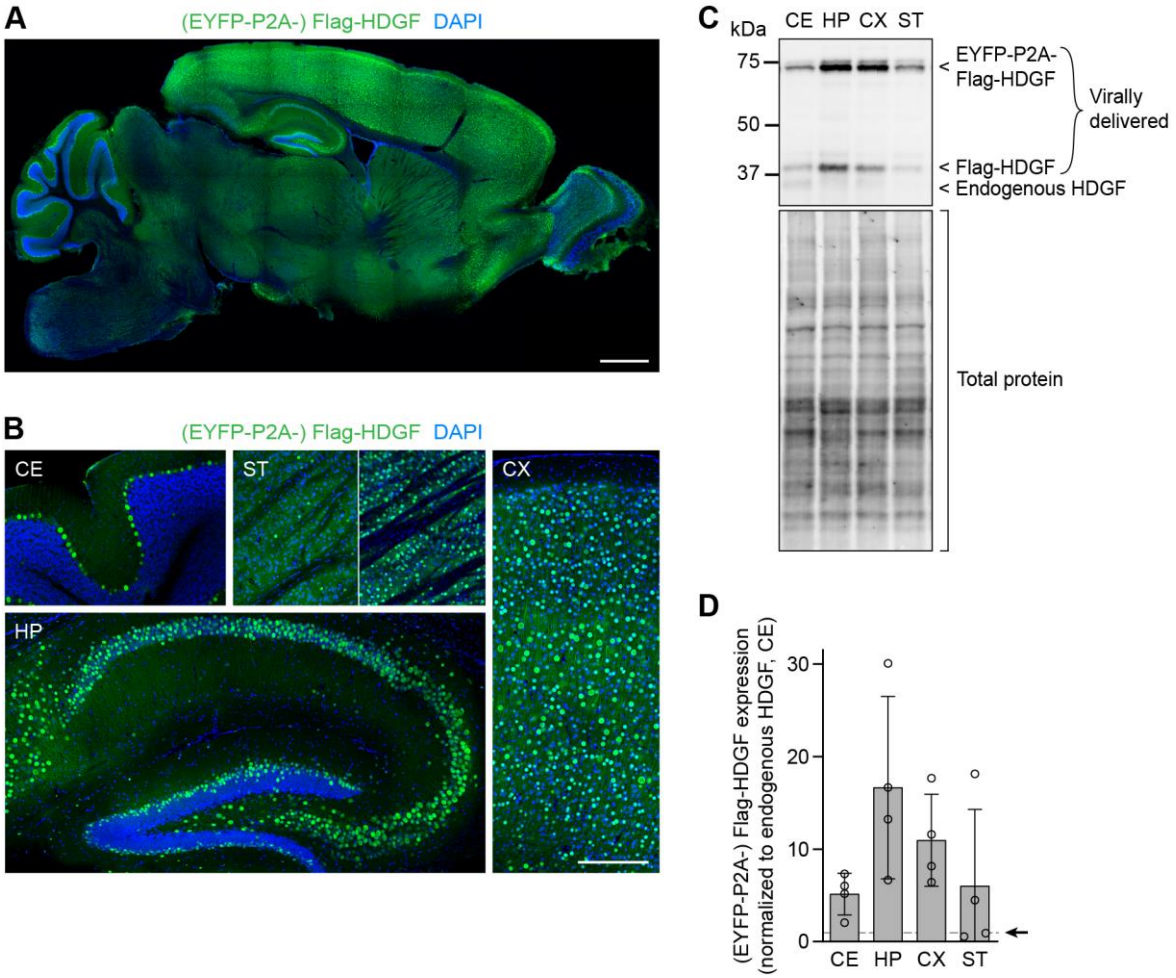

Figure 3.11 Intraventricular viral delivery of HDGF at P0 results in brain-wide expression

Brain-wide expression of virally delivered HDGF was confirmed by immunostaining and western blot analysis in WT mice.

A, B. Brain sections from P0 injected WT mice were immunostained against Flag-tag to detect virally delivered HDGF. Nuclei were counterstained with DAPI. Similar results were obtained from N = 3 (1 ♀, 2 ♂) 3-week-old and 4 (2 ♀, 2 ♂) 22-week-old WT mice. Of note, striatal expression varied between mice ranging from no or very sparse expression (42.9%; 3 out of 7 mice) to a denser, but locally restricted expression, not covering the whole striatum (57.1%; 4 out of 7 mice). (A) Overview image of a representative sagittal brain section collected at 3 weeks of age. (B) Detail images of cerebellum (CE), hippocampus (HP), cortex (CX), and striatum (ST) at 3 weeks of age. Examples of sparse (left) and dense (right) striatal expression are shown.

C, D. HDGF protein levels were measured in the indicated brain regions of P0 injected WT mice by western blot analysis. Total protein, determined using stain-free technology, was used as loading control. N = 4 (2 ♀, 2 ♂) 22-week-old WT mice. (C) Representative western blot of indicated brain lysates. Both cleaved (Flag-HDGF) and uncleaved (EYFP-P2A-Flag-HDGF) forms of virally delivered HDGF, were detected. In comparison, the endogenous HDGF band was faint and only reliably quantifiable for cerebellar lysates. (D) Protein quantity of virally delivered HDGF normalized to total protein and to cerebellar endogenous HDGF. The area under the curve was quantified at the band heights of EYFP-P2A-Flag-HDGF and Flag-HDGF irrespective of presence or absence of a protein band, and the sum calculated for normalization. Arrow highlights dashed line marking endogenous HDGF expression level in cerebellum. Virally delivered HDGF levels were on average 5-17 times higher than cerebellar endogenous HDGF levels. Note the absence of striatal overexpression in two mice (50%; 2 out of 4 mice).

Data information: Columns with error bars represent mean ± standard deviation. Scale bars in A, 1 mm; B, 250 µm.

With support from Nicole Martin in tissue homogenization, determination of protein concentration, western blotting, and image quantification.

Behavior of EYFP- and HDGF-injected R6/2 mice and WT littermates was assessed at 12 weeks of age. Remarkably, distance traveled and rearing frequency of HDGF-injected R6/2 mice were significantly rescued in the open field test (Figure 3.12 A, B). In contrast, rotarod performance and grip strength were not recovered by HDGF (Figure 3.12 C, D). The trend towards prolonged survival of HDGF-injected mice was likely due to slightly longer CAG repeat tracts in this cohort, a parameter strongly correlated with life span (Figure 3.12 E, F, G) (Morton *et al.*, 2009). Importantly, CAG repeat length was not predictive of locomotor activity in the range of repeat sizes detected in our cohorts of R6/2 mice (Figure 3.12 H, I). Hence, although not able to fully prevent disease progression, early HDGF treatment combined with widespread delivery caused a striking improvement in spontaneous motor activity.

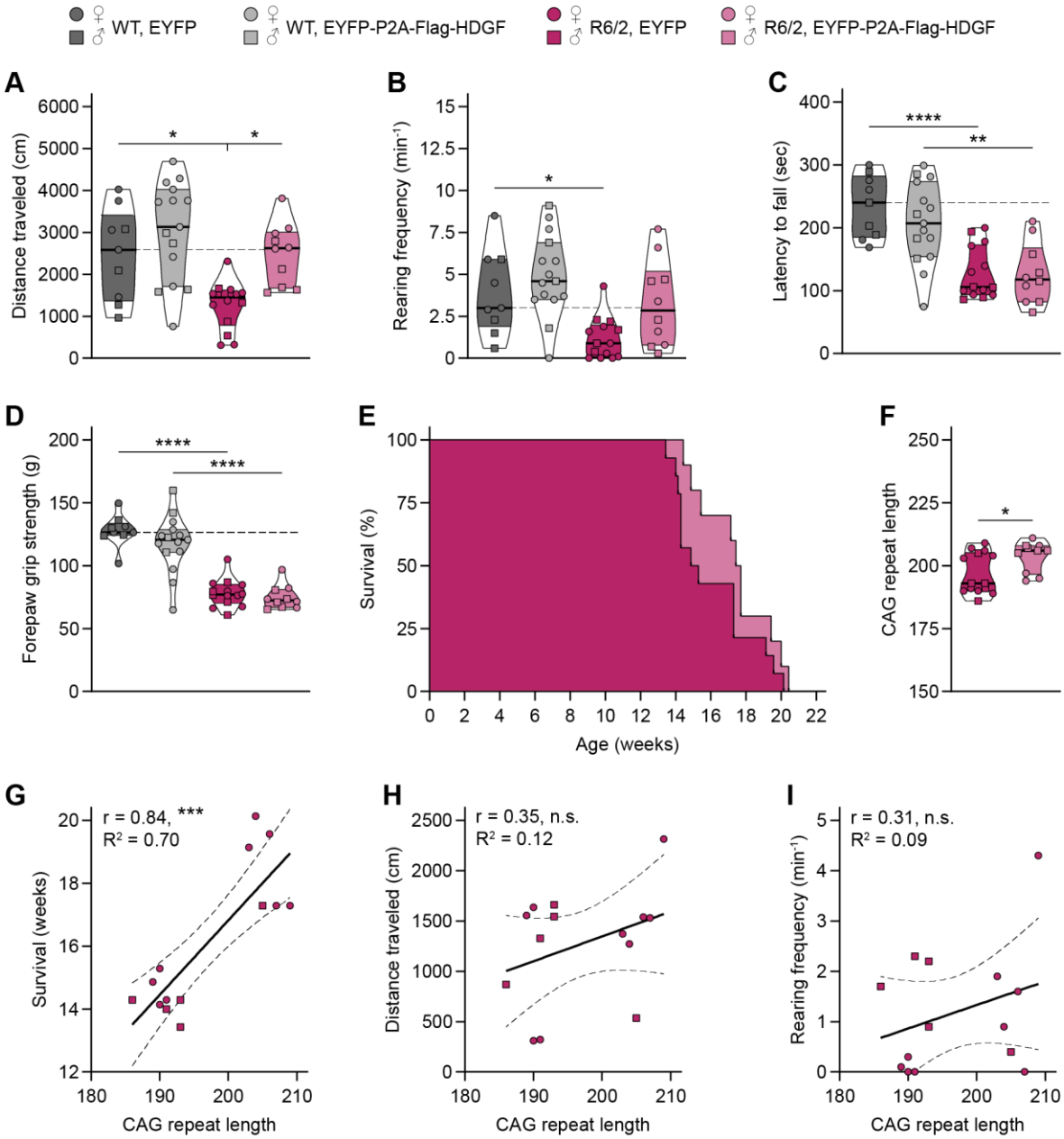

Figure 3.12 Brain-wide HDGF overexpression restores spontaneous locomotor activity in R6/2 mice

Behavior of 12-week-old R6/2 and WT mice injected at P0 with AAV8-EYFP-P2A-Flag-HDGF or AAV8-EYFP control was assessed followed by life span analysis. N = 9 (5 ♀, 4 ♂) EYFP-injected WT mice, 15 (11 ♀, 4 ♂) HDGF-injected WT mice, 14 (9 ♀, 5 ♂) EYFP-injected R6/2 mice, and 10 (5 ♀, 5 ♂) HDGF-injected R6/2 mice.

A. Distance traveled in the open field test. Two-way ANOVA with Bonferroni's multiple comparisons test. ANOVA: HTT, ** $P = 0.0029$; HDGF, ** $P = 0.0025$; HTT x HDGF, $P = 0.2303$. Significant pairwise multiple comparisons are indicated on the graph.

B. Rearing frequency in the open field test. Two-way ANOVA with Bonferroni's multiple comparisons test. ANOVA: HTT, ** $P = 0.0016$; HDGF, * $P = 0.0208$; HTT x HDGF, $P = 0.4273$. Significant pairwise multiple comparisons are indicated on the graph.

C. Latency to fall off the accelerating rotarod. Two-way ANOVA with Bonferroni's multiple comparisons test. ANOVA: HTT, **** $P < 0.0001$; HDGF, $P = 0.3778$; HTT x HDGF, $P = 0.4104$. Significant pairwise multiple comparisons are indicated on the graph.

D. Forepaw grip strength. Two-way ANOVA with Bonferroni's multiple comparisons test. ANOVA: HTT, **** $P < 0.0001$; HDGF, $P = 0.1495$; HTT x HDGF, $P = 0.4633$. Significant pairwise multiple comparisons are indicated on the graph.

E. Kaplan-Meier survival curves. Unpaired two-tailed *t*-test, not significant.

F. CAG repeat tract length. Unpaired two-tailed *t*-test.

G-I. Correlation of (G) survival, (H) distance traveled, and (I) rearing frequency with CAG repeat tract length of EYFP-injected R6/2 mice. Pearson correlation coefficient (r), significance, and R-squared (R^2) are indicated on the graphs.

Data information: A-D, and F: Violin plots with thick black line and colored area representing median and interquartile range, respectively. G-I: Thick line with dashed lines represents linear regression line with 95% confidence bands. Significance: n.s. – not significant, * $P < 0.05$, ** $P < 0.01$, *** $P < 0.001$, **** $P < 0.0001$.

In HD, mutation carriers can be identified and treated prior to disease onset. However, clinical trials are only beginning to include patients with late prodromal HD (NCT02481674, NCT04514367). Moreover, brain-wide delivery is challenging in humans. We therefore performed bilateral stereotactic injections into the striatum of 4-week-old R6/2 mice and WT littermates to evaluate efficacy of local HDGF treatment starting at an early disease stage. Overexpression of HDGF was confined to the striatum and limited to the area close to the injection sites (Figure 3.13 A-C). While exploratory activity of EYFP-injected R6/2 mice was reduced compared to EYFP-injected WT controls, distance traveled and rearing frequency of HDGF-injected R6/2 mice were not significantly different from their WT controls at 12 weeks of age (Figure 3.13 D, E). In addition, histological assessment revealed a reduction in mHTT inclusion body size within the infected area of HDGF-injected animals (Figure 3.13 F, G). Together, these data suggest that HDGF is beneficial in HD even upon local treatment after disease onset. Collectively, our findings in R6/2 mice demonstrate the potential of HDGF to ameliorate HD-related phenotypes *in vivo*.

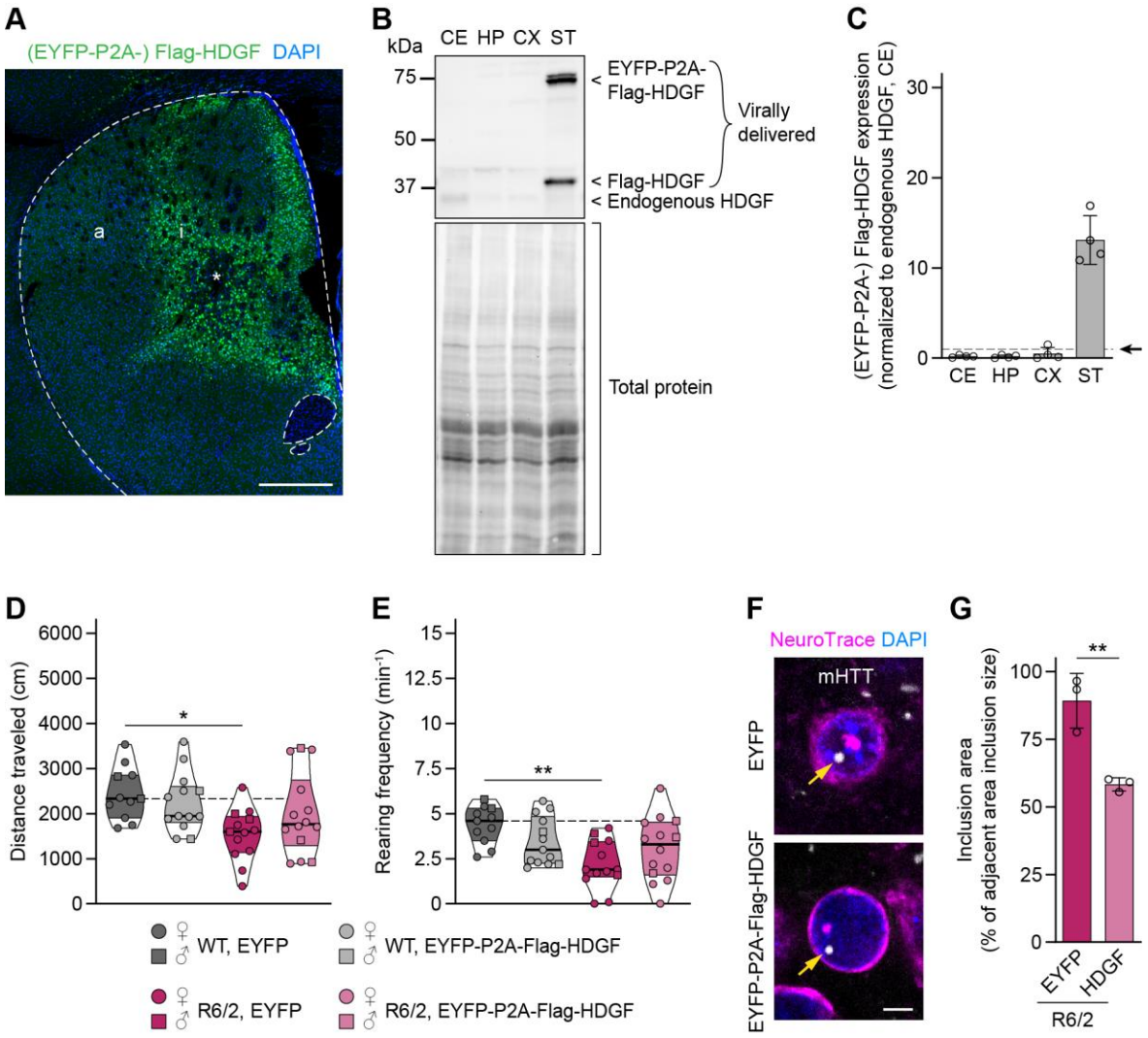

Figure 3.13 Striatal HDGF overexpression early in disease ameliorates HD phenotypes in R6/2 mice

HDGF was virally delivered into the striatum of R6/2 mice and WT littermates via bilateral stereotactic injections at 4 weeks of age. Expression in the striatum and efficacy of local HDGF treatment on HD phenotypes was evaluated.

A. Representative overview image of the striatum from an AAV8-EYFP-P2A-Flag-HDGF-injected mouse brain. Virally delivered HDGF was detected by immunostaining against Flag-tag in coronal brain sections. Nuclei were counterstained with DAPI. Dashed lines denote striatal borders. The striatum can be divided into the infected area (i) close to the injection site (asterisk) and the adjacent non-infected area (a). Similar results were obtained from N = 6 (WT: 1 ♀, 2 ♂; R6/2: 1 ♀, 2 ♂) 12 to 13-week-old mice.

B, C. HDGF protein levels were measured in brain lysates from cerebellum (CE), hippocampus (HP), cortex (CX), and striatum (ST) by western blot analysis. Total protein, determined using stain-free technology, was used as loading control. N = 4 (WT: 2 ♀; R6/2: 2 ♀) 12-week-old mice. (B) Representative western blot of indicated brain lysates. Both cleaved (Flag-HDGF) and uncleaved (EYFP-P2A-Flag-HDGF)

forms of virally delivered HDGF, were detected. In comparison, the endogenous HDGF band was faint and only reliably quantifiable for cerebellar lysates. (C) Protein quantity of virally delivered HDGF normalized to total protein and to cerebellar endogenous HDGF. The area under the curve was quantified at the band heights of EYFP-P2A-Flag-HDGF and Flag-HDGF irrespective of presence or absence of a protein band, and the sum calculated for normalization. Arrow highlights dashed line marking endogenous HDGF expression level in cerebellum. Virally delivered HDGF levels in the striatum were on average 13 times higher than cerebellar endogenous HDGF levels.

D, E. Behavior of R6/2 and WT mice injected with AAV8-EYFP-P2A-Flag-HDGF or AAV8-EYFP control was analyzed at 12 weeks of age. N = 11 (9 ♀, 2 ♂) EYFP-injected WT mice, 13 (11 ♀, 2 ♂) HDGF-injected WT mice, 13 (10 ♀, 3 ♂) EYFP-injected R6/2 mice, and 14 (11 ♀, 3 ♂) HDGF-injected R6/2 mice. (D) Distance traveled in the open field test. Two-way ANOVA with Bonferroni's multiple comparisons test. ANOVA: HTT, ** $P = 0.0050$; HDGF, $P = 0.4980$; HTT x HDGF, $P = 0.1038$. Significant pairwise multiple comparisons are indicated on the graph. (E) Rearing frequency in the open field test. Two-way ANOVA with Bonferroni's multiple comparisons test. ANOVA: HTT, ** $P = 0.0018$; HDGF, $P = 0.9772$; HTT x HDGF, * $P = 0.0277$. Significant pairwise multiple comparisons are indicated on the graph.

F, G. Brain sections of EYFP- and HDGF-injected R6/2 mice were immunostained against mHTT to detect mHTT inclusions. Nuclei were counterstained with DAPI and neurons identified with NeuroTrace. N = 3 (1 ♀, 2 ♂) EYFP-injected and 3 (1 ♀, 2 ♂) HDGF-injected 12 to 13-week-old R6/2 mice. (F) Examples of neurons with mHTT inclusions (yellow arrows) within the infected area of the striatum. (G) Quantification of neuronal mHTT inclusion size within the infected area normalized to mean neuronal inclusion size in the adjacent striatal area per mouse. Unpaired two-tailed *t*-test.

Data information: C, G: Columns with error bars represent mean ± standard deviation. D, E: Violin plots with thick black line and colored area representing median and interquartile range, respectively. Significance: * $P < 0.05$, ** $P < 0.01$. Scale bar in A, 500 µm.

With support from Nicole Martin in tissue homogenization, determination of protein concentration, western blotting, and image quantification. Sara Gutiérrez-Ángel performed stereotactic injections into the striatum, assessed behavior, and collected brains of injected mice.

3.6 Cytoplasmic HDGF rescues mHTT toxicity without promoting nuclear expansion

While our experiments revealed that HDGF provides neuroprotection in HD, downstream effects of HDGF are largely unexplored in neurons. Histological analysis of striatal injected mice pointed towards changes within the nuclear compartment. Nuclei were markedly expanded within the transduced area of HDGF-injected R6/2 and WT mice. In contrast, no change in nucleus area was observed for uninfected striatal neurons (Figure 3.14 A, B), suggesting that potential paracrine action of HDGF is not effective in inducing nuclear expansion. Interestingly, while rescuing mHTT toxicity (Figure 3.1), short-term overexpression of HDGF had no effect on nucleus size in transfected primary neurons (Figure 3.14 C, D). Thus, nuclear expansion might be a side effect of long-term overexpression in neurons, rather than linked to neuroprotection.

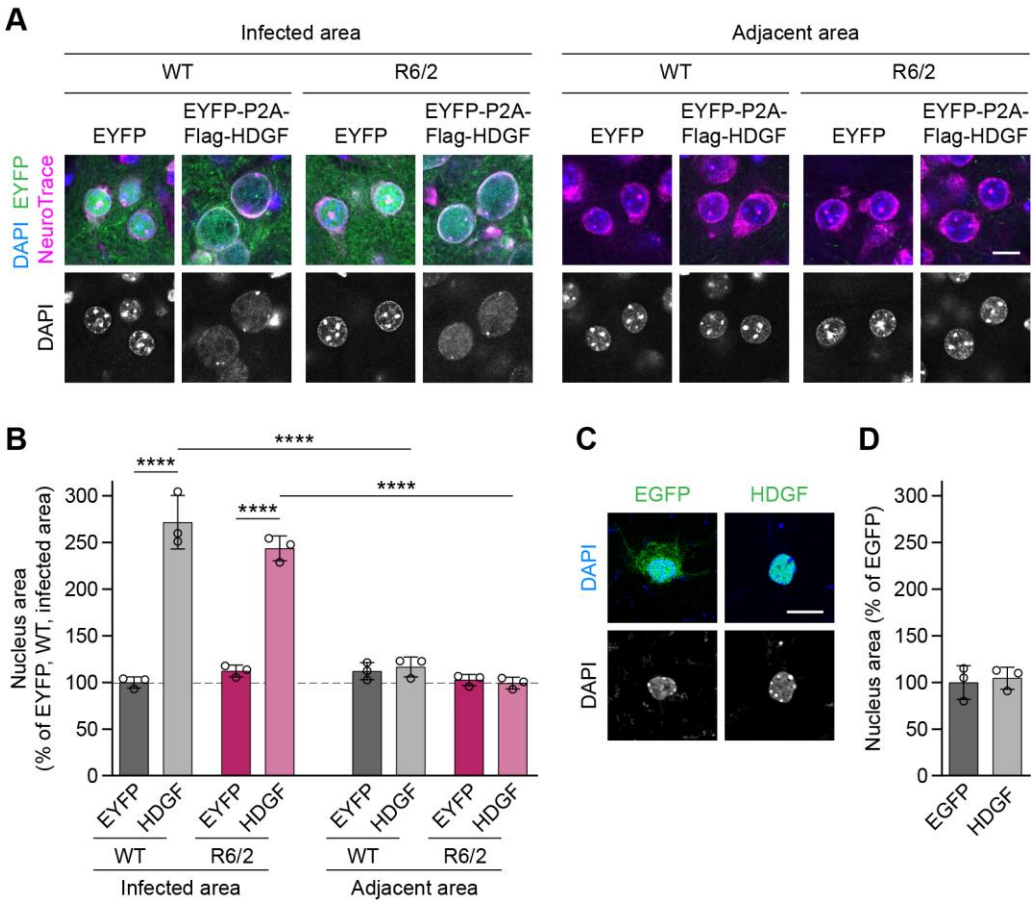

Figure 3.14 HDGF causes nuclear expansion upon long-term overexpression in neurons

Neuronal nucleus area was analyzed in striatal injected mouse brains and transfected primary cortical neurons.

A, B. Brain sections of EYFP- and HDGF-injected R6/2 and WT mice were stained with DAPI to visualize nuclei. Neurons were identified with NeuroTrace. N = 3 (1 ♀, 2 ♂) 12 to 13-week-old mice per group. (A) Examples of neurons within the infected area or adjacent to the transduced area in the striatum. (B) Quantification of neuronal nucleus area normalized to mean nucleus area of neurons within the infected area of EYFP-injected WT brain. Three-way ANOVA with Bonferroni's multiple comparisons test. ANOVA: Area, **** $P < 0.0001$; HTT, $P = 0.0621$; HDGF, **** $P < 0.0001$; Area x HTT, $P = 0.6099$; Area x HDGF, **** $P < 0.0001$; HTT x HDGF, * $P = 0.0376$; Area x HTT x HDGF, $P = 0.1480$. Significant pairwise multiple comparisons are indicated on the graph.

C, D. DIV 7 cortical neurons were transfected with EGFP or HDGF and fixed 2 days later. HDGF-transfected neurons were identified by immunostaining against Flag-tag. Nuclei were labeled with DAPI. N = 3 biological replicates. (C) Examples of neurons transfected with EGFP or HDGF. (D) Quantification of nucleus area normalized to mean nucleus area of EGFP-transfected neurons. Unpaired two-tailed *t*-test, not significant.

Data information: Columns with error bars represent mean ± standard deviation. Significance: **** $P < 0.0001$. Scale bars in A and C, 10 µm.

Since in human motor cortex, HDGF was localized in the cytoplasm of neurons (Figure 3.8), we were prompted to study whether redirecting HDGF from the nucleus to the cytoplasmic compartment can prevent nuclear enlargement, but preserve the neuroprotective properties of HDGF. To this end, we introduced 12 point mutations into the two NLS sequences of HDGF, resulting in 9 amino acid substitutions, as previously described (Kishima *et al.*, 2002). Additionally, a C-terminal NES sequence was added for proper nuclear exclusion of HDGF (Figure 3.15 A). We then transduced primary neurons with either cytoplasmic HDGF (cytHDGF), nuclear wild-type HDGF (from here on nucHDGF), or EYFP control virus for long-term expression. Similar to *in vivo*, nuclei of nucHDGF-transduced, but not of neighboring untransduced primary neurons were markedly enlarged at 11 days post transduction. In contrast, nucleus area was unaltered by cytHDGF expression (Figure 3.15 B, C). Similar results were observed in transfected HEK 293T cells (Figure 3.15 D, E); hence, nuclear expansion as response to nucHDGF overexpression is not specific to post-mitotic neuronal cells. Together, these findings show that overexpression of nuclear, but not cytoplasmic HDGF promotes nuclear expansion in cells.

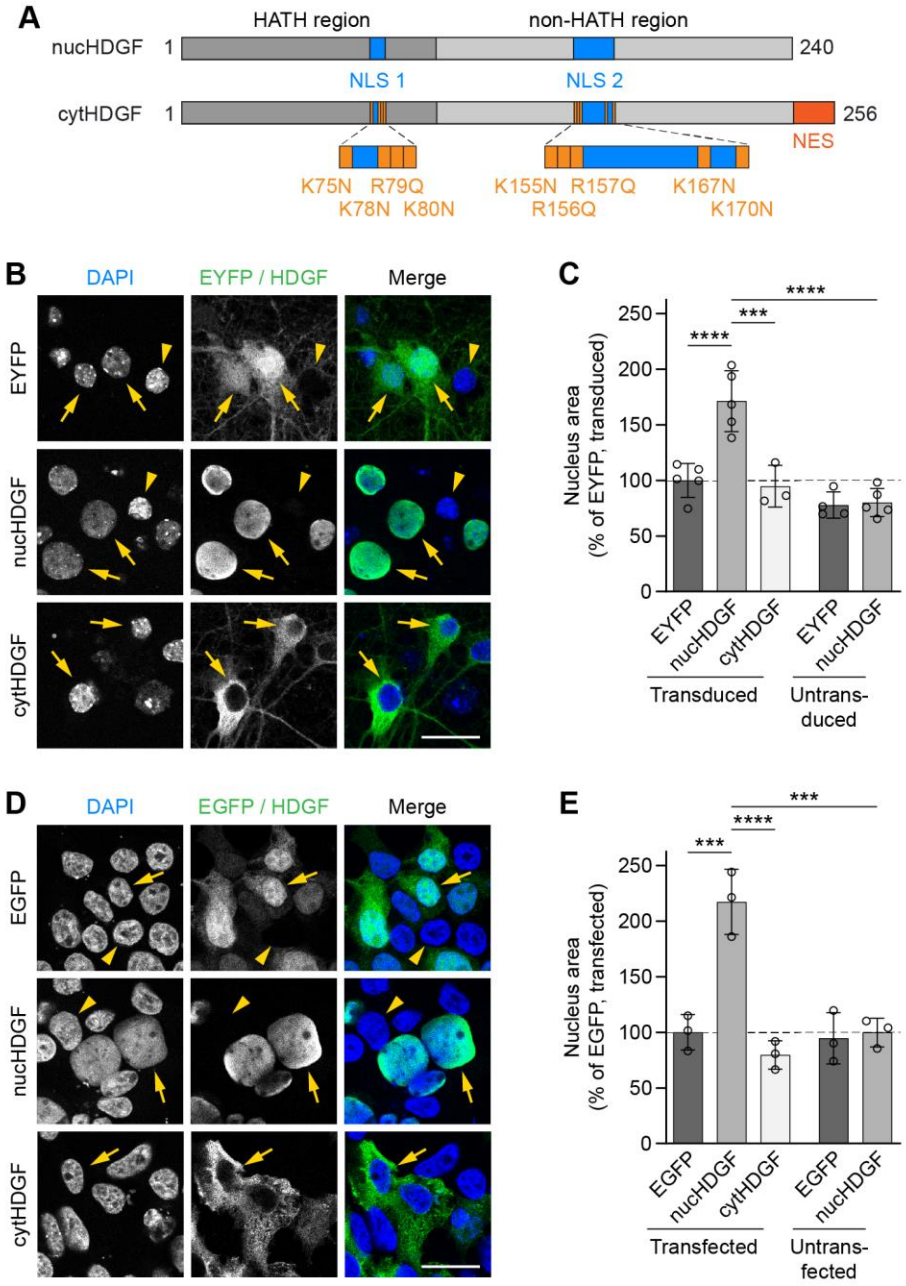

Figure 3.15 Nuclear, but not cytoplasmic HDGF promotes nuclear expansion

The role of HDGF localization for nuclear enlargement was studied in primary neurons and HEK 293T cells.

A. Scheme of wild-type HDGF with nuclear localization (nucHDGF) and cytoplasmic HDGF (cytHDGF). Changes in the amino acid sequence are indicated in orange. Protein length is given in amino acids.

B, C. DIV 7 cortical neurons were transduced with the indicated lentiviral vectors and fixed 11 days later. HDGF-transduced neurons were identified by immunostaining against Flag-tag. Nuclei were labeled with DAPI. N = 3-5 biological replicates. (B) Examples of transduced neurons (arrows) and untransduced

neighboring cells (arrowheads). (C) Quantification of nucleus area normalized to mean nucleus area of EYFP-transduced neurons. Two-way ANOVA with Bonferroni's multiple comparisons test. ANOVA: Transduction, **** $P < 0.0001$; HDGF, ** $P = 0.0023$. Significant pairwise multiple comparisons are indicated on the graph.

D, E. HEK 293T cells were transfected with the indicated constructs and fixed after 24 h. HDGF-transfected cells were identified by immunostaining against Flag-tag. Nuclei were labeled with DAPI. N = 3 independent experiments. (D) Examples of transfected cells (arrows) and untransfected neighboring cells (arrowheads). (E) Quantification of nucleus area normalized to mean nucleus area of EGFP-transfected cells. Two-way ANOVA with Bonferroni's multiple comparisons test. ANOVA: Transfection, * $P = 0.0111$; HDGF, ** $P = 0.0037$. Significant pairwise multiple comparisons are indicated on the graph.

Data information: Columns with error bars represent mean ± standard deviation. Significance: *** $P < 0.001$, **** $P < 0.0001$. Scale bars in B and D, 20 μm.

With support from Sophie Keeling in cell culture, transduction, transfection, immunostaining, and image quantification.

To investigate the potential of cytHDGF to alleviate mHTT toxicity, we assessed neuronal cell death and mHTT aggregation in co-transfected primary neurons by immunostaining. Two mHTT constructs with different aggregation properties, HTTQ97-mCherry and HTTQ72-His, were included in the analysis. Whereas aggregates form mainly in the cytoplasm in HTTQ97-mCherry-transfected neurons, HTTQ72-His is often localized and aggregated in the nucleus (Figure 3.16 A, magenta arrowheads). In cultured neurons, both mHTT versions conveyed similar toxicity (Figure 3.16 B). Remarkably, not only nucHDGF, but also cytHDGF co-expression rescued survival of mHTT-expressing cells, irrespective of which mHTT construct was co-transfected (Figure 3.16 A, B). Moreover, we found the frequency of HTTQ97-mCherry aggregates decreased by either HDGF version (Figure 3.16 A, C). In contrast, for HTTQ72-His-transfected cells, the number of neurons with aggregates was high in all conditions, but formation of large (≥ 1 μm) inclusion bodies was reduced by nucHDGF and cytHDGF (Figure 3.16 A, C, D). These findings demonstrate that nuclear localization of HDGF is not required to ameliorate mHTT-induced toxicity in neurons. In conclusion, our data point to a neuroprotective effect of cytoplasmic HDGF in HD decoupled from nuclear enlargement.

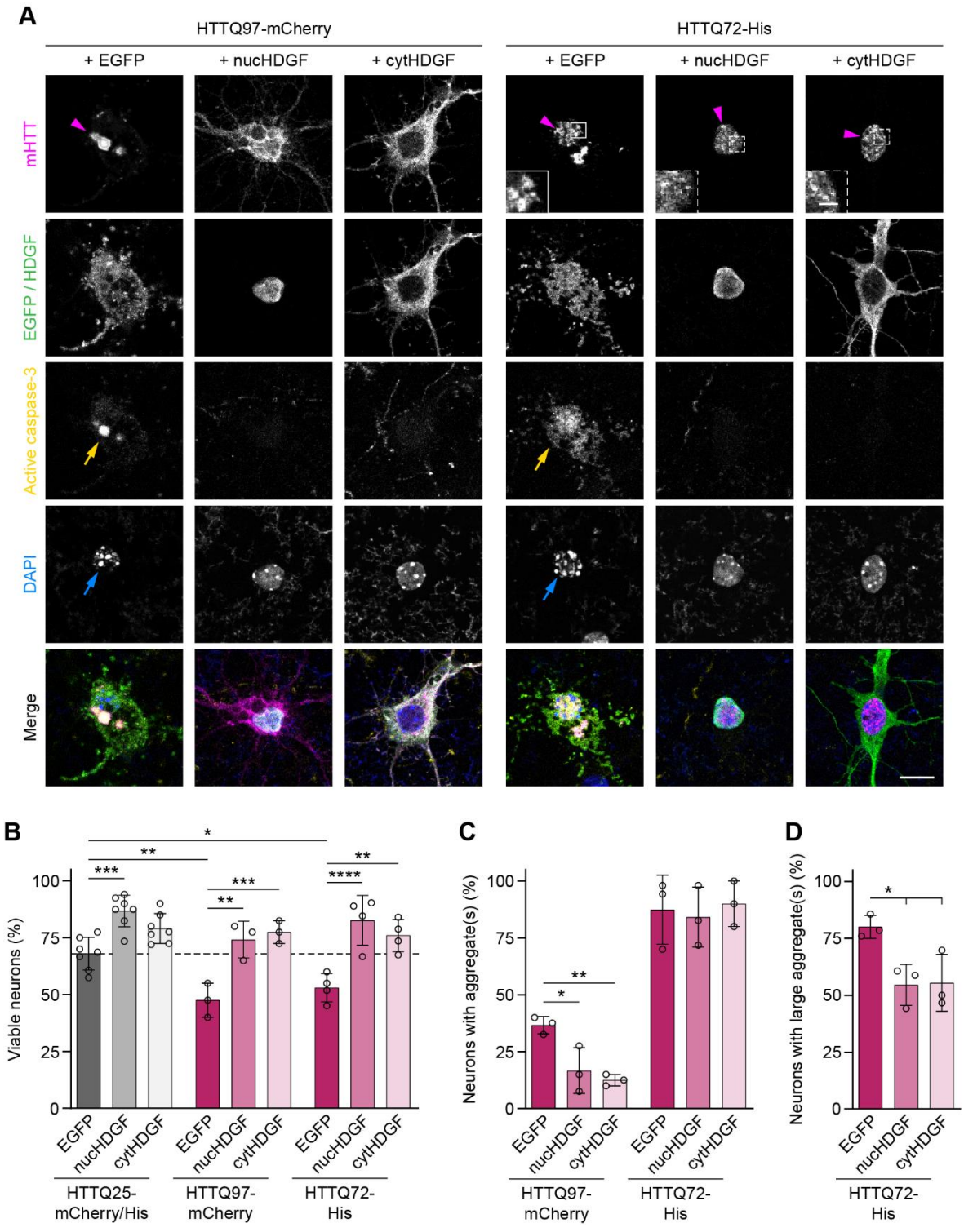

Figure 3.16 Nuclear localization of HDGF is not required for rescuing mHTT toxicity

Cortical neurons were co-transfected with the indicated constructs at DIV 7 and fixed 2 days later. HDGF-transfected cells were identified by immunostaining against Flag-tag. Viability was assessed by immunostaining for active caspase-3 and nuclear labeling with DAPI.

A. Examples of neurons for the indicated conditions. Arrows mark apoptotic neurons with active caspase-3 staining (yellow) and fragmented nuclei (blue). Magenta arrowheads label neurons with mHTT aggregates. Insets show magnifications of boxed areas. Note the difference between large aggregates (solid line box) and small foci (dashed line boxes) formed by HTTQ72-His.

B. Quantification of the fraction of viable neurons. Cells negative for active caspase-3 with intact nuclear morphology were categorized as viable. N = 3-7 biological replicates. HTTQ25-mCherry and HTTQ25-His did not differ from each other and were pooled as controls. Two-way ANOVA with Bonferroni's multiple comparisons test. ANOVA: HTT, **** $P < 0.0001$; HDGF, **** $P < 0.0001$; HTT x HDGF, * $P < 0.0107$. Significant pairwise multiple comparisons are indicated on the graph.

C. Quantification of the fraction of neurons with mHTT aggregates. N = 3 biological replicates. One-way ANOVA with Tukey's multiple comparisons test for each mHTT construct. ANOVA: HTTQ97-mCherry, ** $P = 0.0077$; HTTQ72-His, not significant. Significant pairwise multiple comparisons are indicated on the graph.

D. Quantification of the fraction of HTTQ72-His-transfected neurons with large mHTT aggregates. N = 3 biological replicates. One-way ANOVA with Tukey's multiple comparisons test. ANOVA: * $P = 0.0258$. Significant pairwise multiple comparisons are indicated on the graph.

Data information: Columns with error bars represent mean ± standard deviation. Significance: * $P < 0.05$, ** $P < 0.01$, *** $P < 0.001$, **** $P < 0.0001$. Scale bar in A, 10 µm; insets, 2 µm.

3.7 Extracellular HDGF mitigates mHTT toxicity in primary neurons without activating ERK or AKT signaling

Since HDGF can be secreted and extracellular HDGF has been shown to promote neuronal survival (Zhou *et al.*, 2004; Marubuchi *et al.*, 2006; Hollander *et al.*, 2012), we next investigated the potential of extracellular HDGF to alleviate mHTT toxicity in primary neurons. To this end, we first generated recombinant HDGF and confirmed survival-promoting activity in cortical neuron cultures (Figure 3.17 A). By MTT assay, viability was assessed 24 h after medium exchange to B27-free culture medium supplemented with different concentrations of recombinant nucHDGF. Recombinant BDNF and complete culture medium were used as positive controls, whereas B27-free culture medium with PBS served as negative control. In agreement with published data (Zhou *et al.*, 2004), we observed an increase in neuronal viability in the presence of HDGF. The strongest survival-enhancing effect of extracellular nucHDGF was detected

at a concentration of 250 ng/ml (Figure 3.17 A), which was chosen for further experiments. We then added recombinant nucHDGF or cytHDGF to primary neurons transfected with pathological HTTQ97-mCherry or HTTQ25-mCherry control, and analyzed viability two days later by immunostaining. For comparison, recombinant BDNF, known to improve neuronal survival in the context of HD (Saudou *et al.*, 1998; Zala *et al.*, 2005), was used as positive control. Both recombinant HDGF variants significantly increased viability of mHTT-transfected neurons similar to BDNF, while the frequency of HTTQ97-mCherry aggregates was not significantly altered by BDNF or either HDGF version (Figure 3.17 B, C). These results indicate that extracellular HDGF is a potent modulator of mHTT toxicity which might act beyond modulation of aggregation.

Many growth factors, including BDNF, confer neuroprotection through activation of canonical phosphoinositide 3-kinase (PI3K)/AKT and mitogen-activated protein kinase (MAPK)/extracellular signal-regulated kinase (ERK) signaling (Nasrolahi *et al.*, 2018; Yusuf *et al.*, 2018). We therefore monitored activation of these pathways in primary neurons 10-20 min after application of recombinant HDGF. Western blot analysis revealed that, contrary to BDNF, both HDGF variants failed to increase levels of phosphorylated AKT and ERK1/2 (Figure 3.17 D-F). Together, our findings suggest that extracellular HDGF mitigates mHTT toxicity in neurons by a mechanism distinct from BDNF that does not involve activation of AKT or ERK1/2 signaling.

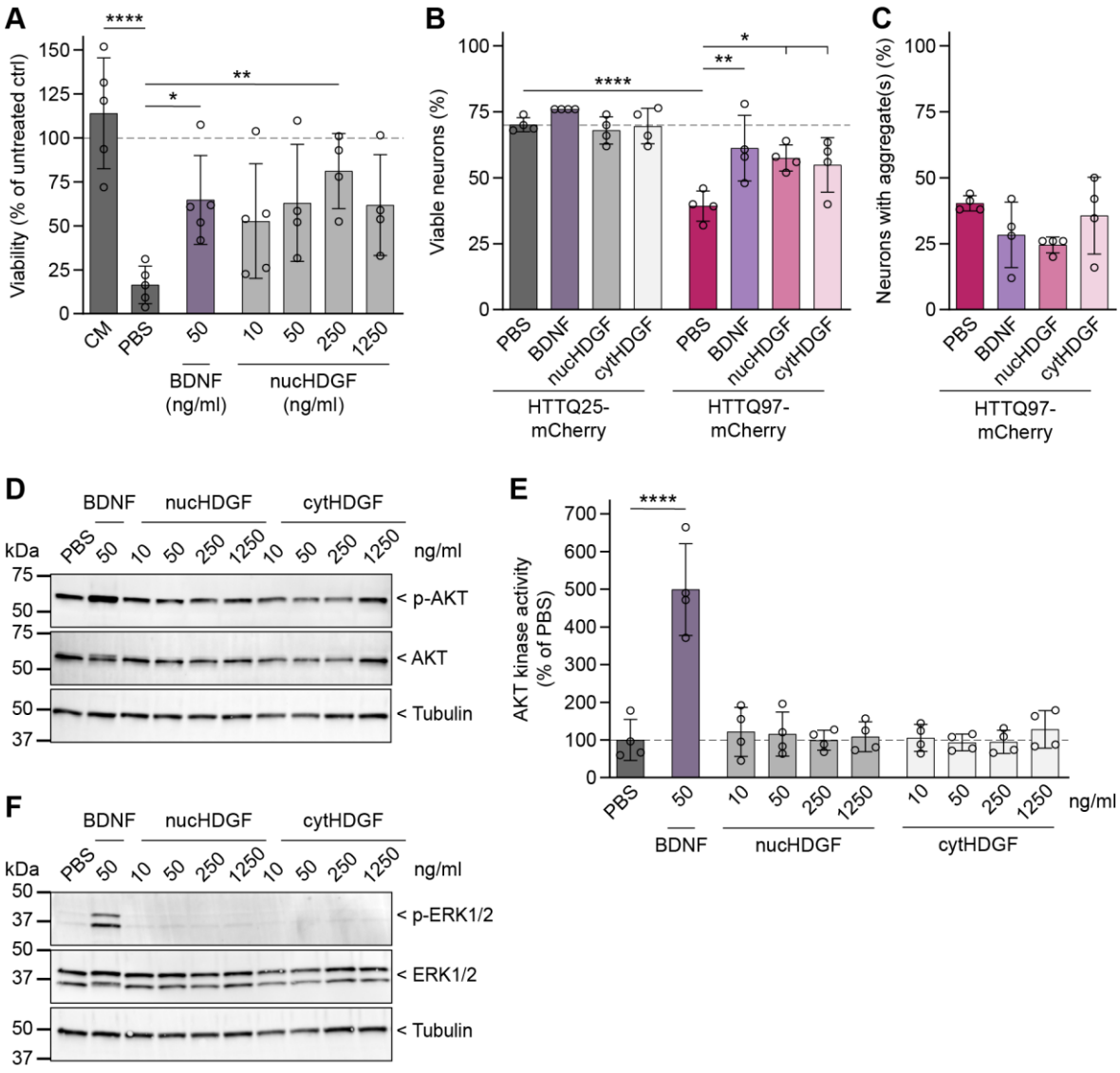

Figure 3.17 Extracellular HDGF mitigates mHTT toxicity independent of AKT and ERK1/2 signaling

Neuroprotective properties of extracellular HDGF were studied in primary cortical neurons.

A. Quantification of neuronal viability by MTT assay 24 h after medium exchange. Medium of DIV 7 cortical neurons was replaced by complete culture medium (CM) or B27-free culture medium supplemented with PBS as vehicle control, recombinant BDNF or nucHDGF as indicated. Viability was normalized to untreated control per experiment. N = 4-5 biological replicates. One-way ANOVA with Dunnett's multiple comparisons test. ANOVA: *** $P = 0.0007$. Significant pairwise multiple comparisons to PBS control are indicated on the graph.

B, C. Cortical neurons were co-transfected with EGFP and the indicated HTT constructs at DIV 7 and treated with PBS, recombinant BDNF (50 ng/ml) or HDGF (250 ng/ml) at the time of transfection. Cells were fixed two days later and immunostained for active caspase-3. Nuclei were counterstained with DAPI. N = 4 biological replicates. (B) Quantification of the fraction of viable neurons. Cells negative for active

caspase-3 with intact nuclear morphology were categorized as viable. Two-way ANOVA with Bonferroni's multiple comparisons test. ANOVA: HTT, **** $P < 0.0001$; Treatment, ** $P = 0.0072$; HTT x Treatment, * $P = 0.0408$. Significant pairwise multiple comparisons are indicated on the graph. (C) Quantification of the fraction of neurons with mHTT aggregates. One-way ANOVA, not significant.

D, E, F. Cortical neurons were treated as indicated at DIV 7 and harvested 10-20 min later. AKT and ERK1/2 kinase activity were assessed by western blot analysis. Tubulin was used as loading control. N = 4 biological replicates. (D) Representative western blot for phosphorylated (p-AKT) and total AKT. (E) Quantification of p-AKT/AKT, normalized to PBS-treated control. One-way ANOVA with Dunnett's multiple comparisons test. ANOVA: **** $P < 0.0001$. Significant pairwise multiple comparisons to PBS control are indicated on the graph. (F) Representative western blot for phosphorylated (p-ERK1/2) and total ERK1/2. No quantification was performed since p-ERK1/2 was only detectable in BDNF-treated cells.

Data information: Columns with error bars represent mean ± standard deviation. Significance: * $P < 0.05$, ** $P < 0.01$, **** $P < 0.0001$.

A, D-F, with support from Sophie Keeling in cell culture, MTT assays, western blotting, and image quantification.

4 Discussion

Despite the fact that the genetic cause of HD is known for almost three decades, disease pathogenesis has not yet been fully resolved and effective treatments to slow or halt disease progression are still lacking. In this study, we investigated the neuroprotective ability of HDGF in HD. Disease-modifying potential of HDGF was demonstrated in cellular and mouse HD models. Moreover, a detailed characterization of HDGF expression in mouse brain revealed inverse correlation of HDGF levels and neuronal vulnerability to HD. Finally, we provided first hints pointing towards a non-canonical mode of action. We therefore propose HDGF as an interesting candidate for HD therapy.

4.1 Neuroprotection by endogenous HDGF

Neuroprotective properties of HDGF have so far only been observed in cell culture and following treatment with recombinant protein after nerve transection in rats (Zhou *et al.*, 2004; Marubuchi *et al.*, 2006; Hollander *et al.*, 2012). Here, we show that *Hdgf* knockout exacerbates motor defects and shortens life span in R6/2 mice (Figure 3.9, 3.10), thereby providing *in vivo* evidence that endogenous HDGF is required for neuroprotection in disease. Of note, HDGF deficiency alone caused behavioral abnormalities as revealed by increased exploratory activity of *Hdgf* $^{-/-}$ mice in the open field test (Figure 3.9 A, B). In contrast, Gallitzendoerfer *et al.* (2008) reported reduced rearing time in 6-month-old *Hdgf* $^{-/-}$ mice, while other locomotive measures were unaltered. Since the latest time point of behavioral analysis in our study was 3 months of age, compensatory adaptions during further aging might explain the observed differences in behavioral phenotypes. Overall, loss of HDGF is well tolerated under physiological conditions (Gallitzendoerfer *et al.*, 2008), suggesting that other proteins largely counterbalance HDGF deficiency. The HRP protein family comprises six

members, including HDGF, all of which contain a N-terminal HATH domain while the C-terminal region is variable (Dietz *et al.*, 2002). Besides HDGF, HRP-2 and HRP-3 are expressed in the brain and, similar to HDGF, neurotrophic properties have been demonstrated for HRP-3 in neuronal cultures (El-Tahir *et al.*, 2006; Abouzied *et al.*, 2010). The presence of other HRPs might therefore compensate loss of HDGF in the nervous system. Interestingly, in a recent genome-wide shRNA screen, *Hdgf* was identified as one of the essential genes required for neuronal survival in the striatum of adult WT mice (Wertz *et al.*, 2020). This finding indicates that disturbances of HDGF levels in adult mouse brain might be less tolerated, whereas early knockdown during development may pave the way for long-term adaptive responses.

Our observations in *Hdgf* $^{-/-}$; R6/2 mice support the idea that HDGF becomes particularly important under pathological conditions. In addition to active secretion, HDGF can be passively released by necrotic as well as late apoptotic cells and has been classified as putative alarmin, an endogenous molecule signaling cell and tissue damage (Zhou *et al.*, 2004; Bianchi, 2007; Giri *et al.*, 2016). Upregulation of HDGF expression was detected in two mouse models of spinal motor neuron degeneration prior to symptom onset, which was proposed to convey neuroprotection (Marubuchi *et al.*, 2006). Moreover, consistent with our results, Wertz *et al.* (2020) reported *Hdgf* not only as neuronal essential gene in WT mice, but also among the genes protecting against mHTT toxicity in R6/2 striatum. *Hdgf* targeting shRNAs were clearly underrepresented in striatal R6/2 tissue compared to WT control striata four weeks after delivery of a lentiviral genome-wide shRNA library, indicating that knockdown of *Hdgf* promoted cell death in the context of HD. It is therefore conceivable, that differential HDGF expression in neurons impacts susceptibility to mHTT toxicity.

Our expression studies in WT mouse brain indeed suggest that endogenous HDGF levels correlate with vulnerability of neuronal populations and brain regions to HD. MSNs and PCs express HDGF at lower levels than cell types with a higher resistance in striatum and cortex, respectively (Figure 3.4 A, C). In the cerebellum, which is rather spared in HD, HDGF levels are high (Figure 3.5), matching human protein expression data (Uhlén *et al.*, 2015) (Human Protein Atlas available from http://www.proteinatlas.org). However, we found no indication for dysregulated

HDGF expression in mouse and human HD brain (Figure 3.6, 3.7, 3.8). Although we cannot exclude alterations in the mechanism of action and desensitization of downstream pathways, the observed beneficial effects of HDGF overexpression and exogenous treatment imply that the neuroprotective cascade can still be triggered in disease, hence enabling neuroprotective intervention.

Contrary to the nuclear localization that we and others observed in mouse brain (Figure 3.2 C) (Zhou *et al.*, 2004; El-Tahir *et al.*, 2006), intracellular distribution of endogenous HDGF was cytoplasmic in human neurons of the primary motor cortex (Figure 3.8). In line with these findings, neurons with cytoplasmic HDGF can also be detected in other regions of the human brain as verified via open access histological images (Uhlén *et al.*, 2015) (Human Protein Atlas available from http://www.proteinatlas.org). While representing an exception in mouse CNS, we found HDGF localized to the cytoplasm in some neurons of the spinal cord (Figure 3.2 B), similar as shown for spinal motor neurons in a previous study (Marubuchi *et al.*, 2006). Together with the observation, that overexpressed human HDGF is largely confined to the nuclear compartment in mouse cortical neurons *in vitro* and *in vivo* (Figure 3.11 B, 3.15 B), these findings clearly argue against differences in the amino acid sequence of human HDGF and its murine ortholog as determinant of HDGF localization in neuronal cells. Most likely differential distribution of HDGF depends on cellular properties and HDGF function. A maturation-dependent change in localization has been reported for HRP-3: During development, HRP-3 first resides in neurites and the cytoplasm where it interacts with the cytoskeleton, before it redistributes to the nucleus upon CNS maturation (El-Tahir *et al.*, 2009). How this process is regulated is yet unclear. For HDGF, two alternative N-terminal splice variants have been described, that were not completely restricted to the nucleus, but also detected in the cytoplasm of fibroblast-like cells (Nüße *et al.*, 2016). However, whether alternative splicing or post-translational processing plays a role in regulation of cellular localization and to what extent the function of nuclear versus cytoplasmic HDGF differs in neurons remains to be studied.

4.2 Augmenting HDGF levels as novel therapeutic strategy for HD

Whereas HDGF depletion worsened HD phenotypes in R6/2 mice, an increase in HDGF levels conveyed neuroprotection both *in vitro* and *in vivo*. Early treatment with brain-wide HDGF delivery preserved spontaneous locomotion and rearing activity in diseased mice (Figure 3.12 A, B). Contrary to *Hdgf* knockout, HDGF overexpression had, however, no effect on rotarod performance and survival (Figure 3.12 C, E). This difference could be explained by ubiquitous deletion of HDGF in *Hdgf* $^{-/-}$; R6/2 mice as opposed to mosaicism for overexpression. Since pathology is very strong and wide-spread in the R6/2 mouse model, we may not have sufficiently targeted all affected neuronal populations and brain regions by viral injections. Although intracerebroventricular delivery resulted in HDGF expression throughout the brain, striatal transduction efficiency was generally rather low (Figure 3.11). Thus, pronounced expression in a brain region central to HD pathology was lacking, possibly limiting treatment efficiency. Simultaneous targeting of cortical and striatal neurons may in fact be key for optimal HD therapy. In conditional HD mice, reduced mHTT expression in either cortex or striatum partially improved disease phenotypes, but amelioration of behavioral deficits and brain atrophy was greatest for mHTT lowering in both cortex and striatum (Wang *et al.*, 2014). Whether combined cortical and striatal overexpression of HDGF can further mitigate symptomology remains to be elucidated in future experiments. Furthermore, we cannot fully rule out peripheral contribution to phenotype aggravation in *Hdgf* $^{-/-}$; R6/2 mice. While brain dysfunction drives symptomology in HD, growing evidence suggests that systemic signaling and pathology in peripheral tissues can modify HD progression in the CNS (Chuang and Demontis, 2021). Similar to HTT, HDGF is widely expressed in mouse and human body (Abouzied *et al.*, 2004; Uhlén *et al.*, 2015) (Human Protein Atlas available from http://www.proteinatlas.org). Its ubiquitous knockdown could therefore impact HD pathology beyond the brain. The prominent muscle wasting phenotype, however,

seems to be unaffected, since grip strength was not modulated by HDGF depletion (Figure 3.9 D).

Despite these ambiguities, our results clearly reveal the therapeutic potential of HDGF in HD. Not only early treatment with brain-wide delivery of HDGF, but also local striatal treatment after disease onset has proven beneficial for disease progression in R6/2 mice (Figure 3.13). In future experiments, it will be important to validate our findings in a second HD model, preferably a full-length model. Moreover, a more detailed characterization of locomotion including analysis of gait parameters, time until movement initiation and duration of movement bouts will help to clarify how HDGF improves spontaneous locomotor activity. In addition to behavioral studies, monitoring plasma and cerebrospinal fluid levels of neurofilament light chain constitutes an interesting option to consider in future studies. Neurofilament light chain is a prospective HD biomarker (Constantinescu *et al.*, 2009; Vinther-Jensen *et al.*, 2016; Byrne *et al.*, 2017; Niemelä *et al.*, 2017; Soylu-Kucharz *et al.*, 2017; Johnson *et al.*, 2018), which has already been included in Roche's tominersen phase III clinical trial (NCT03761849) and may provide a complementary readout to assess treatment response. Eventually, analysis of molecular markers and electrophysiological properties altered in HD will yield more insights into HDGF induced changes in the brain and could help to elucidate the mechanism of HDGF action.

While we are the first to propose HDGF as candidate for HD therapy, previous studies have revealed therapeutic potential of other neurotrophic factors in HD. One of them is BDNF, which provides trophic support to striatal MSNs through release from cortical afferents (Altar *et al.*, 1997; Baquet, 2004). Defects in BDNF production, transport and signaling have been implicated in HD pathogenesis; hence, restoring BDNF function has emerged as promising therapeutic strategy (Zuccato and Cattaneo, 2009; Kim *et al.*, 2021). Stem cell-based BDNF delivery and LM11A-31, a small molecule normalizing BDNF receptor signaling, have proven beneficial in HD mouse models and are now close to clinical testing in HD (Pollock *et al.*, 2016; Simmons *et al.*, 2016). Another neuroprotective factor suggested for HD therapy is the glial derived neurotrophic factor (GDNF). Favorable effects have been demonstrated in toxin-induced lesion models and transgenic HD mice (Araujo and Hilt, 1997; McBride *et al.*,

2003; Kells *et al.*, 2004; McBride *et al.*, 2006; Ebert *et al.*, 2010; Lin *et al.*, 2019). BDNF and GDNF convey neuroprotection through binding to their cell surface receptors, thereby activating intracellular canonical signaling cascades such as PI3K/AKT and MAPK/ERK pathways (Nasrolahi *et al.*, 2018). In contrast, our results indicate that HDGF exerts its neuroprotective activity independent of PI3K/AKT and MAPK/ERK signaling by a non-canonical mode of action (Figure 3.17). Further exploring the mechanism of HDGF's neuroprotective effects will not only enhance our understanding of HDGF action in the brain, but might also entail new interesting strategies for HD therapy beyond augmenting HDGF levels.

More profound knowledge about the neuroprotective action of HDGF could, for instance, open the door for the development of more convenient small molecule drugs that act in a similar manner as HDGF. Such an approach is attractive, since the delivery of neurotrophic factors to human brain is challenging. Systemic administration is not preferable due to the limited ability of neurotrophic factors to cross the blood-brain barrier, their rapid degradation and potential off-target effects (Thorne and Frey, 2001). Direct delivery of recombinant protein into the brain requires catheter placement and regular infusions or periodical refilling of an implanted pump which possesses the risk of infections (Thorne and Frey, 2001; Lang *et al.*, 2006; Whone *et al.*, 2019). Current clinical trials for AD and PD employ AAV-mediated gene transfer to deliver BDNF and GDNF, respectively (NCT05040217, NCT01621581, NCT04167540). This approach allows continuous and long-lasting expression in the target tissue, however, is still surgically invasive and adjusting or stopping protein expression in case of adverse events is not possible (Hudry and Vandenberghe, 2019). AAV vectors enabling regulable gene expression in humans and less invasive techniques to deliver AAVs to the brain such as focused ultrasound-induced blood-brain barrier opening are under development (Thévenot *et al.*, 2012; Hsu *et al.*, 2013; Lipsman *et al.*, 2018; Abrahao *et al.*, 2019; Domenger and Grimm, 2019; Zhong *et al.*, 2020; Cheng *et al.*, 2021; Gasca-Salas *et al.*, 2021). Meanwhile, brain-penetrant and orally bioavailable small molecules acting similarly as neurotrophic factors might provide the most attractive treatment approach for patients. Several small molecules targeting specific neurotrophin receptors have been developed (Mitra *et al.*, 2019). One of them is LM11A-31-BHS, a

modified version of LM11A-31, which has recently been evaluated in a Phase 1/2 clinical trial for AD with results to be expected soon (NCT03069014). However, to facilitate the development of HDGF mimetics or of drugs acting in a similar manner as HDGF, the mechanism behind HDGF's neuroprotective function needs to be elucidated first.

4.3 HDGF action and neuroprotection

In our study, neuroprotection was conveyed by HDGF located to the nucleus *in vitro* and *in vivo*. This observation, together with the fact that HDGF harbors a PWWP-domain and evidence indicating that HDGF is implicated in chromatin-associated processes (Lukasik *et al.*, 2006; Yang and Everett, 2007; Zhao *et al.*, 2011), suggested that neuroprotective properties are linked to nuclear action of HDGF. In line with this idea, localization to the nucleus was shown to be key for mitogenic activity of HDGF in non-neuronal cells (Everett *et al.*, 2001; Kishima *et al.*, 2002). However, to our surprise, we found that nuclear HDGF and a cytoplasmic HDGF variant had comparable neuroprotective effects when co-expressed with mHTT in primary neuron cultures (Figure 3.16). Hence, nuclear localization of HDGF is not required for neuroprotection.

Although HDGF-injected WT mice were phenotypically normal, we cannot rule out that, over longer time periods, enhanced HDGF activity in the nucleus causes unwanted side effects. Nuclear enlargement was prominent in HDGF-transduced neurons *in vivo* and *in vitro* (Figure 3.14 A, B; 3.15 B, C), a feature reminiscent of pathological rather than physiological cell state (Zink *et al.*, 2004; Dehghani *et al.*, 2018). Homeostasis of nuclear size is tightly controlled in cells, but alteration of bulk nucleocytoplasmic transport, RNA processing, chromatin to cytoskeleton linkage, and membrane expansion can promote size increase (Cantwell and Nurse, 2019). HDGF has been suggested to be involved in such processes, namely, RNA processing and chromatin remodeling (Zhao *et al.*, 2011), which could explain nuclear enlargement upon overexpression. Of note, changes in nuclear morphology are among the abnormalities observed in tumor cells and might directly contribute to tumorigenesis (Zink *et al.*, 2004; Chow *et al.*, 2012). A study from Sedlmaier *et al.* (2011) indicated that

HDGF overexpression per se does not induce cancer formation. However, HDGF is upregulated in various tumors, including hepatocellular carcinoma, breast cancer, Ewing's sarcoma family of tumors, and gliomas (Bao *et al.*, 2014). Increased HDGF expression in cancer tissue is correlated with poor outcome and has been shown to promote tumor growth and metastasis (Bao *et al.*, 2014; Liu *et al.*, 2019; Enomoto *et al.*, 2020; Yang *et al.*, 2021). Interestingly, only nuclear, not cytoplasmic HDGF levels serve as independent prognostic factor in various cancers (Bao *et al.*, 2014), suggesting that especially nuclear HDGF activity drives tumor progression. Here, we show that nuclear expansion is specific to HDGF overexpression in the nucleus. Redirecting HDGF to the cytoplasm prevented nuclear size alterations, but preserved HDGF's neuroprotective properties (Figure 3.15, 3.16). Since safety of therapeutic approaches is key, future studies should focus on cytoplasmic HDGF as candidate for long-term therapeutic use in HD.

Besides direct intracrine action, HDGF might convey neuroprotection in an autocrine and/or paracrine manner. Previous studies have demonstrated neuroprotective effects of recombinant HDGF treatment (Zhou *et al.*, 2004; Marubuchi *et al.*, 2006; Hollander *et al.*, 2012). Similarly, extracellular HDGF improved survival of mHTT-transfected primary neurons in our study (Figure 3.17 B). While PI3K/AKT and MAPK/ERK pathway activity in the retina seems to contribute to HDGF-mediated rescue of retinal ganglion cells after axotomy (Hollander *et al.*, 2012), we did not detect activation of these signaling cascades in cultured neurons following application of recombinant HDGF. Increased PI3K/AKT and MAPK/ERK signaling has been related to HDGF's growth factor activity in mitogenic cells (Everett *et al.*, 2004; Ooi *et al.*, 2010; Wang *et al.*, 2011; Kung *et al.*, 2012; Giri *et al.*, 2016), and might contribute to retinal neuroprotection mediated by glial cells (García-Bermúdez *et al.*, 2021). Our findings, however, suggest that direct survival-promoting effects on neurons through HDGF are independent of these canonical signaling pathways. Recently, another growth factor, insulin-like growth factor 2 (IGF2), was also proposed to act through a non-canonical mechanism. IGF2 reduces mHTT aggregation by stimulating secretion of soluble mHTT species via exosomes and microvesicles (García-Huerta *et al.*, 2020). Contrary to IGF2, extracellular application of HDGF does not alter the frequency of mHTT aggregates,

despite promoting neuronal viability (Figure 3.17 B, C). Hence, how HDGF conveys neuroprotection remains unclear. Whether receptor-mediated signaling pathways play a role, or if neuroprotection against mHTT toxicity requires internalization of extracellular HDGF needs to be addressed in future studies.

An HDGF-interacting protein of interest is nucleolin, which can act as cell surface receptor for extracellular HDGF and forms intracellular ribonucleoprotein complexes with HDGF (Bremer *et al.*, 2013; Chen *et al.*, 2015). Nucleolin is a multifaceted protein and known to stabilize B cell lymphoma 2 (BCL2) mRNA, thereby increasing expression of the anti-apoptotic BCL2 protein (Sengupta *et al.*, 2004; Otake *et al.*, 2007; Ishimaru *et al.*, 2010; Jia *et al.*, 2017). Notably, intracellular HDGF-nucleolin complex formation involves BCL2 mRNA (Bremer *et al.*, 2013). In future, it will be exciting to explore whether HDGF provides neuroprotection in a nucleolin-dependent manner.

Overall, HDGF is a versatile protein, which functions are barely studied in the nervous system despite widespread neuronal expression. This study underscores HDGF's neuroprotective properties and unravels its potential to enhance neuronal resistance in HD. In future studies, it will be interesting to explore the neuroprotective ability of HDGF beyond HD in other neurodegenerative diseases.

REFERENCES

Abouzied MM, Baader SL, Dietz F, Kappler J, Gieselmann V, Franken S (2004) Expression patterns and different subcellular localization of the growth factors HDGF (hepatoma-derived growth factor) and HRP-3 (HDGF-related protein-3) suggest functions in addition to their mitogenic activity. *Biochem J* 378:169-176.

Abouzied MM, El-Tahir HM, Gieselmann V, Franken S (2010) Hepatoma-derived growth factor-related protein-3: A new neurotrophic and neurite outgrowth-promoting factor for cortical neurons. *J Neurosci Res* 88:3610-3620.

Abrahao A, Meng Y, Llinas M, Huang Y, Hamani C, Mainprize T, Aubert I, Heyn C, Black SE, Hynynen K, Lipsman N, Zinman L (2019) First-in-human trial of blood–brain barrier opening in amyotrophic lateral sclerosis using MR-guided focused ultrasound. *Nat Commun* 10:4373.

Achenbach J, Thiels C, Lücke T, Saft C (2020) Clinical Manifestation of Juvenile and Pediatric HD Patients: A Retrospective Case Series. *Brain Sci* 10:340.

Alexander GE, Crutcher MD (1990) Functional architecture of basal ganglia circuits: neural substrates of parallel processing. *Trends Neurosci* 13:266-271.

Altar CA, Cai N, Bliven T, Juhasz M, Conner JM, Acheson AL, Lindsay RM, Wiegand SJ (1997) Anterograde transport of brain-derived neurotrophic factor and its role in the brain. *Nature* 389:856-860.

Ambrose CM, Duyao MP, Barnes G, Bates GP, Lin CS, Srinidhi J, Baxendale S, Hummerich H, Lehrach H, Altherr M, Wasmuth J, Buckler A, Church D, Housman D, Berks M, Micklem G, Durbin R, Dodge A, Read A, Gusella J, Macdonald ME (1994) Structure and expression of the Huntington's disease gene: Evidence against simple inactivation due to an expanded CAG repeat. *Somat Cell Mol Genet* 20:27-38.

Andrew SE, Goldberg YP, Kremer B, Telenius H, Theilmann J, Adam S, Starr E, Squitieri F, Lin B, Kalchman MA, Graham RK, Hayden MR (1993) The relationship between trinucleotide (CAG) repeat length and clinical features of Huntington's disease. *Nat Genet* 4:398-403.

Araujo DM, Hilt DC (1997) Glial cell line-derived neurotrophic factor attenuates the excitotoxin-induced behavioral and neurochemical deficits in a rodent model of Huntington's disease. *Neuroscience* 81:1099-1110.

Bañez-Coronel M, Ayhan F, Tarabochia AD, Zu T, Perez BA, Khoramian Tusi S, Pletnikova O, Borchelt DR, Ross CA, Margolis RL, Yachnis AT, Troncoso JC, Ranum LPW (2015) RAN Translation in Huntington Disease. *Neuron* 88:667-677.

Bao C, Wang J, Ma W, Wang X, Cheng Y (2014) HDGF: a novel jack-of-all-trades in cancer. *Future Oncol* 10:2675-2685.

Baquet ZC (2004) Early Striatal Dendrite Deficits followed by Neuron Loss with Advanced Age in the Absence of Anterograde Cortical Brain-Derived Neurotrophic Factor. *J Neurosci* 24:4250-4258.

Barron JC, Hurley EP, Parsons MP (2021) Huntingtin and the Synapse. *Front Cell Neurosci* 15:689332.

Bianchi ME (2007) DAMPs, PAMPs and alarmins: all we need to know about danger. *J Leukoc Biol* 81:1-5.

Bremer S, Klein K, Sedlmaier A, Abouzied M, Gieselmann V, Franken S (2013) Hepatoma-derived growth factor and nucleolin exist in the same ribonucleoprotein complex. *BMC Biochem* 14:2.

Byrne LM, Rodrigues FB, Blennow K, Durr A, Leavitt BR, Roos RAC, Scahill RI, Tabrizi SJ, Zetterberg H, Langbehn D, Wild EJ (2017) Neurofilament light protein in blood as a potential biomarker of neurodegeneration in Huntington's disease: a retrospective cohort analysis. *Lancet Neurol* 16:601-609.

Cantwell H, Nurse P (2019) Unravelling nuclear size control. *Curr Genet* 65:1281-1285.

Carter RJ, Lione LA, Humby T, Mangiarini L, Mahal A, Bates GP, Dunnett SB, Morton AJ (1999) Characterization of Progressive Motor Deficits in Mice Transgenic for the Human Huntington's Disease Mutation. *J Neurosci* 19:3248-3257.

Cepeda-Prado E, Popp S, Khan U, Stefanov D, Rodriguez J, Menalled LB, Dow-Edwards D, Small SA, Moreno H (2012) R6/2 Huntington's Disease Mice Develop Early and Progressive Abnormal Brain Metabolism and Seizures. *J Neurosci* 32:6456-6467.

Chang R, Liu X, Li S, Li XJ (2015) Transgenic animal models for study of the pathogenesis of Huntington's disease and therapy. *Drug Des Devel Ther* 9:2179-2188.

CHDI Foundation (2021) 16th Annual HD Therapeutics Conference. https://chdifoundation.org/2021-conference/ (Accessed: 09 November 2021).

Chen SC, Hu TH, Huang CC, Kung ML, Chu TH, Yi LN, Huang ST, Chan HH, Chuang JH, Liu LF, Wu HC, Wu DC, Chang MC, Tai MH (2015) Hepatoma-derived growth factor/nucleolin axis as a novel oncogenic pathway in liver carcinogenesis. *Oncotarget* 6:16253-16270.

Cheng S, van Gaalen MM, Bähr M, Garea-Rodriguez E, Kügler S (2021) Optimized pharmacological control over the AAV-Gene-Switch vector for regulable gene therapy. *Mol Ther Methods Clin Dev* 23:1-10.

Chow KH, Factor RE, Ullman KS (2012) The nuclear envelope environment and its cancer connections. *Nat Rev Cancer* 12:196-209.

Chuang CL, Demontis F (2021) Systemic manifestation and contribution of peripheral tissues to Huntington's disease pathogenesis. *Ageing Res Rev* 69:101358.

Cloud LJ, Rosenblatt A, Margolis RL, Ross CA, Pillai JA, Corey-Bloom J, Tully HM, Bird T, Panegyres PK, Nichter CA, Higgins DS, Helmers SL, Factor SA, Jones R, Testa CM (2012) Seizures in juvenile Huntington's disease: Frequency and characterization in a multicenter cohort. *Mov Disord* 27:1797-1800.

Constantinescu R, Romer M, Oakes D, Rosengren L, Kieburtz K (2009) Levels of the light subunit of neurofilament triplet protein in cerebrospinal fluid in Huntington's disease. *Parkinsonism Relat Disord* 15:245-248.

Cowin RM, Bui N, Graham D, Green JR, Grueninger S, Yuva-Paylor LA, Syed AU, Weiss A, Paylor R (2011) Onset and progression of behavioral and molecular phenotypes in a novel congenic R6/2 line exhibiting intergenerational CAG repeat stability. *PLoS One* 6:e28409.

Cummings DM, Alaghband Y, Hickey MA, Joshi PR, Hong SC, Zhu C, Ando TK, André VM, Cepeda C, Watson JB, Levine MS (2012) A critical window of CAG repeat-length correlates with phenotype severity in the R6/2 mouse model of Huntington's disease. *J Neurophysiol* 107:677-691.

Davies SW, Turmaine M, Cozens BA, Difiglia M, Sharp AH, Ross CA, Scherzinger E, Wanker EE, Mangiarini L, Bates GP (1997) Formation of Neuronal Intranuclear Inclusions Underlies the Neurological Dysfunction in Mice Transgenic for the HD Mutation. *Cell* 90:537-548.

Dehghani A, Karatas H, Can A, Erdemli E, Yemisci M, Eren-Kocak E, Dalkara T (2018) Nuclear expansion and pore opening are instant signs of neuronal hypoxia and can identify poorly fixed brains. *Sci Rep* 8:14770.

Dietz F, Franken S, Yoshida K, Nakamura H, Kappler J, Gieselmann V (2002) The family of hepatoma-derived growth factor proteins: characterization of a new member HRP-4 and classification of its subfamilies. *Biochem J* 366:491-500.

DiFiglia M, Sapp E, Chase KO, Davies SW, Bates GP, Vonsattel JP, Aronin N (1997) Aggregation of huntingtin in neuronal intranuclear inclusions and dystrophic neurites in brain. *Science* 277:1990-1993.

Djoussé L, Knowlton B, Hayden M, Almqvist EW, Brinkman R, Ross C, Margolis R, Rosenblatt A, Durr A, Dode C, Morrison PJ, Novelletto A, Frontali M, Trent RJA, McCusker E, Gómez-Tortosa E, Mayo D, Jones R, Zanko A, Nance M, Abramson R, Suchowersky O, Paulsen J, Harrison M, Yang Q, Cupples LA, Gusella JF, Macdonald ME, Myers RH (2003) Interaction of normal and expanded CAG repeat sizes influences age at onset of Huntington disease. *Am J Med Genet A* 119A:279-282.

Dodds L, Chen J, Berggren K, Fox J (2014) Characterization of Striatal Neuronal Loss and Atrophy in the R6/2 Mouse Model of Huntington's Disease. *PLoS Curr* 6.

Domenger C, Grimm D (2019) Next-generation AAV vectors—do not judge a virus (only) by its cover. *Hum Mol Genet* 28:R3-R14.

Dragatsis I, Goldowitz D, Del Mar N, Deng YP, Meade CA, Liu L, Sun Z, Dietrich P, Yue J, Reiner A (2009) CAG repeat lengths ≥335 attenuate the phenotype in the R6/2 Huntington's disease transgenic mouse. *Neurobiol Dis* 33:315-330.

Duyao MP, Auerbach AB, Ryan A, Persichetti F, Barnes GT, McNeil SM, Ge P, Vonsattel JP, Gusella JF, Joyner AL, MacDonald ME (1995) Inactivation of the mouse Huntington's disease gene homolog Hdh. *Science* 269:407-410.

Ebert AD, Barber AE, Heins BM, Svendsen CN (2010) Ex vivo delivery of GDNF maintains motor function and prevents neuronal loss in a transgenic mouse model of Huntington's disease. *Exp Neurol* 224:155-162.

El-Tahir HM, Dietz F, Dringen R, Schwabe K, Strenge K, Kelm S, Abouzied MM, Gieselmann V, Franken S (2006) Expression of hepatoma-derived growth factor family members in the adult central nervous system. *BMC Neurosci* 7:6.

El-Tahir HM, Abouzied MM, Gallitzendoerfer R, Gieselmann V, Franken S (2009) Hepatoma-derived growth factor-related protein-3 interacts with microtubules and promotes neurite outgrowth in mouse cortical neurons. *J Biol Chem* 284:11637-11651.

Enomoto H, Nakamura H, Nishikawa H, Nishiguchi S, Iijima H (2020) Hepatoma-Derived Growth Factor: An Overview and Its Role as a Potential Therapeutic Target Molecule for Digestive Malignancies. *Int J Mol Sci* 21:4216.

Everett AD, Lobe DR, Matsumura ME, Nakamura H, McNamara CA (2000) Hepatoma-derived growth factor stimulates smooth muscle cell growth and is expressed in vascular development. *J Clin Invest* 105:567-575.

Everett AD, Stoops T, McNamara CA (2001) Nuclear Targeting Is Required for Hepatoma-derived Growth Factor-stimulated Mitogenesis in Vascular Smooth Muscle Cells. *J Biol Chem* 276:37564-37568.

Everett AD, Narron JV, Stoops T, Nakamura H, Tucker A (2004) Hepatoma-derived growth factor is a pulmonary endothelial cell-expressed angiogenic factor. *Am J Physiol Lung Cell Mol Physiol* 286:L1194-1201.

Flower M, Lomeikaite V, Ciosi M, Cumming S, Morales F, Lo K, Hensman Moss D, Jones L, Holmans P, the TRACK-HD Investigators, the OPTIMISTIC Consortium, Monckton DG, Tabrizi SJ (2019) MSH3 modifies somatic instability and disease severity in Huntington's and myotonic dystrophy type 1. *Brain* 142:1876-1886.

Foroud T, Gray J, Ivashina J, Conneally PM (1999) Differences in duration of Huntington's disease based on age at onset. *J Neurol Neurosurg Psychiatry* 66:52-56.

Fu H, Hardy J, Duff KE (2018) Selective vulnerability in neurodegenerative diseases. *Nat Neurosci* 21:1350-1358.

Fusilli C, Migliore S, Mazza T, Consoli F, De Luca A, Barbagallo G, Ciammola A, Gatto EM, Cesarini M, Etcheverry JL, Parisi V, Al-Oraimi M, Al-Harrasi S, Al-Salmi Q, Marano M, Vonsattel JPG, Sabatini U, Landwehrmeyer GB, Squitieri F (2018) Biological and clinical manifestations of juvenile Huntington's disease: a retrospective analysis. *Lancet Neurol* 17:986-993.

Gallitzendoerfer R, Abouzied MM, Hartmann D, Dobrowolski R, Gieselmann V, Franken S (2008) Hepatoma-derived growth factor (HDGF) is dispensable for normal mouse development. *Dev Dyn* 237:1875-1885.

Gan L, Cookson MR, Petrucelli L, La Spada AR (2018) Converging pathways in neurodegeneration, from genetics to mechanisms. *Nat Neurosci* 21:1300-1309.

García-Bermúdez MY, Freude KK, Mouhammad ZA, van Wijngaarden P, Martin KK, Kolko M (2021) Glial Cells in Glaucoma: Friends, Foes, and Potential Therapeutic Targets. *Front Neurol* 12:624983.

García-Huerta P, Troncoso-Escudero P, Wu D, Thiruvalluvan A, Cisternas-Olmedo M, Henríquez DR, Plate L, Chana-Cuevas P, Saquel C, Thielen P, Longo KA, Geddes BJ, Lederkremer GZ, Sharma N, Shenkman M, Naphade S, Sardi SP, Spichiger C, Richter HG, Court FA, Tshilenge KT, Ellerby LM, Wiseman RL, Gonzalez-Billault C, Bergink S, Vidal RL, Hetz C (2020) Insulin-like growth factor 2 (IGF2) protects against Huntington's disease through the extracellular disposal of protein aggregates. *Acta Neuropathol* 140:737-764.

Gasca-Salas C, Fernández-Rodríguez B, Pineda-Pardo JA, Rodríguez-Rojas R, Obeso I, Hernández-Fernández F, Del Álamo M, Mata D, Guida P, Ordás-Bandera C, Montero-Roblas JI, Martínez-Fernández R, Foffani G, Rachmilevitch I, Obeso JA (2021) Blood-brain barrier opening with focused ultrasound in Parkinson's disease dementia. *Nat Commun* 12:779.

Genetic Modifiers of Huntington's Disease (GeM-HD) Consortium (2015) Identification of Genetic Factors that Modify Clinical Onset of Huntington's Disease. *Cell* 162:516-526.

Genetic Modifiers of Huntington's Disease (GeM-HD) Consortium (2019) CAG Repeat Not Polyglutamine Length Determines Timing of Huntington's Disease Onset. *Cell* 178:887-900.e14.

Giri K, Pabelick CM, Mukherjee P, Prakash YS (2016) Hepatoma derived growth factor (HDGF) dynamics in ovarian cancer cells. *Apoptosis* 21:329-339.

Goedhart J, von Stetten D, Noirclerc-Savoye M, Lelimousin M, Joosen L, Hink MA, van Weeren L, Gadella TWJ, Royant A (2012) Structure-guided evolution of cyan fluorescent proteins towards a quantum yield of 93%. *Nat Commun* 3:751.

Goodman RA, Lochner KA, Thambisetty M, Wingo TS, Posner SF, Ling SM (2017) Prevalence of dementia subtypes in United States Medicare fee-for-service beneficiaries, 2011–2013. *Alzheimers Dement* 13:28-37.

Goold R, Flower M, Moss DH, Medway C, Wood-Kaczmar A, Andre R, Farshim P, Bates GP, Holmans P, Jones L, Tabrizi SJ (2019) FAN1 modifies Huntington's disease progression by stabilizing the expanded HTT CAG repeat. *Hum Mol Genet* 28:650-661.

Gray M, Shirasaki DI, Cepeda C, André VM, Wilburn B, Lu XH, Tao J, Yamazaki I, Li SH, Sun YE, Li XJ, Levine MS, Yang XW (2008) Full-Length Human Mutant Huntingtin with a Stable Polyglutamine Repeat Can Elicit Progressive and Selective Neuropathogenesis in BACHD Mice. *J Neurosci* 28:6182-6195.

Grondin R, Kaytor MD, Ai Y, Nelson PT, Thakker DR, Heisel J, Weatherspoon MR, Blum JL, Burright EN, Zhang Z, Kaemmerer WF (2012) Six-month partial suppression of Huntingtin is well tolerated in the adult rhesus striatum. *Brain* 135:1197-1209.

Gusella JF, Wexler NS, Conneally PM, Naylor SL, Anderson MA, Tanzi RE, Watkins PC, Ottina K, Wallace MR, Sakaguchi AY, Young AB, Shoulson I, Bonilla E, Martin JB (1983) A polymorphic DNA marker genetically linked to Huntington's disease. *Nature* 306:234-238.

Gutekunst CA, Li SH, Yi H, Mulroy JS, Kuemmerle S, Jones R, Rye D, Ferrante RJ, Hersch SM, Li XJ (1999) Nuclear and neuropil aggregates in Huntington's disease: relationship to neuropathology. *J Neurosci* 19:2522-2534.

Gutiérrez-Ángel S (2019) Mutant Huntingtin toxicity modifiers revealed by a spatiotemporal proteomic profiling. Dissertation, LMU Munich: Faculty of Biology.

Hackam AS, Singaraja R, Wellington CL, Metzler M, McCutcheon K, Zhang T, Kalchman M, Hayden MR (1998) The Influence of Huntingtin Protein Size on Nuclear Localization and Cellular Toxicity. *J Cell Biol* 141:1097-1105.

Han I, You Y, Kordower JH, Brady ST, Morfini GA (2010) Differential vulnerability of neurons in Huntington's disease: the role of cell type-specific features. *J Neurochem* 113:1073-1091.

Hedreen JC, Peyser CE, Folstein SE, Ross CA (1991) Neuronal loss in layers V and VI of cerebral cortex in Huntington's disease. *Neurosci Lett* 133:257-261.

Heemskerk AW, Roos RAC (2012) Aspiration pneumonia and death in Huntington's disease. *PLoS Curr* 4:RRN1293.

Hipp MS, Patel CN, Bersuker K, Riley BE, Kaiser SE, Shaler TA, Brandeis M, Kopito RR (2012) Indirect inhibition of 26S proteasome activity in a cellular model of Huntington's disease. *J Cell Biol* 196:573-587.

Hodgson JG, Agopyan N, Gutekunst CA, Leavitt BR, LePiane F, Singaraja R, Smith DJ, Bissada N, McCutcheon K, Nasir J, Jamot L, Li XJ, Stevens ME, Rosemond E, Roder JC, Phillips AG, Rubin EM, Hersch SM, Hayden MR (1999) A YAC Mouse Model for Huntington's Disease with Full-Length Mutant Huntingtin, Cytoplasmic Toxicity, and Selective Striatal Neurodegeneration. *Neuron* 23:181-192.

Hoffmann J (1888) Ueber Chorea chronica progressiva (Huntington'sche Chorea, Chorea hereditaria). *Arch Pathol Anat Physiol Klin Med* 111:513-548.

Hoffner G, Island ML, Djian P (2005) Purification of neuronal inclusions of patients with Huntington's disease reveals a broad range of N-terminal fragments of expanded huntingtin and insoluble polymers. *J Neurochem* 95:125-136.

Hollander A, D'Onofrio PM, Magharious MM, Lysko MD, Koeberle PD (2012) Quantitative retinal protein analysis after optic nerve transection reveals a neuroprotective role for hepatoma-derived growth factor on injured retinal ganglion cells. *Invest Ophthalmol Vis Sci* 53:3973-3989.

Hsu PH, Wei KC, Huang CY, Wen CJ, Yen TC, Liu CL, Lin YT, Chen JC, Shen CR, Liu HL (2013) Noninvasive and Targeted Gene Delivery into the Brain Using Microbubble-Facilitated Focused Ultrasound. *PLoS One* 8:e57682.

Hudry E, Vandenberghe LH (2019) Therapeutic AAV Gene Transfer to the Nervous System: A Clinical Reality. *Neuron* 101:839-862.

Huntington G (2003) On Chorea. *J Neuropsychiatry Clin Neurosci* 15:109-112.

Ishimaru D, Zuraw L, Ramalingam S, Sengupta TK, Bandyopadhyay S, Reuben A, Fernandes DJ, Spicer EK (2010) Mechanism of Regulation of bcl-2 mRNA by Nucleolin and A+U-rich Element-binding Factor 1 (AUF1). *J Biol Chem* 285:27182-27191.

Jeong H, Cohen DE, Cui L, Supinski A, Savas JN, Mazzulli JR, Yates JR, Bordone L, Guarente L, Krainc D (2012) Sirt1 mediates neuroprotection from mutant huntingtin by activation of the TORC1 and CREB transcriptional pathway. *Nat Med* 18:159-165.

Jia W, Yao Z, Zhao J, Guan Q, Gao L (2017) New perspectives of physiological and pathological functions of nucleolin (NCL). *Life Sci* 186:1-10.

Johnson EB, Byrne LM, Gregory S, Rodrigues FB, Blennow K, Durr A, Leavitt BR, Roos RA, Zetterberg H, Tabrizi SJ, Scahill RI, Wild EJ (2018) Neurofilament light protein in blood predicts regional atrophy in Huntington disease. *Neurology* 90:e717-e723.

Kells AP, Fong DM, Dragunow M, During MJ, Young D, Connor B (2004) AAV-Mediated gene delivery of BDNF or GDNF is neuroprotective in a model of huntington disease. *Mol Ther* 9:682-688.

Kennedy L, Evans E, Chen CM, Craven L, Detloff PJ, Ennis M, Shelbourne PF (2003) Dramatic tissue-specific mutation length increases are an early molecular event in Huntington disease pathogenesis. *Hum Mol Genet* 12:3359-3367.

Keum JW, Shin A, Gillis T, Mysore JS, Elneel KA, Lucente D, Hadzi T, Holmans P, Jones L, Orth M, Kwak S, McDonald ME, Gusella JF, Lee JM (2016) The HTT CAG-Expansion Mutation Determines Age at Death but Not Disease Duration in Huntington Disease. *Am J Hum Genet* 98:287-298.

Khristich AN, Mirkin SM (2020) On the wrong DNA track: Molecular mechanisms of repeat-mediated genome instability. *J Biol Chem* 295:4134-4170.

Kiernan MC, Vucic S, Cheah BC, Turner MR, Eisen A, Hardiman O, Burrell JR, Zoing MC (2011) Amyotrophic lateral sclerosis. *Lancet* 377:942-955.

Kim A, Lalonde K, Truesdell A, Gomes Welter P, Brocardo PS, Rosenstock TR, Gil-Mohapel J (2021) New Avenues for the Treatment of Huntington's Disease. *Int J Mol Sci* 22:8363.

Kim JY, Grunke SD, Levites Y, Golde TE, Jankowsky JL (2014) Intracerebroventricular Viral Injection of the Neonatal Mouse Brain for Persistent and Widespread Neuronal Transduction. *J Vis Exp* :51963.

Kishima Y, Yamamoto H, Izumoto Y, Yoshida K, Enomoto H, Yamamoto M, Kuroda T, Ito H, Yoshizaki K, Nakamura H (2002) Hepatoma-derived growth factor stimulates cell growth after translocation to the nucleus by nuclear localization signals. *J Biol Chem* 277:10315-10322.

Kuhn PH, Wang H, Dislich B, Colombo A, Zeitschel U, Ellwart JW, Kremmer E, Roßner S, Lichtenthaler SF (2010) ADAM10 is the physiologically relevant, constitutive α-secretase of the amyloid precursor protein in primary neurons. *EMBO J* 29:3020-3032.

Kumar A, Kumar V, Singh K, Kumar S, Kim YS, Lee YM, Kim JJ (2020) Therapeutic Advances for Huntington's Disease. *Brain Sci* 10:43.

Kumar MJV, Shah D, Giridharan M, Yadav N, Manjithaya R, Clement JP (2021) Spatiotemporal analysis of soluble aggregates and autophagy markers in the R6/2 mouse model. *Sci Rep* 11:96.

Kung ML, Tsai HE, Hu TH, Kuo HM, Liu LF, Chen SC, Lin PR, Ma YL, Wang EM, Liu GS, Liu JK, Tai MH (2012) Hepatoma-derived growth factor stimulates podosome rosettes formation in NIH/3T3 cells through the activation of phosphatidylinositol 3-kinase/Akt pathway. *Biochem Biophys Res Commun* 425:169-176.

Laforet GA, Sapp E, Chase K, McIntyre C, Boyce FM, Campbell M, Cadigan BA, Warzecki L, Tagle DA, Reddy PH, Cepeda C, Calvert CR, Jokel ES, Klapstein GJ, Ariano MA, Levine MS, DiFiglia M, Aronin N (2001) Changes in Cortical and Striatal Neurons Predict Behavioral and Electrophysiological Abnormalities in a Transgenic Murine Model of Huntington's Disease. *J Neurosci* 21:9112-9123.

Landles C, Sathasivam K, Weiss A, Woodman B, Moffitt H, Finkbeiner S, Sun B, Gafni J, Ellerby LM, Trottier Y, Richards WG, Osmand A, Paganetti P, Bates GP (2010) Proteolysis of Mutant Huntingtin Produces an Exon 1 Fragment That Accumulates as an Aggregated Protein in Neuronal Nuclei in Huntington Disease. *J Biol Chem* 285:8808-8823.

Landles C, Milton RE, Ali N, Flomen R, Flower M, Schindler F, Gomez-Paredes C, Bondulich MK, Osborne GF, Goodwin D, Salsbury G, Benn CL, Sathasivam K, Smith EJ, Tabrizi SJ, Wanker EE, Bates GP (2020) Subcellular Localization And Formation Of Huntingtin Aggregates Correlates With Symptom Onset And Progression In A Huntington'S Disease Model. *Brain Commun* 2:fcaa066.

Lang AE, Gill S, Patel NK, Lozano A, Nutt JG, Penn R, Brooks DJ, Hotton G, Moro E, Heywood P, Brodsky MA, Burchiel K, Kelly P, Dalvi A, Scott B, Stacy M, Turner D, Wooten VGF, Elias WJ, Laws ER, Dhawan V, Stoessl AJ, Matcham J, Coffey RJ, Traub M (2006) Randomized controlled trial of intraputamenal glial cell line-derived neurotrophic factor infusion in Parkinson disease. *Ann Neurol* 59:459-466.

Larson E, Fyfe I, Morton AJ, Monckton DG (2015) Age-, tissue- and length-dependent bidirectional somatic CAG•CTG repeat instability in an allelic series of R6/2 Huntington disease mice. *Neurobiol Dis* 76:98-111.

Lieberman AP, Shakkottai VG, Albin RL (2019) Polyglutamine Repeats in Neurodegenerative Diseases. *Annu Rev Pathol* 14:1-27.

Lin CY, Tsai CH, Feng LY, Chai WY, Lin CJ, Huang CY, Wei KC, Yeh CK, Chen CM, Liu HL (2019) Focused ultrasound-induced blood brain-barrier opening enhanced vascular permeability for GDNF delivery in Huntington's disease mouse model. *Brain Stimul* 12:1143-1150.

Lipsman N, Meng Y, Bethune AJ, Huang Y, Lam B, Masellis M, Herrmann N, Heyn C, Aubert I, Boutet A, Smith GS, Hynynen K, Black SE (2018) Blood–brain barrier opening in Alzheimer's disease using MR-guided focused ultrasound. *Nat Commun* 9:2336.

Liu C, Wang L, Jiang Q, Zhang J, Zhu L, Lin L, Jiang H, Lin D, Xiao Y, Fang W, Guo S (2019) Hepatoma-Derived Growth Factor and DDX5 Promote Carcinogenesis and Progression of Endometrial Cancer by Activating beta-Catenin. *Front Oncol* 9:211.

Lukasik SM, Cierpicki T, Borloz M, Grembecka J, Everett A, Bushweller JH (2006) High resolution structure of the HDGF PWWP domain: A potential DNA binding domain. *Protein Sci* 15:314-323.

Macdonald V, Halliday G (2002) Pyramidal Cell Loss in Motor Cortices in Huntington's Disease. *Neurobiol Dis* 10:378-386.

Madisen L, Zwingman TA, Sunkin SM, Oh SW, Zariwala HA, Gu H, Ng LL, Palmiter RD, Hawrylycz MJ, Jones AR, Lein ES, Zeng H (2010) A robust and high-throughput Cre reporting and characterization system for the whole mouse brain. *Nat Neurosci* 13:133-140.

Malik I, Kelley CP, Wang ET, Todd PK (2021) Molecular mechanisms underlying nucleotide repeat expansion disorders. *Nat Rev Mol Cell Biol* 22:589-607.

Mangiarini L, Sathasivam K, Seller M, Cozens B, Harper A, Hetherington C, Lawton M, Trottier Y, Lehrach H, Davies SW, Bates GP (1996) Exon 1 of the HD gene with an expanded CAG repeat is sufficient to cause a progressive neurological phenotype in transgenic mice. *Cell* 87:493-506.

Mangiarini L, Sathasivam K, Mahal A, Mott R, Seller M, Bates GP (1997) Instability of highly expanded CAG repeats in mice transgenic for the Huntington's disease mutation. *Nat Genet* 15:197-200.

Marubuchi S, Okuda T, Tagawa K, Enokido Y, Horiuchi D, Shimokawa R, Tamura T, Qi ML, Eishi Y, Watabe K, Shibata M, Nakagawa M, Okazawa H (2006) Hepatoma-derived growth factor, a new trophic factor for motor neurons, is up-regulated in the spinal cord of PQBP-1 transgenic mice before onset of degeneration. *J Neurochem* 99:70-83.

May S, Hornburg D, Schludi MH, Arzberger T, Rentzsch K, Schwenk BM, Grässer FA, Mori K, Kremmer E, Banzhaf-Strathmann J, Mann M, Meissner F, Edbauer D (2014) C9orf72 FTLD/ALS-associated Gly-Ala dipeptide repeat proteins cause neuronal toxicity and Unc119 sequestration. *Acta Neuropathol* 128:485-503.

McBride JL, During MJ, Wuu J, Chen EY, Leurgans SE, Kordower JH (2003) Structural and functional neuroprotection in a rat model of Huntington's disease by viral gene transfer of GDNF. *Exp Neurol* 181:213-223.

McBride JL, Ramaswamy S, Gasmi M, Bartus RT, Herzog CD, Brandon EP, Zhou L, Pitzer MR, Berry-Kravis EM, Kordower JH (2006) Viral delivery of glial cell line-derived neurotrophic factor improves behavior and protects striatal neurons in a mouse model of Huntington's disease. *Proc Natl Acad Sci U S A* 103:9345-9350.

McBride JL, Pitzer MR, Boudreau RL, Dufour B, Hobbs T, Ojeda SR, Davidson BL (2011) Preclinical Safety of RNAi-Mediated HTT Suppression in the Rhesus Macaque as a Potential Therapy for Huntington's Disease. *Mol Ther* 19:2152-2162.

McColgan P, Tabrizi SJ (2018) Huntington's disease: a clinical review. *Eur J Neurol* 25:24-34.

Menalled L, El-Khodor BF, Patry M, Suárez-Fariñas M, Orenstein SJ, Zahasky B, Leahy C, Wheeler V, Yang XW, MacDonald M, Morton AJ, Bates G, Leeds J, Park L, Howland D, Signer E, Tobin A, Brunner D (2009) Systematic behavioral evaluation of Huntington's disease transgenic and knock-in mouse models. *Neurobiol Dis* 35:319-336.

Mitra S, Behbahani H, Eriksdotter M (2019) Innovative Therapy for Alzheimer's Disease-With Focus on Biodelivery of NGF. *Front Neurosci* 13:38.

Morton AJ, Lagan MA, Skepper JN, Dunnett SB (2000) Progressive formation of inclusions in the striatum and hippocampus of mice transgenic for the human Huntington's disease mutation. *J Neurocytol* 29:679-702.

Morton AJ, Glynn D, Leavens W, Zheng Z, Faull RLM, Skepper JN, Wight JM (2009) Paradoxical delay in the onset of disease caused by super-long CAG repeat expansions in R6/2 mice. *Neurobiol Dis* 33:331-341.

Moss DJH, Pardiñas AF, Langbehn D, Lo K, Leavitt BR, Roos R, Durr A, Mead S, the TRACK-HD Investigators, the REGISTRY Investigators, Holmans P, Jones L, Tabrizi SJ (2017) Identification of genetic variants associated with Huntington's disease progression: a genome-wide association study. *Lancet Neurol* 16:701-711.

Nakamura H, Izumoto Y, Kambe H, Kuroda T, Mori T, Kawamura K, Yamamoto H, Kishimoto T (1994) Molecular cloning of complementary DNA for a novel human hepatoma-derived growth factor. Its homology with high mobility group-1 protein. *J Biol Chem* 269:25143-25149.

Nance MA, Seltzer W, Ashizawa T, Bennett R, McIntosh N, Myers RH, Potter NT, Shea DK (1998) Laboratory Guidelines for Huntington Disease Genetic Testing. *Am J Hum Genet* 62:1243-1247.

Nasir J, Floresco SB, O'Kusky JR, Diewert VM, Richman JM, Zeisler J, Borowski A, Marth JD, Phillips AG, Hayden MR (1995) Targeted disruption of the Huntington's disease gene results in embryonic lethality and behavioral and morphological changes in heterozygotes. *Cell* 81:811-823.

Nasrolahi A, Mahmoudi J, Akbarzadeh A, Karimipour M, Sadigh-Eteghad S, Salehi R, Farhoudi M (2018) Neurotrophic factors hold promise for the future of Parkinson's disease treatment: is there a light at the end of the tunnel? *Rev Neurosci* 29:475-489.

Neueder A, Landles C, Ghosh R, Howland D, Myers RH, Faull RLM, Tabrizi SJ, Bates GP (2017) The pathogenic exon 1 HTT protein is produced by incomplete splicing in Huntington's disease patients. *Sci Rep* 7:1307.

Niemelä V, Landtblom AM, Blennow K, Sundblom J (2017) Tau or neurofilament light—Which is the more suitable biomarker for Huntington's disease? *PLoS One* 12:e0172762.

Nopoulos PC, Aylward EH, Ross CA, Johnson HJ, Magnotta VA, Juhl AR, Pierson RK, Mills J, Langbehn DR, Paulsen JS, the PREDICT-HD Investigators Coordinators of the Huntington Study Group (HSG) (2010) Cerebral cortex structure in prodromal Huntington disease. *Neurobiol Dis* 40:544-554.

Nüße J, Mirastschijski U, Waespy M, Oetjen J, Brandes N, Rebello O, Paroni F, Kelm S, Dietz F (2016) Two new isoforms of the human hepatoma-derived growth factor interact with components of the cytoskeleton. *Biol Chem* 397:417-436.

Nüße J, Blumrich EM, Mirastschijski U, Kappelmann L, Kelm S, Dietz F (2017) Intra- or extra-exosomal secretion of HDGF isoforms: the extraordinary function of the HDGF-A N-terminal peptide. *Biol Chem* 398:793-811.

Ojima K, Oe M, Nakajima I, Shibata M, Chikuni K, Muroya S, Nishimura T (2014) Proteomic analysis of secreted proteins from skeletal muscle cells during differentiation. *EuPA Open Proteom* 5:1-9.

Oliver JA, Al-Awqati Q (1998) An endothelial growth factor involved in rat renal development. *J Clin Invest* 102:1208-1219.

Ooi BNS, Mukhopadhyay A, Masilamani J, Do DV, Lim CP, Cao XM, Lim IJ, Mao L, Ren HN, Nakamura H, Phan TT (2010) Hepatoma-derived growth factor and its role in keloid pathogenesis. *J Cell Mol Med* 14:1328-1337.

Ordway JM, Tallaksen-Greene S, Gutekunst CA, Bernstein EM, Cearley JA, Wiener HW, Dure LS, Lindsey R, Hersch SM, Jope RS, Albin RL, Detloff PJ (1997) Ectopically Expressed CAG Repeats Cause Intranuclear Inclusions and a Progressive Late Onset Neurological Phenotype in the Mouse. *Cell* 91:753-763.

Otake Y, Soundararajan S, Sengupta TK, Kio EA, Smith JC, Pineda-Roman M, Stuart RK, Spicer EK, Fernandes DJ (2007) Overexpression of nucleolin in chronic lymphocytic leukemia cells induces stabilization of bcl2 mRNA. *Blood* 109:3069-3075.

Palfi S, Brouillet E, Jarraya B, Bloch J, Jan C, Shin M, Condé F, Li XJ, Aebischer P, Hantraye P, Déglon N (2007) Expression of Mutated Huntingtin Fragment in the Putamen Is Sufficient to Produce Abnormal Movement in Non-human Primates. *Mol Ther* 15:1444-1451.

Pearson CE, Edamura KN, Cleary JD (2005) Repeat instability: mechanisms of dynamic mutations. *Nat Rev Genet* 6:729-742.

Peskett TR, Rau F, O'Driscoll J, Patani R, Lowe AR, Saibil HR (2018) A Liquid to Solid Phase Transition Underlying Pathological Huntingtin Exon1 Aggregation. *Mol Cell* 70:588-601.e6.

Pollock K, Dahlenburg H, Nelson H, Fink KD, Cary W, Hendrix K, Annett G, Torrest A, Deng P, Gutierrez J, Nacey C, Pepper K, Kalomoiris S, Anderson JD, McGee J, Gruenloh W, Fury B, Bauer G, Duffy A, Tempkin T, Wheelock V, Nolta JA (2016) Human Mesenchymal Stem Cells Genetically Engineered to Overexpress Brain-derived Neurotrophic Factor Improve Outcomes in Huntington's Disease Mouse Models. *Mol Ther* 24:965-977.

Postuma RB, Berg D, Stern M, Poewe W, Olanow CW, Oertel W, Obeso J, Marek K, Litvan I, Lang AE, Halliday G, Goetz CG, Gasser T, Dubois B, Chan P, Bloem BR, Adler CH, Deuschl G (2015) MDS clinical diagnostic criteria for Parkinson's disease. *Mov Disord* 30:1591-1601.

Pringsheim T, Wiltshire K, Day L, Dykeman J, Steeves T, Jette N (2012) The incidence and prevalence of Huntington's disease: A systematic review and meta-analysis. *Mov Disord* 27:1083-1091.

Qin S, Min J (2014) Structure and function of the nucleosome-binding PWWP domain. *Trends Biochem Sci* 39:536-547.

Rabouille C (2017) Pathways of Unconventional Protein Secretion. *Trends Cell Biol* 27:230-240.

Ranganathan M, Kostyk SK, Allain DC, Race JA, Daley AM (2021) Age of onset and behavioral manifestations in Huntington's disease: An Enroll-HD cohort analysis. *Clin Genet* 99:133-142.

Reddy PH, Williams M, Charles V, Garrett L, Pike-Buchanan L, Whetsell WO, Miller G, Tagle DA (1998) Behavioural abnormalities and selective neuronal loss in HD transgenic mice expressing mutated full-length HD cDNA. *Nat Genet* 20:198-202.

Reiner A, Albin RL, Anderson KD, D'Amato CJ, Penney JB, Young AB (1988) Differential loss of striatal projection neurons in Huntington disease. *Proc Natl Acad Sci U S A* 85:5733-5737.

Roche (2021) Roche provides update on tominersen programme in manifest Huntington's disease. https://www.roche.com/de/media/releases/med-cor-2021-03-22b.html (Accessed: 09 November 2021).

Rodrigues FB, Abreu D, Damásio J, Goncalves N, Correia-Guedes L, Coelho M, Ferreira JJ, the REGISTRY Investigators of the European Huntington's Disease Network (2017) Survival, Mortality, Causes and Places of Death in a European Huntington's Disease Prospective Cohort. *Mov Disord Clin Pract* 4:737-742.

Rosas HD, Salat DH, Lee SY, Zaleta AK, Pappu V, Fischl B, Greve D, Hevelone N, Hersch SM (2008) Cerebral cortex and the clinical expression of Huntington's disease: complexity and heterogeneity. *Brain* 131:1057-1068.

Rubinsztein DC (2002) Lessons from animal models of Huntington's disease. *Trends Genet* 18:202-209.

Sathasivam K, Neueder A, Gipson TA, Landles C, Benjamin AC, Bondulich MK, Smith DL, Faull RLM, Roos RAC, Howland D, Detloff PJ, Housman DE, Bates GP (2013) Aberrant splicing of HTT generates the pathogenic exon 1 protein in Huntington disease. *Proc Natl Acad Sci U S A* 110:2366-2370.

Saudou F, Finkbeiner S, Devys D, Greenberg ME (1998) Huntingtin Acts in the Nucleus to Induce Apoptosis but Death Does Not Correlate with the Formation of Intranuclear Inclusions. *Cell* 95:55-66.

Saudou F, Humbert S (2016) The Biology of Huntingtin. *Neuron* 89:910-926.

Scherzinger E, Lurz R, Turmaine M, Mangiarini L, Hollenbach B, Hasenbank R, Bates GP, Davies SW, Lehrach H, Wanker EE (1997) Huntingtin-Encoded Polyglutamine Expansions Form Amyloid-like Protein Aggregates In Vitro and In Vivo. *Cell* 90:549-558.

Schilling G, Becher MW, Sharp AH, Jinnah HA, Duan K, Kotzuk JA, Slunt HH, Ratovitski T, Cooper JK, Jenkins NA, Copeland NG, Price DL, Ross CA, Borchelt DR (1999) Intranuclear inclusions and neuritic aggregates in transgenic mice expressing a mutant N-terminal fragment of huntingtin. *Hum Mol Genet* 8:397-407.

Schindelin J, Arganda-Carreras I, Frise E, Kaynig V, Longair M, Pietzsch T, Preibisch S, Rueden C, Saalfeld S, Schmid B, Tinevez JY, White DJ, Hartenstein V, Eliceiri K, Tomancak P, Cardona A (2012) Fiji: an open-source platform for biological-image analysis. *Nat Methods* 9:676-682.

Schulz-Trieglaff EK (2018) Alterations of neuronal activity and protein homeostasis in a mouse model of Huntington's disease. Dissertation, LMU Munich: Faculty of Biology.

Sedlmaier A, Wernert N, Gallitzendörfer R, Abouzied MM, Gieselmann V, Franken S (2011) Overexpression of hepatoma-derived growth factor in melanocytes does not lead to oncogenic transformation. *BMC Cancer* 11:457.

Sengupta TK, Bandyopadhyay S, Fernandes DJ, Spicer EK (2004) Identification of Nucleolin as an AU-rich Element Binding Protein Involved in bcl-2 mRNA Stabilization. *J Biol Chem* 279:10855-10863.

Shelbourne PF, Keller-McGandy C, Bi WL, Yoon SR, Dubeau L, Veitch NJ, Vonsattel JP, Wexler NS, the US-Venezuela Collaborative Research Group, Arnheim N, Augood SJ (2007) Triplet repeat mutation length gains correlate with cell-type specific vulnerability in Huntington disease brain. *Hum Mol Genet* 16:1133-1142.

Sieradzan KA, Mechan AO, Jones L, Wanker EE, Nukina N, Mann DMA (1999) Huntington's Disease Intranuclear Inclusions Contain Truncated, Ubiquitinated Huntingtin Protein. *Exp Neurol* 156:92-99.

Simmons DA, Belichenko NP, Ford EC, Semaan S, Monbureau M, Aiyaswamy S, Holman CM, Condon C, Shamloo M, Massa SM, Longo FM (2016) A small molecule p75NTR ligand normalizes signalling and reduces Huntington's disease phenotypes in R6/2 and BACHD mice. *Hum Mol Genet* 25:4920-4938.

Sørensen SA, Fenger K (1992) Causes of death in patients with Huntington's disease and in unaffected first degree relatives. *J Med Genet* 29:911-914.

Soylu-Kucharz R, Sandelius Å, Sjögren M, Blennow K, Wild EJ, Zetterberg H, Björkqvist M (2017) Neurofilament light protein in CSF and blood is associated with neurodegeneration and disease severity in Huntington's disease R6/2 mice. *Sci Rep* 7:14114.

Squitieri F, Gellera C, Cennella M, Mariotti C, Cislaghi G, Rubinsztein DC, Almqvist EW, Turner D, Bachoud-Lévi AC, Simpson SA, Delatycki M, Maglione V, Hyden MR, Di Donato S (2003) Homozygosity for CAG mutation in Huntington disease is associated with a more severe clinical course. *Brain* 126:946-955.

Stack EC, Kubilus JK, Smith K, Cormier K, Del Signore SJ, Guelin E, Ryu H, Hersch SM, Ferrante RJ (2005) Chronology of behavioral symptoms and neuropathological sequela in R6/2 Huntington's disease transgenic mice. *J Comp Neurol* 490:354-370.

Studier FW (2005) Protein production by auto-induction in high density shaking cultures. *Protein Expr Purif* 41:207-234.

Tabrizi SJ, Langbehn DR, Leavitt BR, Roos RA, Durr A, Craufurd D, Kennard C, Hicks SL, Fox NC, Scahill RI, Borowsky B, Tobin AJ, Rosas HD, Johnson H, Reilmann R, Landwehrmeyer B, Stout JC, the TRACK-HD Investigators (2009) Biological and clinical manifestations of Huntington's disease in the longitudinal TRACK-HD study: cross-sectional analysis of baseline data. *Lancet Neurol* 8:791-801.

Tabrizi SJ, Ghosh R, Leavitt BR (2019a) Huntingtin Lowering Strategies for Disease Modification in Huntington's Disease. *Neuron* 101:801-819.

Tabrizi SJ, Leavitt BR, Landwehrmeyer GB, Wild EJ, Saft C, Barker RA, Blair NF, Craufurd D, Priller J, Rickards H, Rosser A, Kordasiewicz HB, Czech C, Swayze EE, Norris DA, Baumann T, Gerlach I, Schobel SA, Paz E, Smith AV, Bennett CF, Lane RM (2019b) Targeting Huntingtin Expression in Patients with Huntington's Disease. *N Engl J Med* 380:2307-2316.

Taniguchi H, He M, Wu P, Kim S, Paik R, Sugino K, Kvitsiani D, Fu Y, Lu J, Lin Y, Miyoshi G, Shima Y, Fishell G, Nelson SB, Huang ZJ (2011) A Resource of Cre Driver Lines for Genetic Targeting of GABAergic Neurons in Cerebral Cortex. *Neuron* 71:995-1013.

Telenius H, Kremer B, Goldberg YP, Theilmann J, Andrew SE, Zeisler J, Adam S, Greenberg C, Ives EJ, Clarke LA, Hayden MR (1994) Somatic and gonadal mosaicism of the Huntington disease gene CAG repeat in brain and sperm. *Nat Genet* 6:409-414.

Thakar K, Kröcher T, Savant S, Gollnast D, Kelm S, Dietz F (2010) Secretion of hepatoma-derived growth factor is regulated by N-terminal processing. *Biol Chem* 391:1401-1410.

The Huntington's Disease Collaborative Research Group (1993) A novel gene containing a trinucleotide repeat that is expanded and unstable on Huntington's disease chromosomes. *Cell* 72:971-983.

The U.S.-Venezuela Collaborative Research Project, Wexler NS (2004) Venezuelan kindreds reveal that genetic and environmental factors modulate Huntington's disease age of onset. *Proc Natl Acad Sci U S A* 101:3498-3503.

Thévenot E, Jordão JF, O'Reilly MA, Markham K, Weng Y-Q, Foust KD, Kaspar BK, Hynynen K, Aubert I (2012) Targeted Delivery of Self-Complementary Adeno-Associated Virus Serotype 9 to the Brain, Using Magnetic Resonance Imaging-Guided Focused Ultrasound. *Hum Gene Ther* 23:1144-1155.

Thorne RG, Frey WH (2001) Delivery of Neurotrophic Factors to the Central Nervous System. *Clin Pharmacokinet* 40:907-946.

Thu DCV, Oorschot DE, Tippett LJ, Nana AL, Hogg VM, Synek BJ, Luthi-Carter R, Waldvogel HJ, Faull RLM (2010) Cell loss in the motor and cingulate cortex correlates with symptomatology in Huntington's disease. *Brain* 133:1094-1110.

Tippett LJ, Waldvogel HJ, Thomas SJ, Hogg VM, van Roon-Mom W, Synek BJ, Graybiel AM, Faull RLM (2007) Striosomes and mood dysfunction in Huntington's disease. *Brain* 130:206-221.

Uhlén M, Fagerberg L, Hallström BM, Lindskog C, Oksvold P, Mardinoglu A, Sivertsson Å, Kampf C, Sjöstedt E, Asplund A, Olsson I, Edlund K, Lundberg E, Navani S, Al-Khalili Szigyarto C, Odeberg J, Djureinovic D, Ottosson Takanen J, Hober S, Alm T, Edqvist PH, Berling H, Tegel H, Mulder J, Rockberg J, Nilsson P, Schwenk JM, Hamsten M, von Feilitzen K, Forsberg M, Persson L, Johansson F, Zwahlen M, von Heijne G, Nielsen J, Pontén F (2015) Tissue-based map of the human proteome. *Science* 347:1260419-1260419.

Vinther-Jensen T, Börnsen L, Budtz-Jørgensen E, Ammitzbøll C, Larsen IU, Hjermind LE, Sellebjerg F, Nielsen JE (2016) Selected CSF biomarkers indicate no evidence of early neuroinflammation in Huntington disease. *Neurol Neuroimmunol Neuroinflamm* 3:e287.

Vonsattel JPG, DiFiglia M (1998) Huntington Disease. *J Neuropathol Exp Neurol* 57:369-384.

Wang CH, Davamani F, Sue SC, Lee SC, Wu PL, Tang F-M, Shih C, Huang TH, Wu WG (2011) Cell surface heparan sulfates mediate internalization of the PWWP/HATH domain of HDGF via macropinocytosis to fine-tune cell signalling processes involved in fibroblast cell migration. *Biochem J* 433:127-138.

Wang G, Liu X, Gaertig MA, Li S, Li XJ (2016) Ablation of huntingtin in adult neurons is nondeleterious but its depletion in young mice causes acute pancreatitis. *Proc Natl Acad Sci U S A* 113:3359-3364.

Wang N, Gray M, Lu XH, Cantle JP, Holley SM, Greiner E, Gu X, Shirasaki D, Cepeda C, Li Y, Dong H, Levine MS, Yang XW (2014) Neuronal targets for reducing mutant huntingtin expression to ameliorate disease in a mouse model of Huntington's disease. *Nat Med* 20:536-541.

Wave Life Sciences (2021) Wave Life Sciences Provides Update on Phase 1b/2a PRECISION-HD Trials. https://ir.wavelifesciences.com/news-releases/news-release-details/wave-life-sciences-provides-update-phase-1b2a-precision-hd (Accessed: 09 November 2021).

Wertz MH, Mitchem MR, Pineda SS, Hachigian LJ, Lee H, Lau V, Powers A, Kulicke R, Madan GK, Colic M, Therrien M, Vernon A, Beja-Glasser VF, Hegde M, Gao F, Kellis M, Hart T, Doench JG, Heiman M (2020) Genome-wide In Vivo CNS Screening Identifies Genes that Modify CNS Neuronal Survival and mHTT Toxicity. *Neuron* 106:76-89.e8.

Wheeler VC, Persichetti F, McNeil SM, Mysore JS, Mysore SS, MacDonald ME, Myers RH, Gusella JF, Wexler NS, the US-Venezuela Collaborative Reasearch Group (2007) Factors associated with HD CAG repeat instability in Huntington disease. *J Med Genet* 44:695-701.

Whone A, Luz M, Boca M, Woolley M, Mooney L, Dharia S, Broadfoot J, Cronin D, Schroers C, Barua NU, Longpre L, Barclay CL, Boiko C, Johnson GA, Fibiger HC, Harrison R, Lewis O, Pritchard G, Howell M, Irving C, Johnson D, Kinch S, Marshall C, Lawrence AD, Blinder S, Sossi V, Stoessl AJ, Skinner P, Mohr E, Gill SS (2019) Randomized trial of intermittent intraputamenal glial cell line-derived neurotrophic factor in Parkinson's disease. *Brain* 142:512-525.

Yamamoto A, Lucas JJ, Hen R (2000) Reversal of Neuropathology and Motor Dysfunction in a Conditional Model of Huntington's Disease. *Cell* 101:57-66.

Yang J, Everett AD (2007) Hepatoma derived growth factor binds DNA through the N-terminal PWWP domain. *BMC Mol Biol* 8:101.

Yang J, Everett AD (2009) Hepatoma-derived growth factor represses SET and MYND domain containing 1 gene expression through interaction with C-terminal binding protein. *J Mol Biol* 386:938-950.

Yang SH, Cheng PH, Banta H, Piotrowska-Nitsche K, Yang JJ, Cheng ECH, Snyder B, Larkin K, Liu J, Orkin J, Fang ZH, Smith Y, Bachevalier J, Zola SM, Li SH, Li XJ, Chan AWS (2008) Towards a transgenic model of Huntington's disease in a non-human primate. *Nature* 453:921-924.

Yang Y, Ma Y, Gao H, Peng T, Shi H, Tang Y, Li H, Chen L, Hu K, Han A (2021) A novel HDGF-ALCAM axis promotes the metastasis of Ewing sarcoma via regulating the GTPases signaling pathway. *Oncogene* 40:731-745.

Yusuf IO, Cheng PH, Chen HM, Chang YF, Chang CY, Yang HI, Lin CW, Tsai SJ, Chuang JI, Wu CC, Huang BM, Sun SH, Yang SH (2018) Fibroblast Growth Factor 9 Suppresses Striatal Cell Death Dominantly Through ERK Signaling in Huntington's Disease. *Cell Physiol Biochem* 48:605-617.

Zala D, Benchoua A, Brouillet E, Perrin V, Gaillard MC, Zurn AD, Aebischer P, Déglon N (2005) Progressive and selective striatal degeneration in primary neuronal cultures using lentiviral vector coding for a mutant huntingtin fragment. *Neurobiol Dis* 20:785-798.

Zeitlin S, Liu JP, Chapman DL, Papaioannou VE, Efstratiadis A (1995) Increased apoptosis and early embryonic lethality in mice nullizygous for the Huntington's disease gene homologue. *Nat Genet* 11:155-163.

Zhao J, Yu H, Lin L, Tu J, Cai L, Chen Y, Zhong F, Lin C, He F, Yang P (2011) Interactome study suggests multiple cellular functions of hepatoma-derived growth factor (HDGF). *J Proteomics* 75:588-602.

Zhong G, Wang H, He W, Li Y, Mou H, Tickner ZJ, Tran MH, Ou T, Yin Y, Diao H, Farzan M (2020) A reversible RNA on-switch that controls gene expression of AAV-delivered therapeutics in vivo. *Nat Biotechnol* 38:169-175.

Zhou Z, Yamamoto Y, Sugai F, Yoshida K, Kishima Y, Sumi H, Nakamura H, Sakoda S (2004) Hepatoma-derived growth factor is a neurotrophic factor harbored in the nucleus. *J Biol Chem* 279:27320-27326.

Zink D, Fischer AH, Nickerson JA (2004) Nuclear structure in cancer cells. *Nat Rev Cancer* 4:677-687.

Zuccato C, Cattaneo E (2009) Brain-derived neurotrophic factor in neurodegenerative diseases. *Nat Rev Neurol* 5:311-322.

ACKNOWLEDGEMENTS

I would like to thank everyone who contributed to the success of this dissertation, for support of all kinds, the great working atmosphere, for inspiring scientific discussions and all conversations beyond science.

In particular, my sincere thanks go to Rüdiger Klein for the opportunity to work in this exceptional international environment, for continuous support and insightful input throughout the last years. I am especially grateful to Irina Dudanova who guided me all the way through my doctorate. Thank you for creating a pleasant working atmosphere of trust and support.

Many thanks to my former colleague Sara Gutiérrez-Ángel for sharing her project with me. I was very lucky to work with her in a great team effort halfway through my doctorate. Heartfelt thanks to my fantastic students Sophie Keeling, Nicole Martin, Maximilian Gantz, and Florian Leiß-Maier for their enthusiasm and remarkable help, as well as to my HiWi Magdalena Böhm for excellent technical support.

I would like to express my gratitude to our collaborators Thomas Arzberger and Michael Schmidt, who enabled immunostaining in human tissue. Thank you to my thesis advisory committee members, Laura Busse and Dieter Edbauer, for valuable advice and scientific input. Moreover, I am grateful to the IMPRS-LS coordination office for their support, the familial atmosphere, and for creating a lively research environment.

Finally, I want to thank my lab mates, friends, and family, who kept me going when the road felt too bumpy and long.

LIST OF PUBLICATIONS

Blumenstock S[†], Schulz-Trieglaff EK[†], **Voelkl K**, Bolender AL, Lapios P, Lindner J, Hipp MS, Hartl FU, Klein R, Dudanova I (2021) Fluc-EGFP reporter mice reveal differential alterations of neuronal proteostasis in aging and disease. *EMBO J* 40:e107260.

Burgold J[†], Schulz-Trieglaff EK[†], **Voelkl K**, Gutiérrez-Ángel S, Bader JM, Hosp F, Mann M, Arzberger T, Klein R[‡], Liebscher S[‡], Dudanova I[‡] (2019) Cortical circuit alterations precede motor impairments in Huntington's disease mice. *Sci Rep* 9:6634.

Hartmann S, Zheng F, Kyncl M, Karch S, **Voelkl K**, Zott B, D'Avanzo C, Lomoio S, Tesco G, Kim DY[‡], Alzheimer C[‡], Huth T[‡] (2018) β-Secretase BACE1 Promotes Surface Expression and Function of Kv3.4 at Hippocampal Mossy Fiber Synapses. *J Neurosci* 38:3480-3494.

[†] These authors share first authorship

[‡] These authors share senior authorship